

AD-A154 947

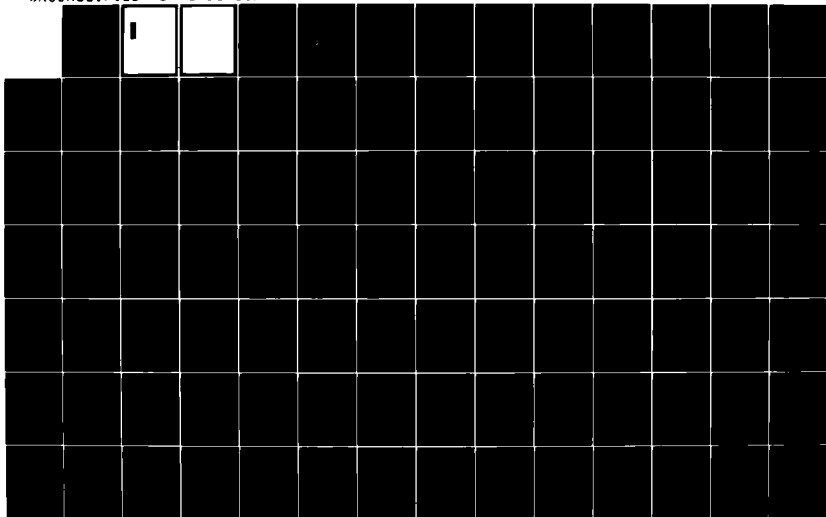
TRAILING EDGE FLOW AND AERODYNAMIC SOUND PART 1 TONAL  
PRESSURE AND VELOC... (U) DAVID W TAYLOR NAVAL SHIP  
RESEARCH AND DEVELOPMENT CENTER BET... W K BLAKE DEC 84  
DTNSRDC-83/113

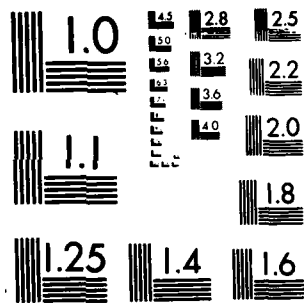
1/2

UNCLASSIFIED

F/G 20/4

NL





MICROCOPY RESOLUTION TEST CHART  
NATIONAL BUREAU OF STANDARDS 1963-A

**AD-A154 947**

UNCLASSIFIED

SECURITY CLASSIFICATION OF THIS PAGE (When Data Entered)

REPORT DOCUMENTATION PAGE		READ INSTRUCTIONS BEFORE COMPLETING FORM
1. REPORT NUMBER DTNSRDC-83/113	2. GOVT ACCESSION NO. <b>A154947</b>	3. AUTHOR'S CATALOG NUMBER
4. TITLE (and Subtitle) TRAILING EDGE FLOW AND AERODYNAMIC SOUND PART 1. TONAL PRESSURE AND VELOCITY FLUCTUATIONS PART 2. RANDOM PRESSURE AND VELOCITY FLUCTUATIONS		5. TYPE OF REPORT & PERIOD COVERED Final
7. AUTHOR(s) William K. Blake		6. PERFORMING ORG. REPORT NUMBER
9. PERFORMING ORGANIZATION NAME AND ADDRESS David Taylor Naval Ship Research and Development Center Bethesda, Maryland 20084-5000		8. CONTRACT OR GRANT NUMBER(s)
11. CONTROLLING OFFICE NAME AND ADDRESS Naval Sea Systems Command Washington, D.C. 20362		10. PROGRAM ELEMENT, PROJECT, TASK AREA & WORK UNIT NUMBERS Task Area SF 43 434 001 Work Unit 1540-002
14. MONITORING AGENCY NAME & ADDRESS (if different from Controlling Office)		12. REPORT DATE December 1984
		13. NUMBER OF PAGES 100
		15. SECURITY CLASS. (of this report) UNCLASSIFIED
		15a. DECLASSIFICATION/DOWNGRADING SCHEDULE
16. DISTRIBUTION STATEMENT (of this Report)  APPROVED FOR PUBLIC RELEASE: DISTRIBUTION UNLIMITED		
17. DISTRIBUTION STATEMENT (of the abstract entered in Block 20, if different from Report)		
18. SUPPLEMENTARY NOTES  <i>with plot</i>		
19. KEY WORDS (Continue on reverse side if necessary and identify by block number) Turbulence Vortex Shedding; Pressure Fluctuations, Singing; → Wake Instability; Trailing Edge Noise. *		
20. ABSTRACT (Continue on reverse side if necessary and identify by block number) → The turbulent field quantities at the trailing edges of lifting surfaces consist of two components. Locally-generated random fluctuations are generated by separation of the turbulent boundary layers and these fluctuations account for weakly correlated surface pressure fields. The second contribution is periodic, or nearly periodic, and is generated by the structured vortex pressure field. The aerodynamic properties of each of these contributions are (Continued on reverse side)		

DD FORM 1473  
1 JAN 73

EDITION OF 1 NOV 65 IS OBSOLETE  
S/N 0102-LF-014-6601

UNCLASSIFIED

SECURITY CLASSIFICATION OF THIS PAGE (When Data Entered)

UNCLASSIFIED

SECURITY CLASSIFICATION OF THIS PAGE (When Data Entered)

(Block 20 continued)

examined for various trailing edge configurations, and the aeroacoustic qualities of each are explored. Rules are given for the prediction of the onset of either predominantly tonal or predominantly random pressure fields. Relationships are given for estimating aerodynamic sound levels from the surface pressures for each class of aerodynamic excitation.

*report - 4:10 → (to p. 1)*

DTIC  
ELECTE  
S JUN 13 1985 D  
B

Number of Pages	
Number of Figures	<input checked="" type="checkbox"/>
Number of Tables	<input type="checkbox"/>
Number of References	<input type="checkbox"/>
Author	
Organization	
Address	
City	
State	
Country	
Availability Codes	
Availability	
Availability	
Availability	

A-1

0148  
0149  
0150

S/N 0102-LF-014-6601

UNCLASSIFIED

SECURITY CLASSIFICATION OF THIS PAGE (When Data Entered)

TABLE OF CONTENTS

<u>Section</u>	<u>Page</u>
LIST OF FIGURES . . . . .	v
LIST OF TABLES . . . . .	ix
ADMINISTRATIVE INFORMATION . . . . .	ix
 <u>PART 1</u>	
ABSTRACT . . . . .	1
1. INTRODUCTION . . . . .	3
2. FACILITY AND INSTRUMENTATION DESCRIPTIONS . . . . .	5
2.1 STRUT AND TRAILING EDGES . . . . .	6
2.2 INSTRUMENTATION . . . . .	7
2.3 CHARACTERISTICS OF FLOW UPSTREAM OF THE EDGES . . . . .	7
3. PRESSURES AND VELOCITIES GENERATED BY PERIODIC VORTEX STREETS . . . . .	12
3.1 SURFACE PRESSURES AND VORTEX STRENGTHS OF BLUNT TRAILING EDGES . . . . .	12
3.2 VORTEX STRUCTURE RELATED TO SURFACE PRESSURE . . . . .	16
3.3 THE WAKE-PRESSURE CONNECTION FOR THE ROUNDED 45° BEVEL TRAILING EDGE . . . . .	19
3.4 SPANWISE STATISTICS OF THE TONAL SURFACE PRESSURES . . . . .	27
4. GENERALITIES REGARDING THE FREQUENCIES AND AMPLITUDES OF TONAL TRAILING-EDGE PRESSURES . . . . .	30
4.1 VORTEX-SHEDDING FREQUENCY . . . . .	30
4.2 MAGNITUDES OF THE SURFACE PRESSURE; ANALYTICAL MODEL . . . . .	33
4.3 RADIATED SOUND FROM VORTEX SHEDDING . . . . .	42
4.4 APPARENT DEPENDENCE ON REYNOLDS NUMBER . . . . .	44
5. CONCLUSIONS . . . . .	49
ACKNOWLEDGMENTS . . . . .	50
REFERENCES . . . . .	51

<u>Section</u>	<u>Page</u>
<u>PART 2</u>	
ABSTRACT . . . . .	55
1. INTRODUCTION . . . . .	57
2. SEPARATED FLOW AT BEVELED TRAILING EDGES . . . . .	60
2.1 TURBULENT FLOW NEAR 25° KNUCKLE-BEVELED EDGE . . . . .	60
2.2 TURBULENT FLOW NEAR 25° ROUNDED-BEVELED EDGE . . . . .	63
3. AUTOSPECTRA OF PRESSURE FLUCTUATIONS: GENERAL FEATURES . . . . .	65
4. CONNECTION BETWEEN SURFACE PRESSURE AND LOCAL FLOW STRUCTURE . . . . .	68
5. DETAILS OF THE PRESSURE SPECTRA IN REGIONS OF SEPARATED TRAILING EDGE FLOW . . . . .	70
5.1 GENERALIZATIONS REGARDING THE STATISTICAL PROPERTIES OF THE SURFACE PRESSURE . . . . .	70
5.2 LARGE-EDDY STRUCTURE IN THE SEPARATION ZONE OF THE BEVELED EDGE . . . . .	74
5.3 WALL PRESSURE STATISTICS ON ROUNDED-BEVEL TRAILING EDGES. . . . .	78
6. IMPLICATIONS FOR AERODYNAMIC SOUND GENERATION AND SPANWISE PRESSURE CORRELATIONS . . . . .	80
6.1 ELEMENTS OF THE THEORY OF AERODYNAMIC SURFACE PRESSURES AT TRAILING EDGES . . . . .	80
6.2 DEDUCTIONS REGARDING AERODYNAMIC SOUND . . . . .	86
7. CONCLUSIONS . . . . .	90
7.1 GENERAL COMMENTS . . . . .	90
7.2 MINIMUM REYNOLDS NUMBER FOR PERIODIC WAKE GENERATION. . . . .	90
7.3 MAGNITUDES OF SURFACE PRESSURE . . . . .	91
ACKNOWLEDGMENTS . . . . .	92
REFERENCES . . . . .	93

LIST OF FIGURES

<u>Figure</u>		<u>Page</u>
PART 1		
1	A View of the Strut Showing the Orientation of Trailing Edges and Schematic Locations of Microphones . . . . .	4
2	Static Pressure Distribution, Cross-Section Shape, and Microphone Locations of the Strut Outfitted with the 25° Rounded Trailing Edge . . . . .	8
3	Mean and Turbulent Velocity Profiles for Positions 4 and B on Strut with the 25° Rounded Trailing Edges. . . . .	10
4	Normalized Mean Velocity Profiles Incident on the Trailing Edges . .	11
5	Flow Patterns and Static Pressure Distribution at the 45° Rounded Trailing Edge of the Strut . . . . .	13
6	Mean-Square Pressures Measured on the Blunt Edge in 12.5 Hz Bands at the Tip . . . . .	15
7	Pressure Velocity Correlations Behind Blunt Edge at $U_\infty = 100$ ft/s . .	18
8	Flow Patterns and Pressure Distributions at the Trailing Edge of the Blunt Trailing Edge at $U_\infty = 100$ ft/s . . . . .	20
9	Dimensionless Longitudinal Velocity Spectral Densities Measured in the Formation Region of the Near-Wake from the 45° Rounded Bevel Edge . . . . .	21
10	Mean-Square Pressures Measured on the 45° Rounded Edge in 12.5-Hz Bands at Position G and at Position 6 for $U_\infty = 50$ ft/s . . . . .	22
11	Chordwise Profiles of Fluctuating Pressure at $f = f_s$ with 45° Rounded Trailing Edge at $U_\infty = 100$ ft/s . . . . .	23
12	Pressure-Velocity Correlations in the Wake Behind the 45° Rounded Beveled Edge at $U_\infty = 50$ ft/s . . . . .	24
13	Pressure-Velocity Correlations Behind the 45° Rounded Beveled Edge at $U_\infty = 100$ ft/s . . . . .	25
14	Spanwise Correlations of Vortex-Shedding Pressures on the Trailing Edges of Flat Airfoils . . . . .	28
15	Bearman's (1967) Universal Strouhal Number Versus $U_s/U_\infty$ for the Blunt and 45° Rounded Trailing Edges . . . . .	29

<u>Figure</u>		<u>Page</u>
16	Idealizations of Vortex Wake Structures for Modeling of Surface Pressures and Radiated Sound . . . . .	34
17	Mean-Square Pressures Measured at Various Streamwise Distances (x) Forward of Trailing-Edge Stagnation Point ( $x_s$ ) . . . . .	35
18	Vortex-Induced Surface Pressures on Trailing Edges of Airfoils . . .	36
19	Profiles of Surface Pressure and Velocity Fluctuations at the Blunt Trailing Edge of a Tapered Airfoil . . . . .	41
20	Radiated Sound and Surface Pressure for Sharp and Blunt Edges of a NACA 0012 Airfoil with Leading Edge Tripping, $U_\infty = 62$ m/s . . . .	45
21	Narrowband Cross-Spectral Densities and Spanwise Integral Scales of Surface Pressures on Blunt-Edged NACA 0012 Airfoil . . . . .	46
22	Mean-Square Vortex Strengths for Various Trailing Edges with Vortex Shedding . . . . .	47

PART 2

1	A View of the Strut Showing the Orientation of Trailing Edges and Schematic Locations of Microphones . . . . .	57
2	Flow Patterns and Static Pressure Distributions on the 25° Knuckle Beveled Edge . . . . .	58
3	Flow Patterns a $U_\infty = 100$ ft/s Pressure Distribution Near 25° Rounded Level . . . . .	59
4	Relationship Between Shape Factor and $\delta^*/\delta$ for Various Positions on the Trailing Edges and for Sanborn and Kline's Experiment with Intermittent Separation . . . . .	64
5	Wall Pressure Spectral Densities at Position B Normalized on Local Wall Shear, Displacement Thickness, and $U_\infty$ . . . . .	66
6	Dimensionless Pressure Spectra of 25° Rounded Bevel Trailing Edge. Open Points, $U_\infty = 100$ ft/s; Closed Points $U_\infty = 60$ ft/s . . . . .	67
7	Dimensionless Pressure Spectra of 25° Knuckle Trailing Edge . . . .	67
8	Pressure-Velocity Correlation in the Near Wake and Separation Zone of the 25° Knuckle Trailing Edge . . . . .	68
9	Pressure-Velocity Correlations in the Near Wake and Separation Zone of the 25° Rounded Trailing Edge. $r_x$ is Measured from Position G . . . . .	69

<u>Figure</u>		<u>Page</u>
10	Surface Pressure Spectra Beneath Flow Separation at Trailing Edges Which Do Not Ordinarily Generate Periodic Vortex Street Wakes . . .	72
11	Surface Pressure Spectra at Trailing Edges for Conditions with Varying Degrees of Vortex Shedding Periodicity . . . . .	73
12	Spectral Densities of Surface Pressures at a Rounded-Bevel Trailing Edge . . . . .	74
13	Distribution and Covariance of Pressures on the Beveled Trailing Edge of Fig. 12 at $N_{Re_h} = 10.4 \times 10^4$ . . . . .	75
14	Cross-Spectral Densities of Surface Pressures with Chordwise Distances in the Separation Zone of the 25° Knuckle Edge . . . . .	77
15	Normalized Longitudinal Cross-Spectral Density Magnitudes of Fluctuating Surface Pressures on 25° Rounded Bevel Edge . . . . .	79
16	Wall Pressure Convection Velocities at Two Positions on the Strut with 25° Rounded Bevel Trailing Edge . . . . .	80
17	Geometry and Coordinate System for Trailing Edge Problems . . . . .	82
18	Normalized Lateral Cross-Spectral Density Magnitudes of Fluctuating Surface Pressure at Position E1 on 25° Rounded Bevel Edge . . . . .	88
19	Cross-Spectral Densities of Pressures in the Zone of Separated Flow on the 25° Knuckle Trailing Edge . . . . .	89

LIST OF TABLES

<u>Table</u>		<u>Page</u>
PART 1		
1	Strouhal Numbers Based on Cross-Wake Length Scale . . . . .	32
2	Parameters for Trailing Edges Which Produce Tones . . . . .	48
PART 2		
1	Mean Boundary-Layer Properties for the 25° Knuckle Trailing Edge . .	59
2	Mean Boundary-Layer Properties for the 25° Round Trailing Edge . . .	60
3	Summary of Parameters for Trailing Edge Flow . . . . .	71

ADMINISTRATIVE INFORMATION

The work reported herein was funded by the Naval Sea Systems Command under Task Area SF 43 434 001, Work Unit 1540-002.

## PART 1. TONAL PRESSURE AND VELOCITY FLUCTUATIONS

### ABSTRACT

A comprehensive evaluation has been made of the vortex structures in the near wakes which exist behind various shapes of trailing edges as used on many lifting surfaces. This structure, in the form of fluctuating velocities and correlation scales, has been related both experimentally and analytically to the surface pressure fluctuations which were measured on these same trailing edges. It is shown herein how the wake structures and the observed behavior of the surface pressures relate to the techniques of theoretical modeling of flow-induced surface pressures and far field sound. In this report which features measurements of wake and pressure fluctuations that are characterized by strong tonal content, the chordwise variation of the magnitudes of the tonal pressures are shown to be determined, through a nearly unique functional form, by the strengths and formation lengths of vortices in the near wake. The frequency of vortex shedding has not only been found to conform to Bearman's (1967) universal Strouhal number based on the far wake, but also on parameters characteristic of the near wake. This Strouhal number is defined as  $\omega_s y_f / U_s \approx 1$ ;  $\omega_s$  is the frequency of vortex shedding,  $y_f$  is a lateral shear-layer dimension defined at formation, and  $U_s$  is Roshko's (1954) shedding velocity. Conditions for the occurrence or non-occurrence of tones are given for the trailing edges examined. A corresponding theory for tonal sound radiation is given and confirmed using measurements by Brooks and Hodgeson (1981).

## 1. INTRODUCTION

Flow past the trailing edge of a lifting surface can be the source of both tonal and continuous spectrum noises occurring either separately or simultaneously. The subject receiving the most attention in previous work, however, has been trailing edge vortex shedding and, in particular, a tonal phenomenon called singing. In general, the flow-body coupling required for singing may be facilitated through a vibration or an acoustic path, and the flow on the surface could be either laminar or turbulent. In typical applications at a high enough Reynolds number that the boundary layers on the surface are fully turbulent, the vortex shedding at the trailing edge may become nonlinearly coupled to vibration of the edge and produce enhanced vibration and sound. This problem is a common hydroelastic phenomenon observed on turbines and propellers. In aeroacoustics it may be the source of some high-frequency helicopter noise measured by Leverton (1973). At large enough Reynolds numbers of practical significance, the boundary layers on both surfaces of the foil are turbulent, and, if the surface is also rigid with a sharp trailing edge, then the trailing edge flow appears to be hydrodynamically stable, as shown by Chevray and Kovaszny (1969). In such turbulent surface flows a certain degree of edge bluntness is required to promote regular vortex shedding. Such bluntness may also be required in a practical sense to preserve structural integrity of the lifting foil. It is noted that when the boundary layers are laminar or transitional, tones may be generated when the trailing edge is sharp, but as Reynolds number is increased, the propensity for tonal excitation diminishes. This report will be restricted to lifting surfaces with fully developed turbulent boundary layers and some degree of edge bluntness.

The earliest work in this general area addressed the frequencies of vortex shedding and the determination of means to reduce turbine and propeller blade singing through the use of modification of trailing edge geometry. Notable work in this area is that of Gongwer (1952), Heskestad and Olberts (1960), Toebis and Eagleson (1961), and Eagleson et al. (1961), in which various definitions of Strouhal number were examined. It was found that the most severe aerohydroelastic oscillations could be attained with either blunt trailing edges or those which are symmetrically leveled. These studies produced only qualitative indications of the driving forces from the wake, although nonsymmetrically leveled edges such as the 30° angle edges



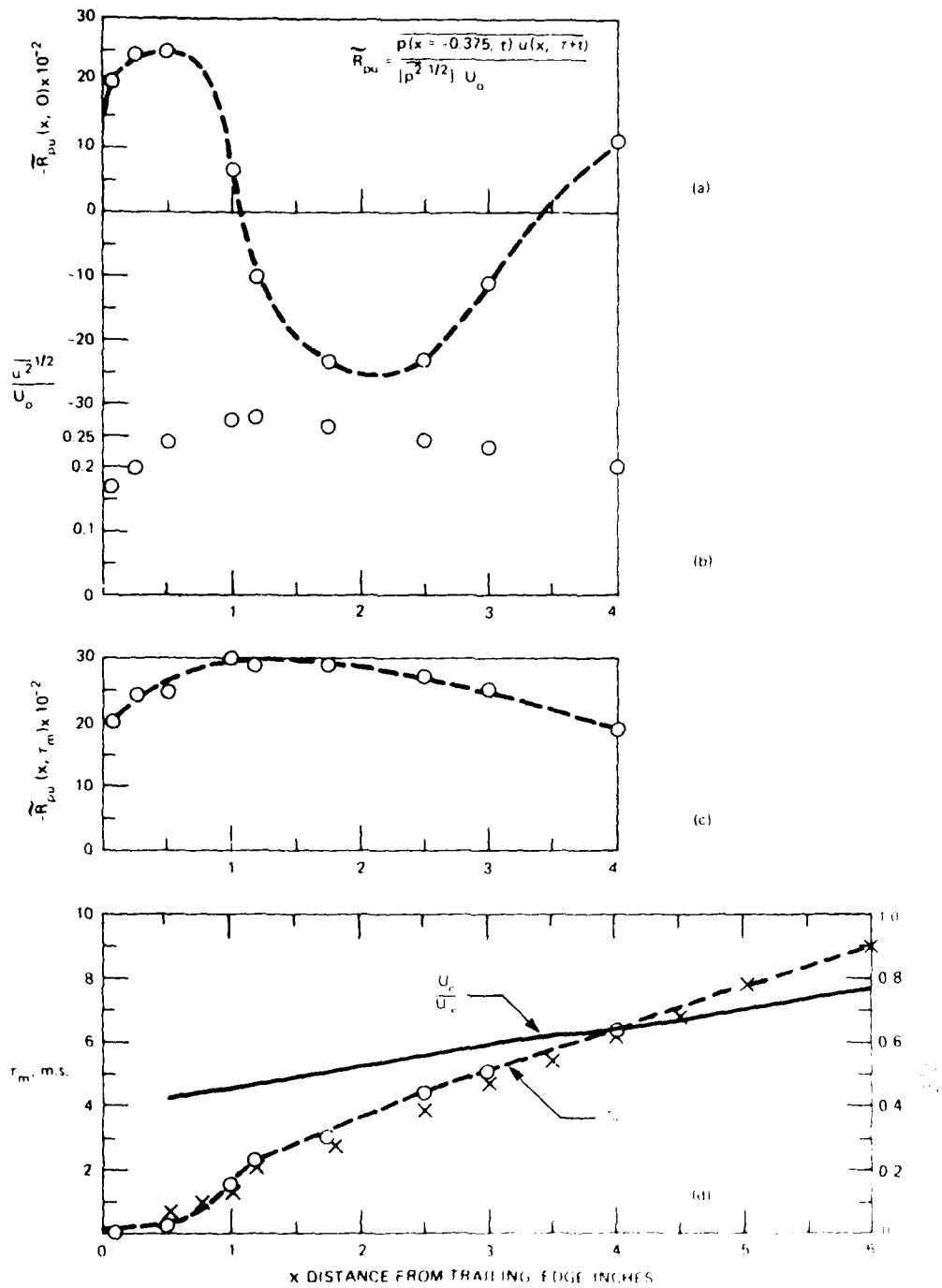


Figure 7 - Pressure Velocity Correlations Behind the Blunt Edge at  $V = 100$  ft/s

and the fluctuating velocity along the  $y = y_0/2$  locus actually reflects the structure of vortices in the wake.

This measurement was performed by moving an anemometer probe along the locus of filtered turbulence maxima in the upper side of the wake that is shown in Figure 5. The space-time correlation of pressure and velocity is written as

$$\tilde{R}_{pu}(r_x, \tau) = \frac{\overline{p(x = -0.3 \text{ in.}, t) u(x, t + \tau)}}{\overline{p_e^2} U_0} \quad (6)$$

where  $P_e(t) = p(x = -0.3 \text{ in.}, t)$  is the unfiltered fluctuating pressure at a location as close as possible to the tip, i.e., at

$$x = -0.3 \text{ in.}$$

$$t = \text{time}$$

$$u(x, t) = \text{the local velocity along } y = y_0/2, \text{ and } x \text{ is measured from the trailing edge.}$$

The correlation has been normalized on the root-mean-square fluctuating pressure at the tip and the local free-stream velocity  $U_0$ . By using  $U_0$  rather than the local root-mean-square velocity,  $\overline{u^2}^{1/2}(f_s)$ , as a normalizing factor, we can determine the relative influences of specific locations of the wake on the fluctuating pressure. The measured correlations for  $U_\infty = 100 \text{ ft/s}$  are shown in Figure 7. The upper curve is the spatial correlation, which reaches a value  $\tilde{R}_{pu}(x, 0) = -0.25$  at  $x = 0.5 \text{ in.}$  and a value  $\tilde{R}_{pu}(x, 0) = +0.25$  at  $x = 2.1 \text{ in.}$  Zero-crossings occur at  $x = 1.1 \text{ in.}$  and  $x = 3.5 \text{ in.}$  The correlation coefficient evaluated at constant phase is determined by  $\tilde{R}_{pu}(x, \tau_m)$ , where  $\tau_m$  increases from zero, and it essentially correlates the pressure with a developing vortical disturbance as it moves downstream. We shall call this the moving-eddy correlation, and it shows that although the coherence is greatest at the end of the formation region  $x = x_f$ , its magnitude essentially follows that of  $\overline{u^2}^{1/2}(f_s)$ . The correlation coefficient based on  $\overline{u^2}^{1/2}(f_s)$ , therefore, is unity, which simply means that the pressure is caused entirely by the fully coherent vortex street. The values of the time delay  $\tau_m$  for the moving-eddy correlation are used to obtain approximate convection velocities defined as  $U_c = \Delta x / \tau_m$ . Terms  $U_c$  and  $\tau_m$  are shown at the bottom of Figure 7. The varying slope in the curve of  $\tau_m$  versus  $x$  shows that when the vortex begins to form from the free shear layer, the pressure has generated the vortex field which is initially slow-moving. As the vortex

characteristic of the shear-layer at the point of separation. Justification for this variable is offered later in paragraph 4.1. This speed has been introduced by Roshko (1954) through the theory of potential flow to be related to the static base-pressure coefficient by

$$U_s = U_\infty \sqrt{1 - C_{pb}} \quad (5)$$

The dimensionless filtered-pressure levels show a maximum at a dimensionless frequency  $\omega_s y_f / U_s \approx 1$ . The bandwidth of the pressure levels appear greater for a speed of 50 than for 100 ft/s. However, at both speeds the bandwidths of the measured pressure are controlled by: the filter for which the dimensionless bandwidths are  $\Delta\omega_y / U_s < 3$ ; and the broadband-pressure levels just upstream of the tip at  $x = 0.3$  in. are a factor of 6 to 10 in excess of those measured upstream at Position 6,  $x = 13$  in. Very close to the edge, it appears that both the tonal and continuous-spectrum levels at low frequency are increased in the same proportions, while far upstream at  $x = 13$  in. the continuous-spectrum levels are typical of those measured in fully-developed turbulent boundary layers with vanishing streamwise pressure gradient.

### 3.2 VORTEX STRUCTURE RELATED TO SURFACE PRESSURE

The magnitudes of the fluctuating pressure generated by the wake depend on both the strength of the vortices shed into the wake and the proximity of the vortices to the edge. The frequency of the pressures is the same as the rate of formation of vortices, and it is given by the ratio of the local speed of the convected vortices (relative to the fixed edge) to the streamwise spacing of adjacent vortices in a single row. The cross-wake spatial variation of local fluctuating velocity shown in Figure 5 is typical of that in a street of fully-developed vortices. The variation has been related to the geometry of the configuration of the vortices by Schaefer and Eskinazi (1959). They have shown that the maximum of  $\overline{u'^2}(f_s)$ , i.e.,  $y = y_0/2$ , coincides with the locus of the peripheries of the vortex cores rather than the locus of centers of the vortices. The diameter of each vortex core was shown to extend approximately from the position of maximum filtered velocity to the centerline of the wake. The strength of each vortex is proportional to the product of the diameter of the vortex core and the tangential velocity at the periphery of the core. Therefore, measurement of the correlation between the fluctuating surface pressure

maximum, according to the Bearman (1965) criterion, signifies the end of the vortex formation region  $x = \lambda_f$ , where  $x$  denotes downstream distance from the edge.

The root-mean-square fluctuating surface pressures, which are set up by the induction field of the vortex street wake, were filtered in a 12.5-Hz band centered on the shedding frequency  $f_s$ , and measured at increasing distances upstream from the trailing edge. As shown in the upper part of Figure 5, their pressures, non-dimensionalized on the dynamic head of the inflow, diminish in level along a direction in line with the chord. They are also in common phase, showing an expected lack of convection. The frequency spectra of these pressures, at two locations along the chord, (shown in Figure 6) have a single dominant peak at  $f = f_s$ . An auto-spectrum of the fluctuating base pressure displayed a single peak at  $f = 2f_s$ . The narrowband, root-mean-square base pressure, filtered at  $f = 2f_s$  has a value of  $0.15 q_w$ . The circular frequency of shedding  $\omega_s = 2\pi f_s$  has been made dimensionless on the cross-wake distance between filtered turbulence maxima  $y_o = y_f$ , and evaluated at  $x = \lambda_f$ . These parameters are indicated in the inset to the figure. The  $U_s$  is

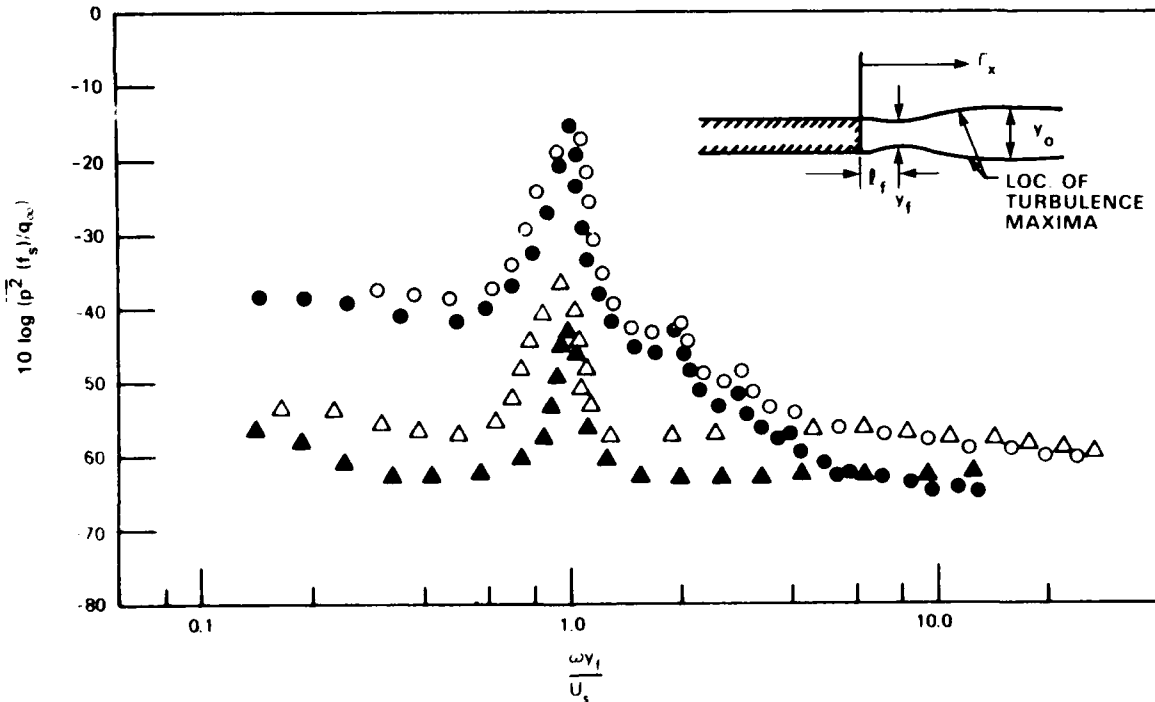


Figure 6 - Mean-Square Pressures Measured on the Blunt Edge in 12.5 Hz Bands at the Tip

to be linearly dependent on  $U_\infty$ . To compare shedding frequencies in this earlier work, we note that the Strouhal number based on the strut thickness is

$$N_{st} = f_s h / U_\infty = 0.23. \quad (4)$$

This number\* is somewhat smaller than that reported by Greenway and Wood at a lower Reynolds number with laminar upstream flow  $N_{st} = 0.286$ ; however it is in agreement with their value of  $N_{st} = 0.24$  obtained at a high Reynolds number with turbulent upstream flow. The current value compares favorably with Bearman's value,  $N_{st} = 0.24$ , for a blunt edge and turbulent upstream flow without a splitter plate. All of the previously mentioned differences in dimensionless shedding frequency are most likely due to variations in the wake thickness occurring in the various experiments, and they reflect the observation (Bearman 1965) that  $N_{st}$  is not a universal scaling number. One of the purposes of the next section will be to review various frequency-scaling hypotheses in light of the current measurements.

The mean velocity profiles of the flow on the strut and in the near wake of the strut are shown at the center of Figure 5. At the bottom of the figure are shown the vertical profiles of root-mean-square filtered fluctuating velocity fluctuations  $\overline{u^{1/2}}(f_s)$  in the wake which were found to be strongly tonal. These velocities were filtered in 1/10-octave bands centered on the shedding frequency  $f_s$ , and are controlled by the vortex street wake. Within 0.5 in. of the strut, the profiles display sharp maxima near the corners of the edge and broader peaks closer to the centerline of the wake. The sharp peaks in intensity are associated with nonlinearly growing disturbances in the shear layers, while the peaks near the centerline are probably caused by a secondary vortex system. For  $x > 5$  in., the profiles of  $\overline{u^{1/2}}(f_s)$  display maxima at each of the corners of the edge and broaden in spatial as the disturbances are convected away from the strut. The locus of the filtered intensity maxima in the upper wake is sketched in the upper part of Figure 5. The values of  $\overline{u^{1/2}}(f_s)/U_\infty$  show an absolute maximum at  $r_x = 1.3$  in. and then diminish with distance downstream. This

---

\*In this case, the definition is practically equivalent to that of Gongwer (1952) which replaces  $h$  by  $h$  plus the sum of momentum thicknesses of the boundary layers shed off the edge. Thus,  $h + 2\theta = 2.14$  in. and  $f_s(h + 2\theta)/U_\infty = 0.25$ , which is somewhat greater than the value of 0.19 obtained by Gongwer.

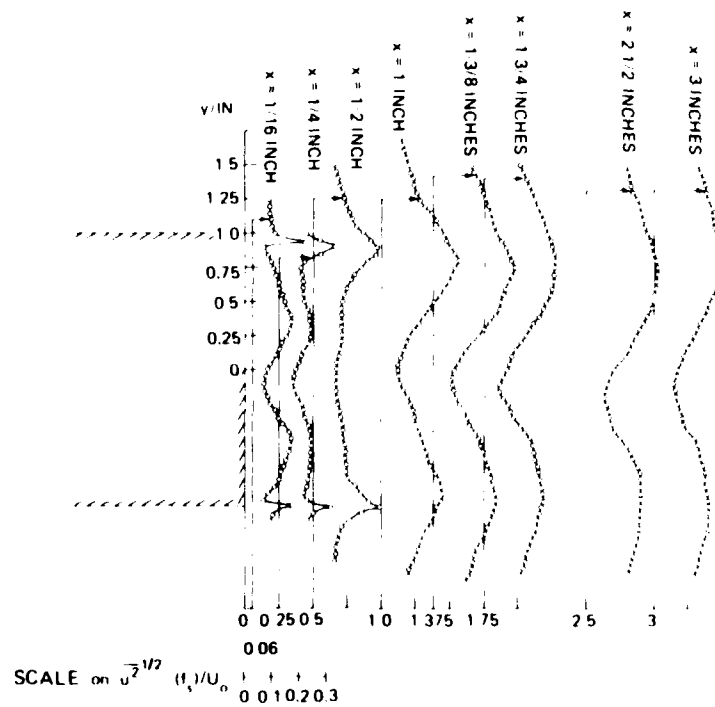
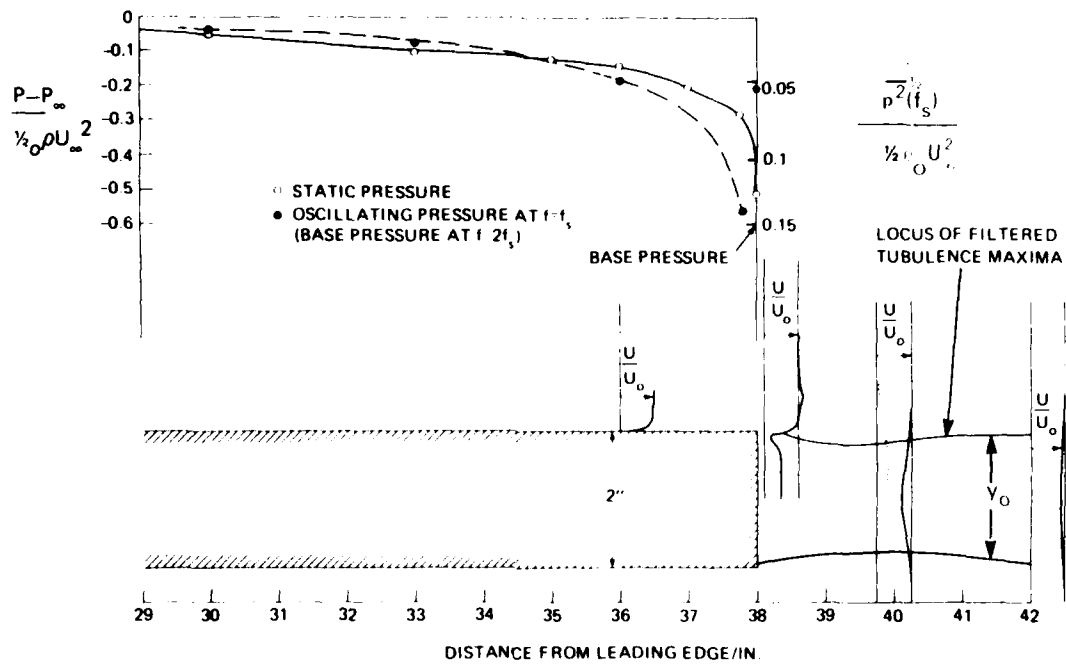


Figure 5 - Flow Patterns and Static Pressure Distribution at the 45° Rounded Trailing Edge of the Strut

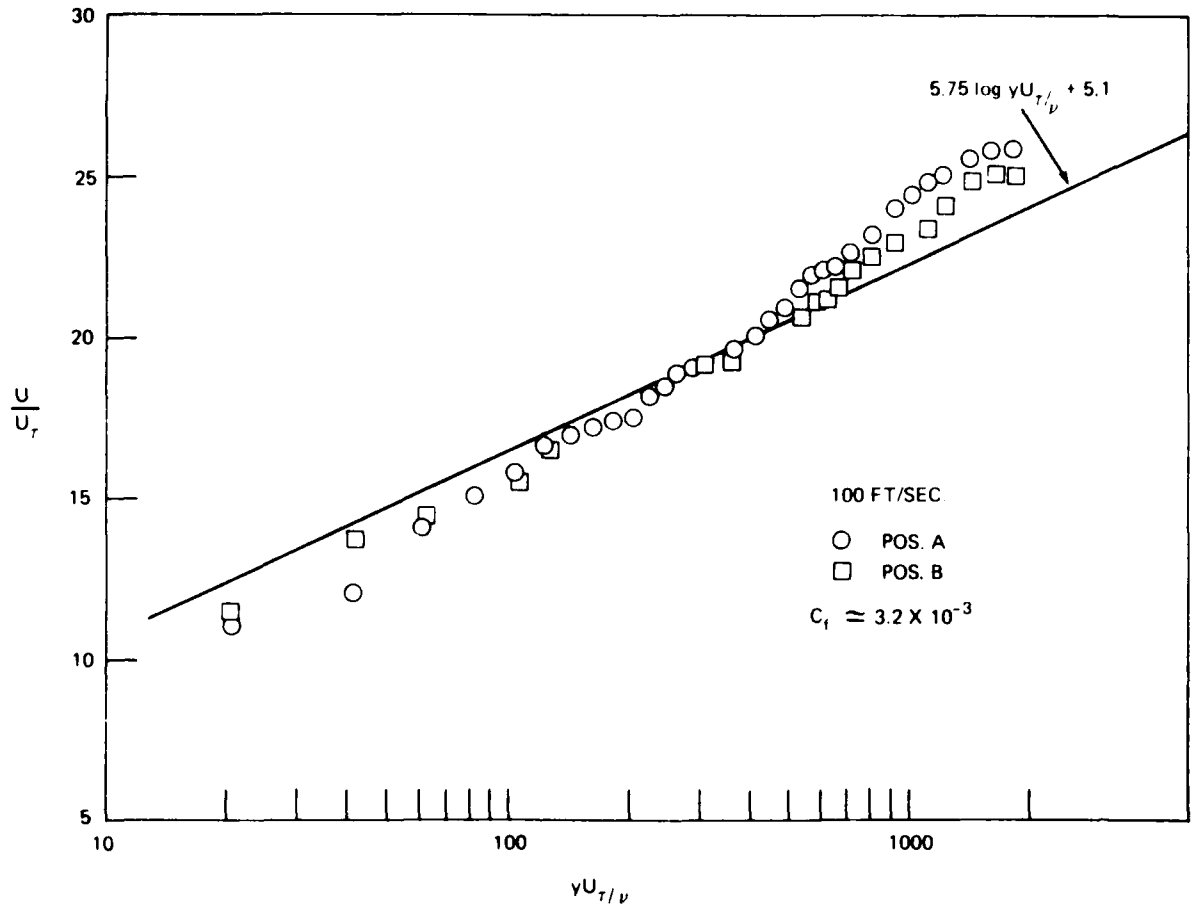


Figure 4 - Normalized Mean Velocity Profiles Incident on the Trailing Edges

and was found to be  $C_f = 3.2 \times 10^{-3}$ , slightly lower than that given by Schlichting (1960) for a naturally developed boundary layer on a smooth wall at the Reynolds number  $U_{\infty}x/\nu$ .

Spectral densities of the turbulent velocities are typically normalized on the local mean velocity  $U(y)$ , the boundary-layer-displacement thickness  $\delta^*$ , and the mean square velocity  $\overline{u^2}$ ; in this paper they are considered two-sided so that

$$\overline{u^2} = \int_{-\infty}^{\infty} \phi_{uu}(\omega) d\omega \quad (3)$$

where  $\omega$  is the radian frequency. Turbulence spectra measured in the attached

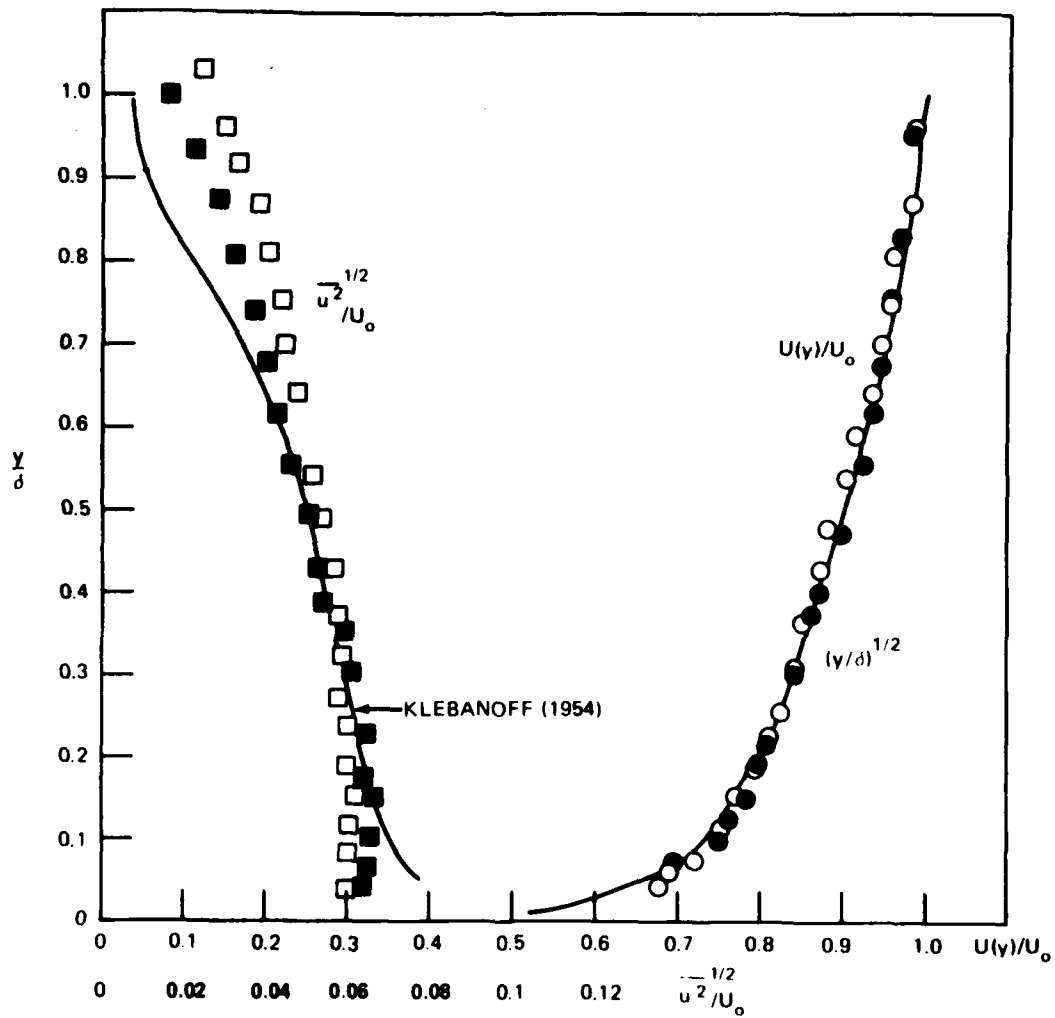


Figure 3 - Mean and Turbulent Velocity Profiles for Position 4 (Open Points) and B (Closed Points) on Strut with the 25° Rounded Trailing Edges

different edges; measurements were performed at those locations for all edges. The results in Figure 2 show the sharp static pressure minimum forward of microphone Position 1, followed by a steep adverse pressure gradient which caused a laminar separation. This, as far as trailing-edge flow was concerned, merely served to trip the boundary layer. Further downstream, the static pressure varied slightly, becoming somewhat favorable forward of the trailing edge. Magnitudes of the favorable and adverse pressure gradients at the trailing edges were dependent on the shape of the edge. For all except the blunt trailing edge, the favorable pressure gradient from  $x = 28$  in. to  $x = 34$  in. shown in Figure 2 is typical. Therefore, the statistics of the boundary layer for all Positions 1 through B were unaltered by changing the bevel-trailing edges, and only slightly modified at Position B by installing the blunt edge. This difference in local static pressure is thought to be caused by the slight change in camber brought about by the use of unsymmetrical versus symmetrical edges.

The mean and turbulent velocity profiles for Positions 4 and B are shown in Figures 3 and 4 in each of two conventional representations. In Figure 3, the mean velocity  $U(y)$  and root-mean-square turbulent velocity  $\overline{u'^2}^{1/2}$  are expressed as fractions of the local free-system velocity  $U_o$ . Distance normal to the plane of the strut  $y$  is normalized on the boundary-layer thickness  $\delta$ , which is defined by  $U(\delta) = 0.99 U_o$ . The mean velocity profiles appear to be similar, indicating that an equilibrium boundary layer has been formed on the strut. Klebanoff's (1955) longitudinal turbulence intensities are shown; levels in the outer region of the boundary layer on the strut are higher than those of Klebanoff. That they decrease from Position 4 to Position B suggests that the levels at Position 4 are influenced by large-scale disturbances associated with the leading-edge separation that are diminished at Position B. Close to the wall  $y/\delta < 0.15$ , the measured intensities are lower than those measured by Klebanoff. In Figure 4, the friction velocity is given by

$$U_\tau = \sqrt{\tau_w / \rho_o}$$

where  $\tau_w$  is the local wall shear used to normalize the velocity. The value of  $U_\tau$  was determined by curve fitting to the law of the wall, as described by Perry and Joubert (1963). The local wall-shear coefficient at  $x = 32$  in. and  $U_\infty = 100$  ft/s is

$$C_f = \tau_w / (\frac{1}{2} \rho_o U_o^2) \quad (2)$$

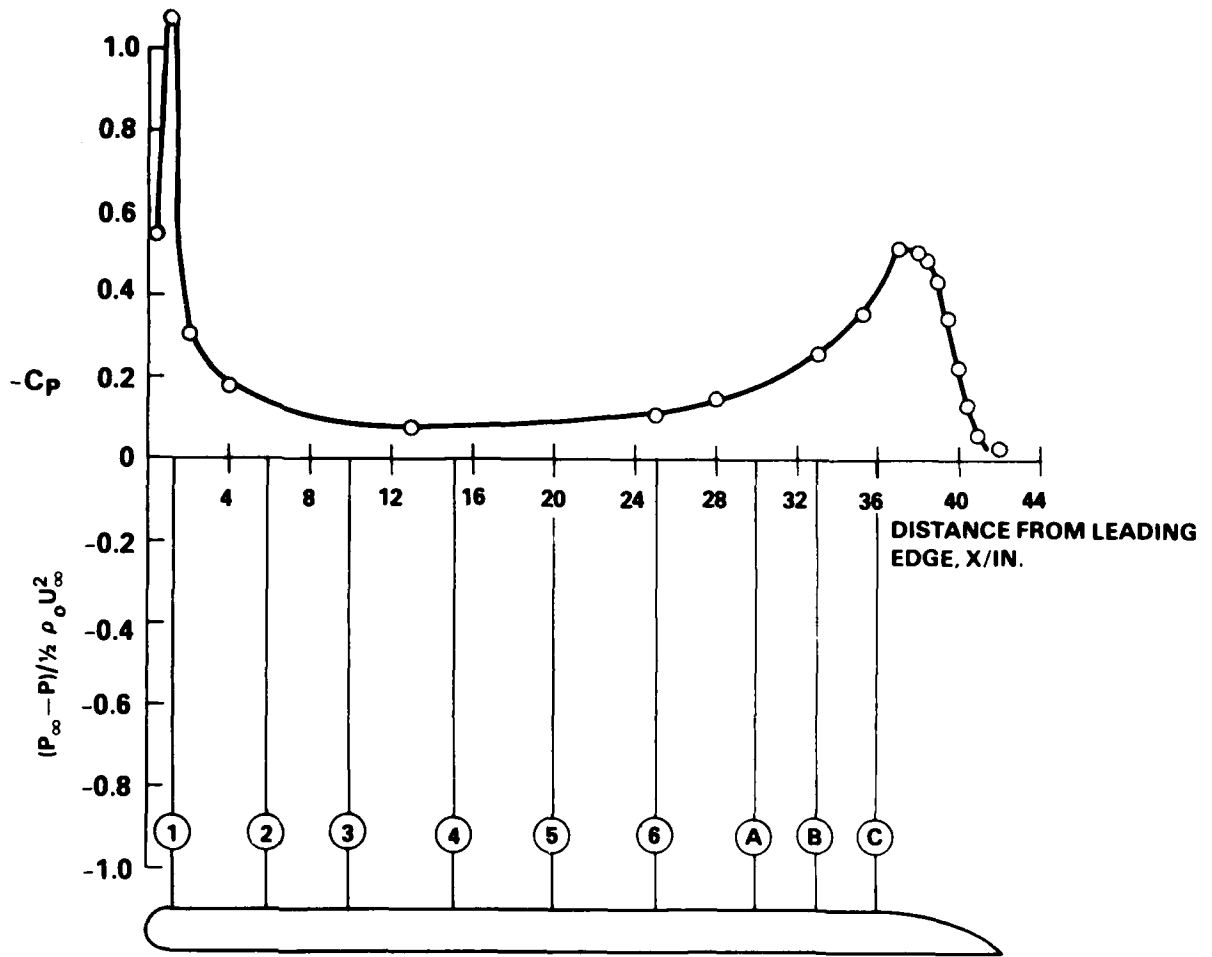


Figure 2 - Static Pressure Distribution, Cross-Section Shape, and Microphone Locations of the Strut Outfitted with the 25° Rounded Trailing Edge

$$-C_p = \frac{P_\infty - P}{\frac{1}{2} \rho_0 U_\infty^2} \quad (1)$$

where  $P_\infty$  is the ambient pressure far from the strut,  $P$  is the local static pressure on the strut,  $\rho_0$  is the fluid density, and  $U_\infty$  is the mean velocity that was trivially altered by modifying the edges. The lettered locations near the trailing edge are those for which the static pressure was influenced to varying degrees by the

## 2.2 INSTRUMENTATION

The static pressure variation along the chord was measured in the standard manner using pressure taps along both sides of the strut, including the stagnation point, (see Blake (1975a)). The flow-induced, surface-pressure fluctuations on the strut were measured using "pinhole" microphones with a 1/32-in.-diam as described by Blake (1970). Probe-tube extensions were used to measure the pressure spectra at narrow thicknesses of the trailing edge. The probe tube acts like a low-pass filter between the microphone and the fluctuating pressure source. The amplitude response was determined to be flat for frequencies less than 2 kHz, see Blake (1975). For certain of the edges miniature Kulite strain gage microphones, of diameter 0.08 in., were used when space limitations did not permit the use of the condenser microphones. Turbulent velocity fluctuations were measured using standard constant-temperature anemometry with a linearizer. Probe and probe supports were aerodynamically shaped to minimize vibration from vortex shedding from the supports.

All of the auto and cross-spectral densities of wall pressure as well as the pressure-velocity, cross-spectral densities were obtained with a real-time analyzer system. The spectral densities were determined digitally using a fast Fourier-transform algorithm with a Hanning window. Sample sizes of at least 256 (occasionally larger) were used with effective analyses bands, ranging from 12.5 to 62.5 Hz. The bandwidths of analyses were constant over each complete frequency range, which was either from 0 to 2 or 0 to 20 kHz.

Broadband correlations were made with a digital correlator instrument that displayed both auto and cross correlation functions at 100 computed points, with time delays from 100  $\mu$ s to 100 s possible. The digital equivalent of resistor-capacitor circuit (RC) averaging was used.

## 2.3 CHARACTERISTICS OF FLOW UPSTREAM OF THE EDGES

The measurements of the boundary-layer velocity profiles on the body of the strut served to establish that the turbulent flow field upstream of the edges was typical of that which exists in fully developed boundary layers on flat surfaces. Because of the flow separation at the leading-edge, the boundary layers incident on the edge were extensively surveyed to establish that both turbulence streams of the edges could be taken as typical. Figure 2 shows the chordwise static pressure distribution and the cross-section shape of the strut, which was outfitted with the 25° rounded trailing edge. The static pressures are expressed as the coefficient. Thus,

tunnel with an anechoic chamber. The broadband turbulence intensity level in the tunnel at a centerline speed of 150 ft/s has been shown by DeMetz and Casarella (1973) to be about 0.08%. A full account of the equipment and instrumentation for the studies comprising this report is given in a report (Blake (1975a) and in subsequent papers Blake (1975b) and (1977); therefore, only salient features will be summarized here.

## 2.1 STRUT AND TRAILING EDGES

The working strut (Figure 1) on which most of the work in this paper was done, had a circular leading edge, which, due to laminar separation, tripped the turbulent boundary layer on the downstream flat section. Excluding the removable trailing-edge sections, the strut was 3 ft in chord with a uniform thickness of 2 in. and a span of 4 ft. Four trailing edges were used; one was squared off and three were unsymmetrically beveled. Of the beveled edges, one had an included tip angle of  $45^\circ$  and a length of 4 in. The other had an included tip angle of  $25^\circ$  and a length of 6 1/4 in. The  $45^\circ$  edge and one of the  $25^\circ$  edges were faired with 5- and 10-in. radii, respectively, to give a continuously increasing pressure gradient. The other  $25^\circ$  edge had a knuckle, 2 in. from the strut attachment point. Both the strut and the trailing edges were constructed from pine and plywood and were painted to maintain a smooth surface. The characteristics of both of the trailing edges with  $25^\circ$  bevel will be discussed in the sequel paper because throughout most of the Reynolds number range of these experiments, the two edges with  $25^\circ$  bevels did not generate wakes with tonal character. The edges have been categorized in Figure 1 as producing tonal or continuous-spectrum flow fields.

Discussions in Section 4 of this paper will draw on an additional strut utilized for hydroelastic observations, Blake (1975b). The strut was rigidly fastened in a vertical position to the floor of the tunnel at the end of the upstream test section, adjacent to the anechoic chamber. An end plate in the form of a plywood panel (8 ft long and 5 ft wide) was attached to the top of the strut and to the walls of the tunnel in half. The measured values of fluctuating wall pressures on the blunt trailing edge of the strut were uniform over an 8-in. spanwise section, showing that the flow was essentially two-dimensional across the span of the strut.

The flow parameters selected for measurement in this work were selected on the basis of their theoretical importance for vibration and aerodynamic sound generation. Thus, to answer the questions of whether or not tonal or nontonal sound or vibration will be generated, and of what the magnitude of the disturbance will be, in either case, requires knowledge of the correlation properties of the surface pressure at the trailing edge. In the case of aerodynamic tone generation, for example, available theoretical models give the radiated sound in terms of wake vorticity and the convection velocity of that vorticity relative to the trailing edge. The analytically-determined surface pressure generated is dependent on whether or not a Kutta condition is imposed at the trailing edge. It is shown in this paper by using an analytical model of the vortex-induced surface pressures at the edge, that a full Kutta condition should not be applied in this case.

The discussions will, therefore, be divided into two parts. This Part 1 will deal with the unsteady flow fields of the near wakes characterized by periodic disturbances. Also, dimensionless representations of the wake-induced surface pressures and their frequencies will be derived. Analytical expressions for the surface and far-field acoustic pressure will be derived and compared with measurements of Brooks and Hodgeson. In Part 2 the sequel part, the disturbance fields of the near wakes behind other trailing edges that were observed to generate primarily continuous-spectrum disturbances, will be discussed particularly with regard to general features of the wake field, as compared to the case of tone generation. Finally, the conditions for the establishment of periodic versus random near wakes will also be discussed in Part 2.

## 2. FACILITY AND INSTRUMENTATION DESCRIPTIONS

A principle objective of the work herein was the simultaneous measurement of fluctuating velocity and surface pressure; thus, the experimental facility for this work was selected for its low acoustic noise background. The experimental arrangement made it impossible to use the more modern laser velocimetry techniques, so hot-wire anemometry was used for wake traverses. The high speeds and high Reynolds numbers made the use of flow visualization methods unacceptable so that flow structures had to be deduced from correlation measurements.

All measurements were performed in the Anechoic Flow Facility (AFF) of the David W. Taylor Naval Ship R&D Center. This facility combines a low-turbulence wind

in Figure 1 were found to be least likely to produce tonal excitations. The mechanics of vortex shedding and measurements of shed vortex strengths and frequencies were the subject of later studies by Greenway and Wood (1973) and Bearman (1965 and 1967), respectively.

Disturbances at trailing edges become continuous spectrum when the edge is sharpened or unsymmetrically beveled to included angles of  $30^\circ$  or less. In such cases, intense tonal vibrations are not problematic, but continuous-spectrum aerodynamic sound often is. Analytical work by Chase (1975), Chandiramani (1974), and Howe (1978) has in fact identified the prominent physical variables that affect trailing edge noise for thin, sharp, rigid edges. Experiments by Brooks and Hodgson (1980) have generally confirmed the theory. The problem with many practical airfoils is that they are not necessarily sharp, and it remains to be established what flows exist on edge shapes that are intermediate between blunt and sharp. This report examines flows on the trailing edge shapes shown in Figure 1. These shapes were selected to be representative of geometrics examined in the earlier work on vortex shedding cited above.

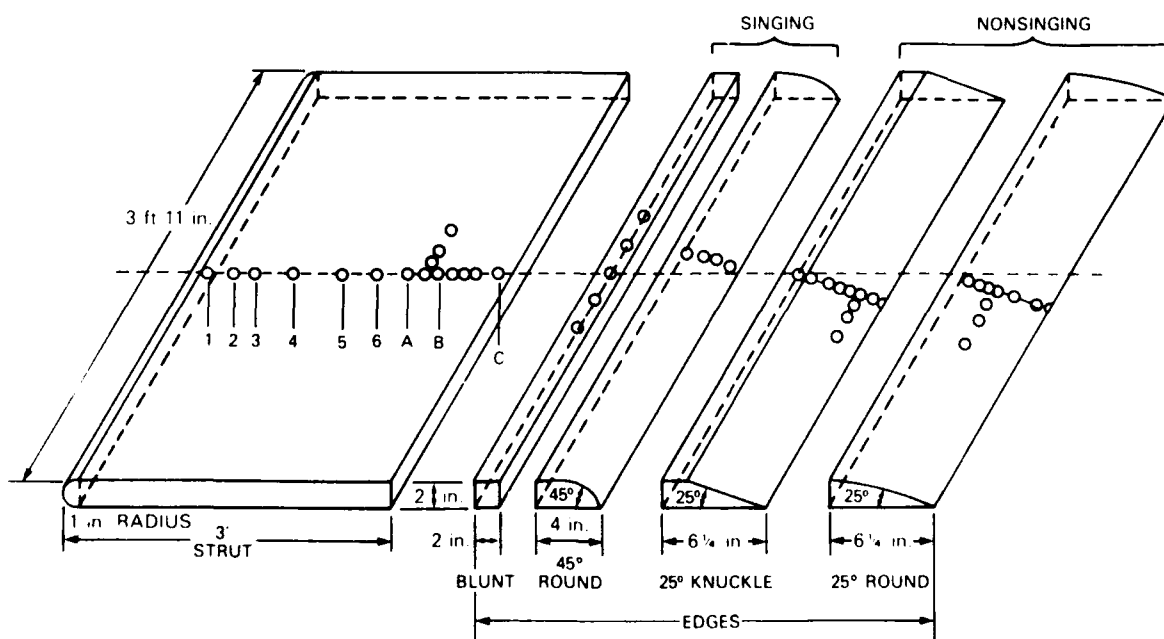


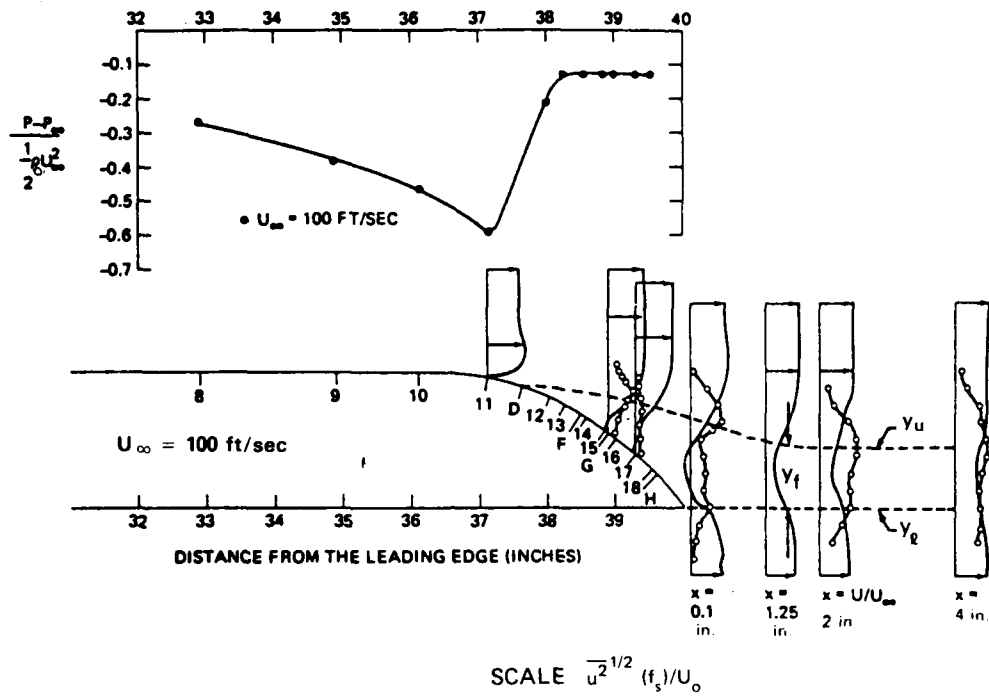
Figure 1 - A View of the Strut Showing the Orientation of Trailing Edges and Schematic Locations of Microphones

continues to form, it begins to move downstream from the edge while its strength increases. This acceleration continues until  $x = 1.3$  in., at which point the acceleration diminishes, and it begins to move with a slowly varying speed of convection. This convection behavior is indicated by either pressure-velocity or velocity-velocity correlations. In the far wake, i.e., for  $x = 9$  in. or  $x/h = 4.5$ , the velocity-velocity correlations give  $\bar{U}_c = 0.81 U_o$ . According to Bearman's (1965) measurements of velocity correlations, the convection velocity of disturbances in the far wake became constant and equal to  $0.88 U_\infty$  for  $x/h > 4$ .

### 3.3 THE WAKE-PRESSURE CONNECTION FOR THE ROUNDED 45° BEVEL TRAILING EDGE

When the trailing edge is unsymmetrically rounded, using the 45° angle and a 5-in. fairing radius of curvature as shown in Figure 1, the separation point for the boundary layer on the curved side becomes less distinct. This degree of disorder, as well as the streamwise displacement of the free-shear layer formation points, detunes interaction of the upper and lower shear layers. Characteristics of the boundary layer and near-wake are shown in Figure 8. The figure shows a favorable pressure gradient upstream from Tap 11, followed by an adverse gradient downstream from this point and constant pressure downstream from Tap 13. Observation of oil-streak patterns disclosed concentrations of oil along spanwise-oriented lines at Taps 13 and 17. The former is interpreted as an upper separation point, the latter, as the stagnation point for the trailing edge. The constant static pressure and the oil-film patterns indicate that flow is separated downstream from Tap 13.

The center diagrams of Figure 8 show both the mean and broadband rms velocity profiles in the trailing-edge region. Speeds measured at various points above the surface have been made dimensionless by using a local approximation of the free-stream speed,  $U_o$ , which was determined at each measurement station. The bulge in the profile at Tap 11, showing a somewhat higher speed near the wall than in the outer flow, reflects the negative pressure coefficient at this point. The dimensionless mean and turbulent velocity profiles at Position G, between Taps 15 and 16, have behavior typical of separated boundary layers. In these flows, which form the near wake, the velocity profiles show the flow reversal that is characteristic of regions of separated flow. The velocity fluctuations display local maxima at locations that correspond to maxima in the vertical gradient of mean velocity  $du/dy$ . The velocity spectral densities, examples of which are shown in Figure 9, and



SCALE  $u^2/2 (f_s)/U_0$

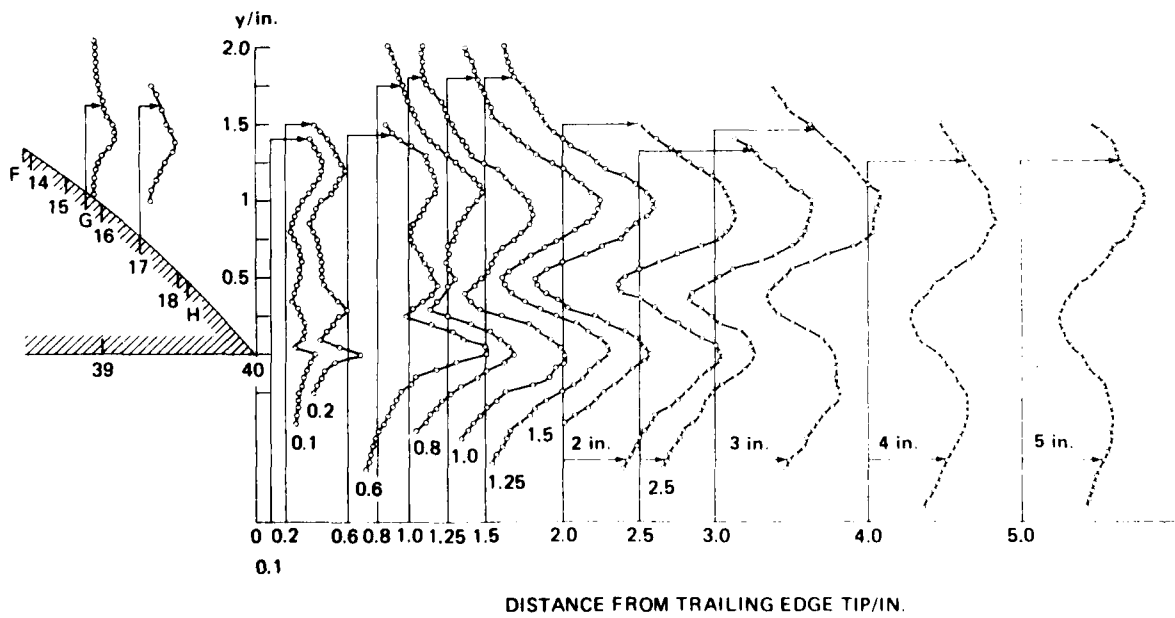


Figure 8 - Flow Patterns and Pressure Distributions at the Trailing Edge of the Blunt Trailing Edge at  $U_\infty = 100$  ft/s

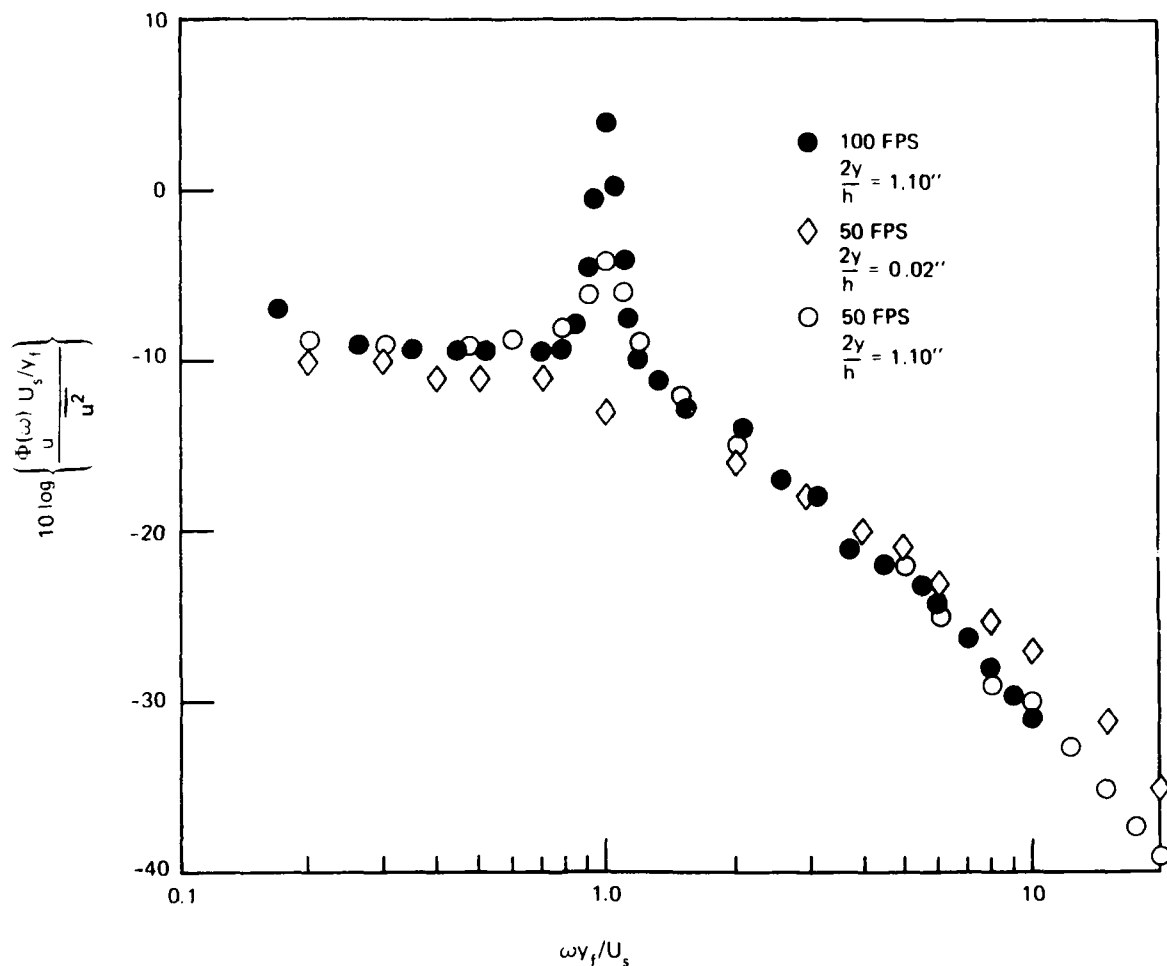


Figure 9 - Dimensionless Longitudinal Velocity Spectral Densities Measured in the Formation Region of the Near-Wake from the 45° Rounded Bevel Edge

normalized on the wake variables described below, disclosed a periodic contribution  $\omega = \omega_s$  which is interpreted as due to a vortex street. Profiles of narrowband fluctuating velocity, filtered in 1/10-octave bands at the shedding frequency  $\omega = \omega_s$ , i.e.,  $\overline{u^{2^{1/2}}}(f_s)/U_0$ , are shown at the bottom of Figure 8. Above the surface of the edge and in the wake at downstream distances  $x > 1$  in., there are secondary maxima which are probably associated with a secondary bound vortex system similar to that already proposed behind the blunt edge. In contrast to the wake of the blunt edge,

however, there is an asymmetry in the wake which persists at least 2.5 h downstream from the trailing edge. In this case, local maxima in filtered intensities occur at the upper- and lower-cross wake positions  $y = y_u$  and  $y = y_l$  as illustrated in the center portion of Figure 8. A characteristic shedding velocity  $U_s$  is again defined in terms of the pressure coefficient  $-C_{p_s}$  beneath the separated boundary layer downstream from Tap 13. Following the Roshko (1954) definition we write

$$U_s = U_\infty \sqrt{1 - C_{p_s}} \quad (7)$$

which is the same as the separation velocity of the blunt edge.

At a distance  $x = 1.25$  in. downstream from the edge, and  $2y/h = 1.10$  above the tip, the dimensionless frequency spectrum in Figure 9 shows the periodic contribution at  $\omega_s y_f / U_s = 1$  for  $U_\infty = 100$  and 50 ft/s. The intensity of the contribution is substantially higher at 100 than at 50 ft/s. Velocity fluctuations at  $U_\infty = 50$  ft/s and  $2y/h = 0$  are entirely broadband. A similar nondimensionalization of fluctuating surface pressures on the edge also shows a periodic contribution at  $\omega_s y_f / U_s = 1$ . Figure 10 shows the dimensionless spectral densities of pressure fluctuations at

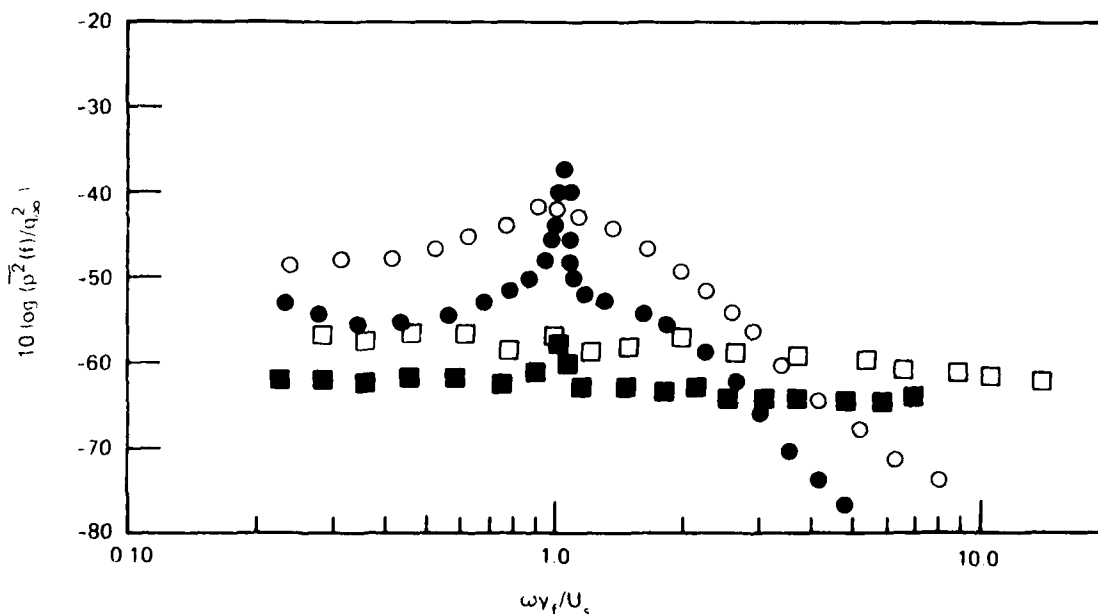


Figure 10 - Mean-Square Pressures Measured on the  $45^\circ$  Round Edge in 12.5-Hz Bands at Position G and at Position 6 (Flagged Points) for  $U_\infty = 50$  ft/s (Open Points,  $\Delta\omega y_f / U_s = 0.09$ ) and for 100 ft/s (Closed Points,  $\Delta\omega y_f / U_s = 0.045$ )

Positions 6 and G. For  $U_\infty = 100$  ft/s, the periodic contribution is greatest at Position G and substantially diminishes at Position 6. At 50 ft/s, however, the spectrum at Position G shows a broadly peaked contribution that contrasts the weak periodicity indicated by the velocity spectrum of Figure 9. It appears that the pressure fluctuations extant on the edge at 50 ft/s are determined more by local separation than by the vorticity in the wake field. At 100 ft/s, the pressures are generated by the system of vortices in the wake; these pressures, incidentally, were not affected by the presence of the anemometer probe used in the correlation measurements described below. Tonal root-mean-square filtered pressures  $\overline{p^{2^{1/2}}}(f_s)/q_\infty$  on the  $45^\circ$  rounded edge are shown to have maximum at Position G ( $x = -1.1$  in.) as shown by the profile in Figure 11. At the downstream Position H ( $x = -0.4$  in.) the periodic contributions at  $f = f_s$  are missing; this position is nearly coincident with the stagnation point  $x = -0.6$  in. Further upstream, the pressures diminish monotonically just as observed, that the periodic pressures on the blunt edge and the tonal pressures at  $\omega y_f/U_s = 1$  remain in phase.

Space-time cross-correlation between the unfiltered trailing-edge pressure at Position G and the wake-velocity fluctuations filtered in 1/10-octave bands at  $f = f_s$ , shown in Figures 12 and 13 disclose a connection between the vortex structure and surface pressure similar to that of the blunt edge. For  $U_\infty = 50$  ft/s, correlations between the pressure fluctuations at Position G and the wake velocities along

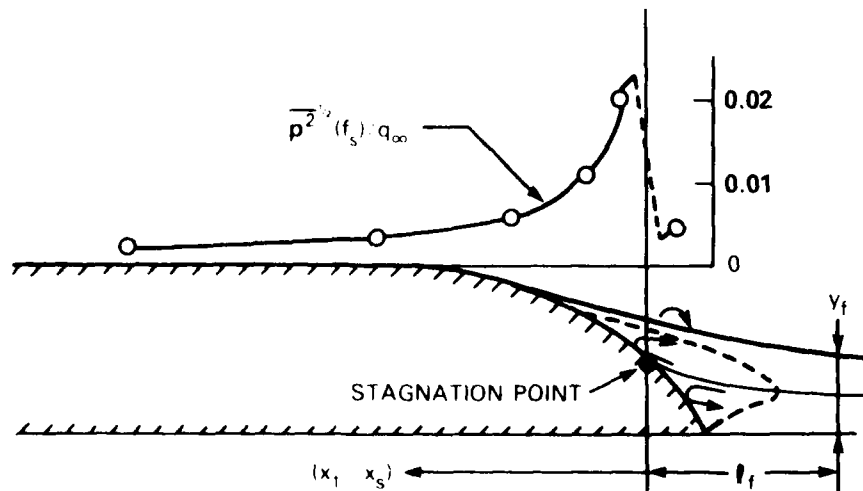


Figure 11 - Chordwise Profiles of Fluctuating Pressure at  $f = f_s$  with  $45^\circ$  Rounded Trailing Edge at  $U_\infty = 100$  ft/s

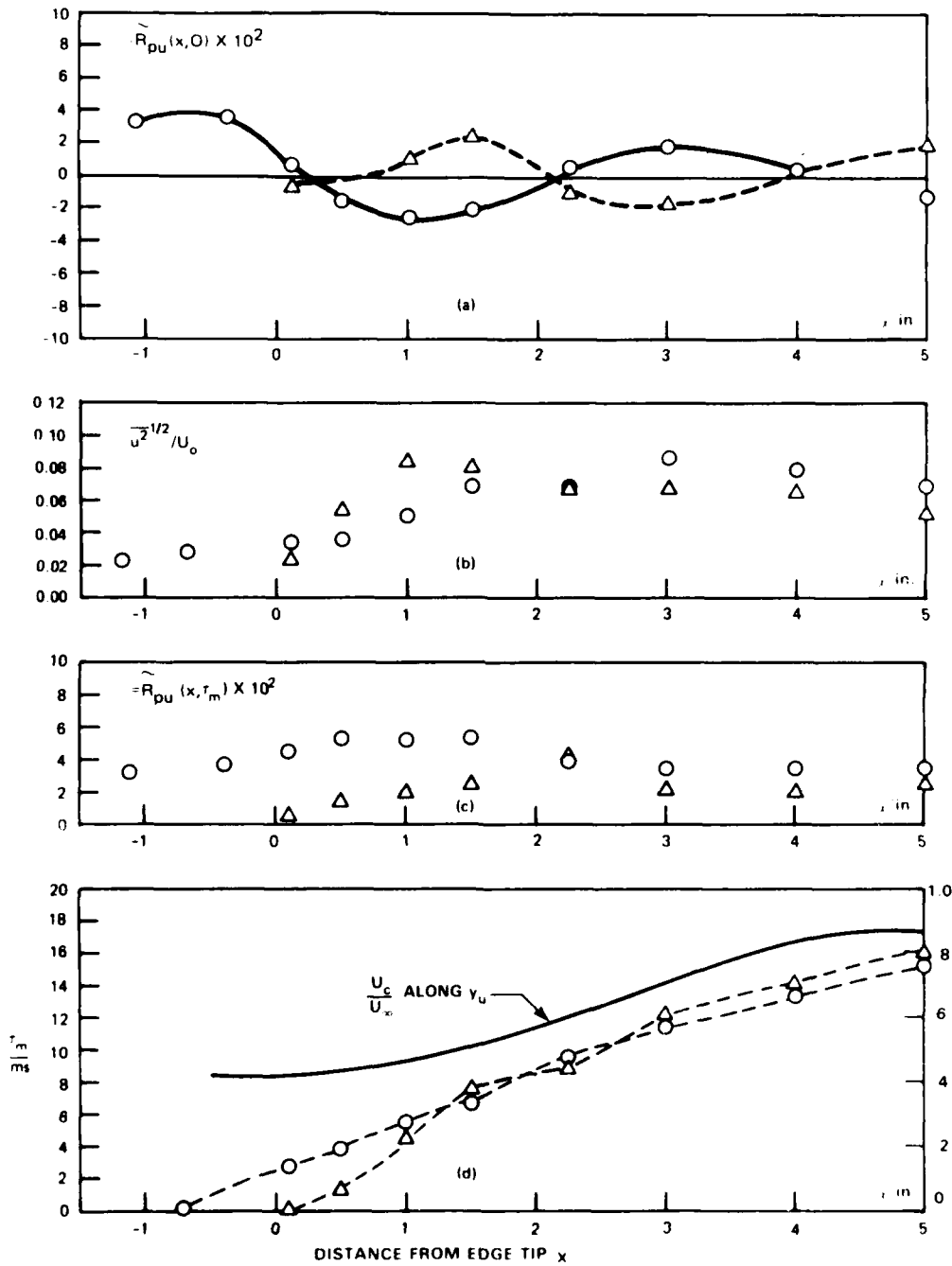


Figure 12 - Pressure-Velocity Correlations in the Wake Behind the 45° Rounded Beveled Edge at  $U_w = 50$  ft/s;  $x$  Measured from the Lip. Points Marked  $\circ$  along  $y = y_u$ ,  $\Delta$  along  $y = y_r$ . Velocity filtered in  $y_r$ -octave band at frequency  $f_s$

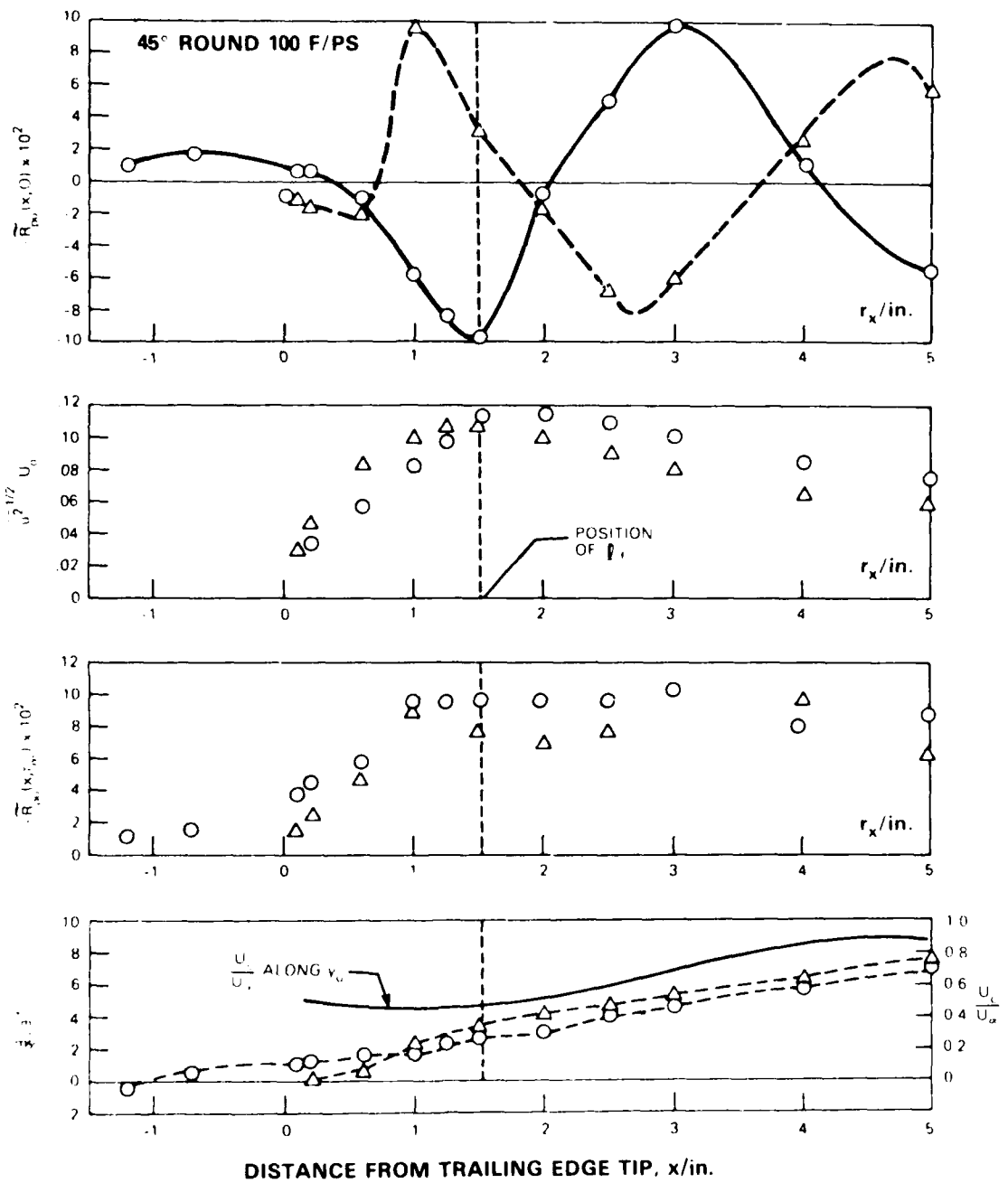


Figure 13 - Pressure-Velocity Correlations Behind the 45° Rounded Beveled Edge at  $U_r = 100$  ft/s; Distances  $r_x$  are Measured from the Tip of the Edge. Points Marked O Along  $y = y_u$ ,  $\Delta$  Along  $y = y_v$ . Velocity Filtered in 1/100-Octave Band at Frequency

both  $y = y_u$  and  $y = y_l$  are shown in Figure 12. Normalized as before (Equation (6)), the spatial correlation along the locus  $(x, y_u)$  shows a minimum of  $\tilde{R}_{pu}(0, x, y_u) = -0.04$  over the edge, and this value is never exceeded in the wake for  $x > 0$ , showing that the pressure at Position G is dominated by local separation. The correlations also indicate that the shear layers along  $y_u$  and  $y_l$  interact to form a coherent wake of paired vorticity concentrations; however, the level of coherence with the pressure at Position G decreases as  $x$  increases. The spatial correlation indicates that the formation of vortices from the upper and lower shear layer, although facilitated by mutual interaction of the layers, does not involve a growing entrainment of one layer by the other. The maxima in velocity fluctuations shown in the figure suggest that the upper layer forms a vortex first near  $x = 1$ , while the lower layer forms a vortex near  $x = 1.5$  in. which is approximately one-eighth wavelength further downstream. Continuing downstream, the mutual interaction brings the vortices into a more coherent alignment, but the intensity of the vortex street decays. These local maxima are similar for both low and high speeds, as seen by comparing Figures 12 and 13, but the growth, streamwise coherence and tonal quality of the disturbances at  $U_s = 100$  ft/s, shown in Figures 13a and 13b, compared to that at 50 ft/s, show how dependent the development of the regular vortex structure is for edges such as this. Of course, tonal pressures are not generated unless a periodic disturbance is developed downstream of the edge.

The convection velocities determined with  $t_m$ , as above, show similar behavior to those in the wake of the blunt edge. Here, the streamwise velocity disturbance is approximately  $180^\circ$  out of phase with the fluctuating pressure at Position G, and its phase slowly varies as the eddy moves downstream. Along the lower layer  $y = y_l$ , an opposite behavior appears; the disturbance convection velocity decreases slightly, i.e.,  $\Delta X/\Delta t_m$  decreases. This contrasting behavior could be caused by an uncertainty in determining the peak in the space-time correlation and would be discounted altogether, except that Hanson (1970) noted a similar observation in the wake behind a notched, lifting airfoil in observing "convection velocities" on the order of  $1.7 U_s$ . The current measurement indicates that the upper disturbance speeds up briefly, while the lower disturbance is convected at a lower speed. As an extension of our modeling of blunt-edged vortex streets, the formation length will be defined as the distance from the trailing-edge stagnation point on the foil to the value of  $x$  corresponding to the maximum in the filtered velocity fluctuation in the wake. This distance is approximately  $\ell_f = 2.3$  in. and it nearly corresponds to the location of

the minimum shear layer spacing  $y_0 = y_\lambda$  (see Figure 8). In the more distant wake,  $x > 2$  in., the two convection velocities become equal and approach 0.8 to 0.9 of the free-stream velocity.

#### 3.4 SPANWISE STATISTICS OF THE TONAL SURFACE PRESSURES

The preceding discussion has shown that the wake generates a pressure field with deterministic behavior along the chord. Along the span, these pressures are stochastic, a behavior which is quite analogous to the unsteady lift fluctuations induced on circular cylinders by vortex street wakes. Span-wise correlations for the blunt and the 45° rounded edges were determined at chord points for which the fluctuations were maximum; i.e.,  $x = -0.3$  in. on the blunt edge, Position G on the 45° rounded edge. These correlations, defined as

$$R_{pp}(r_z, \tau) = \frac{\overline{[p(z, t) p(z+r_z, t+\tau)]}}{\overline{[p^2(z, t) p^2(t, z+r_z)]}^{1/2}} \quad (8)$$

where  $r_z$  is spanwise separation, are shown in Figure 14 as a function of  $r_z/y_f$ . As is often typical in such measurements, the time delay for maximum correlation,  $\tau_m$ , is not always zero but slowly increases with  $r_z$ . This is because the vortices shed behind rigid bodies may take a preferred, yet small, yaw angle to the edge. In the case of the blunt trailing edge (this angle was approximately 17°) it is probably not natural to the edge flow, but rather an artifact of some asymmetry in the strut fixture. Therefore since the correlation values at  $\tau = \tau_m$  represent the maximum spanwise correlation, only those values are shown.

In the case of the 45° rounded edge, correlation functions obtained at a velocity of  $U_\infty = 200$  ft/s anomalously approached unity through the entire range of  $r_z$ . This behavior has now been regarded as due largely to flow induced vibration. As shown in work subsequent to Blake (1975a), see Blake et al. (1977), displacements of only 0.005  $y_f$  are necessary to increase the spanwise correlation of the vortex street wakes of airfoils.

Aside from the question of the effects of vibration, Figure 15 shows that the length scale of the spanwise correlation of natural vortex shedding is apparently set by  $y_f$ . In fact, for both trailing edges a correlation length defined as

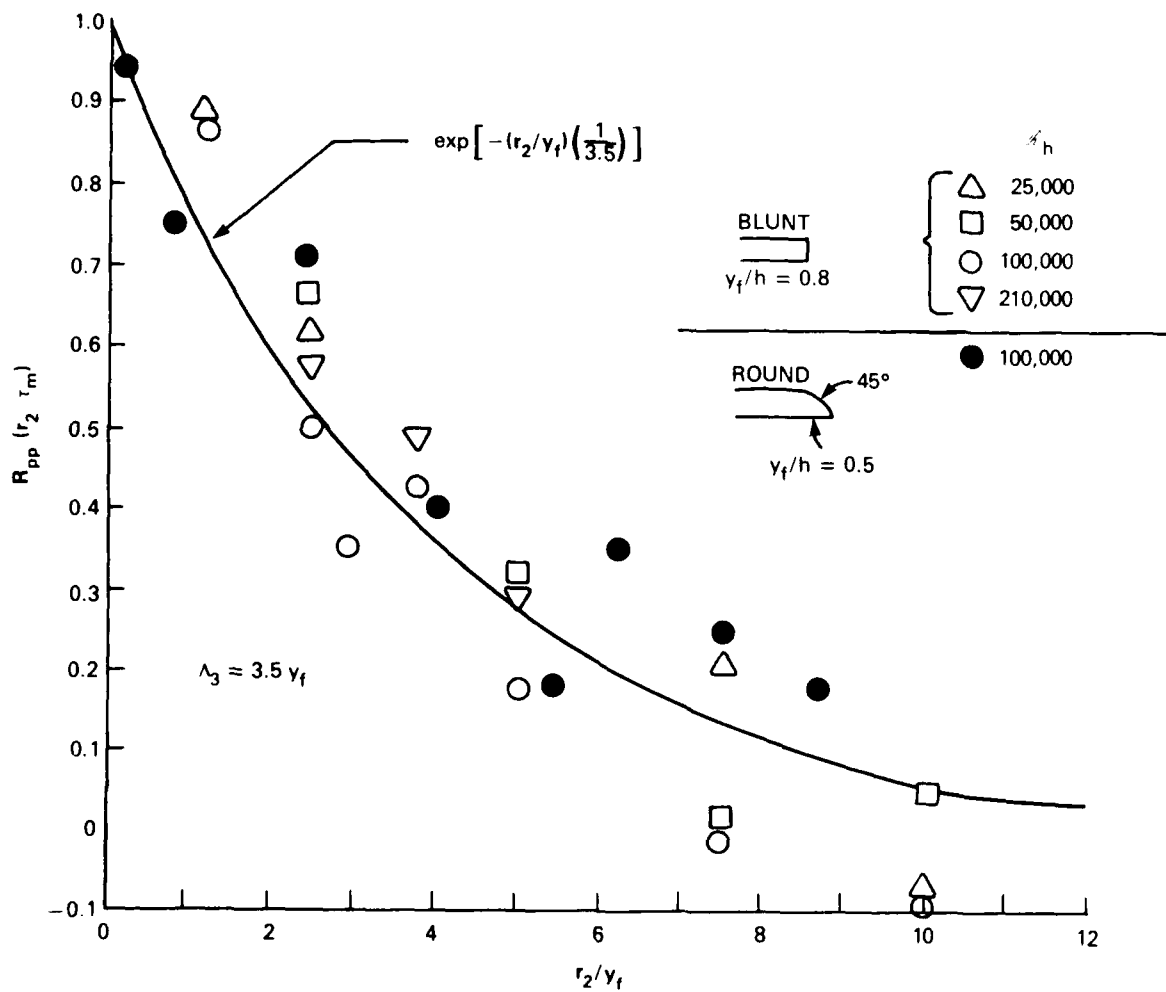


Figure 14 - Spanwise Correlations of Vortex-Shedding Pressures on the Trailing Edges of Flat Airfoils

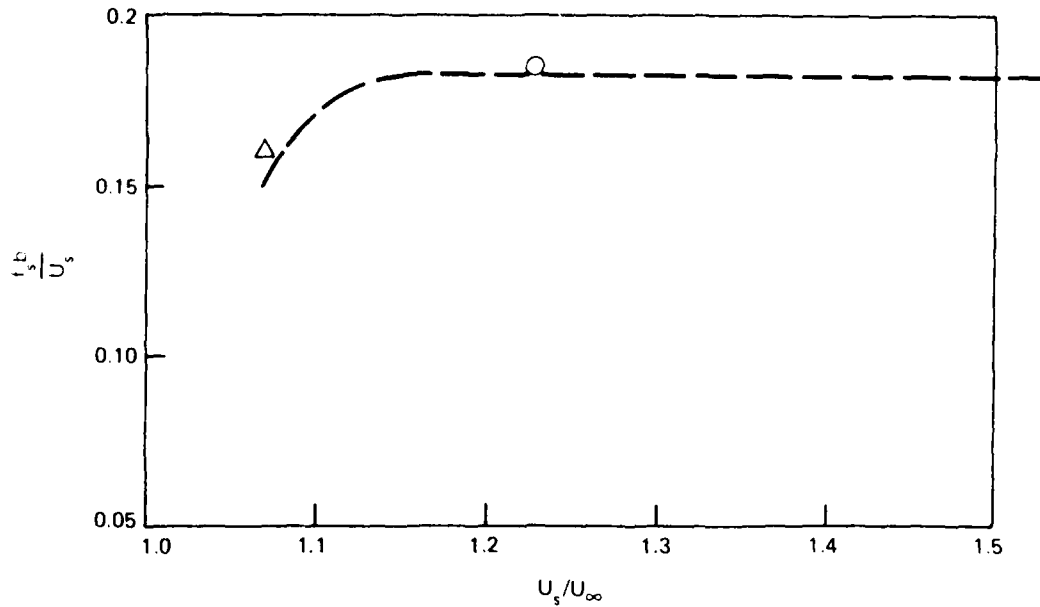


Figure 15 - Bearman's (1967) Universal Strouhal Number Versus  $U_s/U_\infty$  for the Blunt and  $45^\circ$  Round Trailing Edges.  $\Delta$   $45^\circ$  Round, 100 ft/s,  $O$  Blunt, 100 ft/s; ---- Representative of Data for a Wide Range of Bluff Body Shapes

$$\Lambda_3 = \int_0^\infty |R_{pp}(r_z, \tau_m)| dr_z \quad (9)$$

can be easily deduced from the figure by fitting a correlation function of the form

$$R_{pp}(r_z, 0) = \exp[-|r_z|/\Lambda_3] \quad (10)$$

to the measurements as shown. It appears that  $\Lambda_3 = 3.5 y_f$  is a representative value for both trailing edges; similarly defined correlation lengths have been found for vortex streets behind rigid cylinders to be as low as 1.5 and as large as 5 cylinder diameters. This value gusted above holds over a considerable range of velocities for the blunt trailing edge; it is unknown how it behaves on the  $45^\circ$  rounded edge.

#### 4. GENERALITIES REGARDING THE FREQUENCIES AND AMPLITUDES OF TONAL TRAILING-EDGE PRESSURES

##### 4.1 VORTEX-SHEDDING FREQUENCY

Treatment of the frequency spectral qualities of the surface pressures in this paper has adopted the wake thickness dimension  $y_f$  on which to base the nondimensionalized frequency  $\omega y_f / U_s$ . Tones, or near-tones have been observed at  $\omega y_f / U_s \approx 1$  on the two edges discussed. Before proceeding with this point we wish to review briefly some alternative methods of definition.

The previously-used definition of Strouhal number based on the base thickness, Equation (4), does not yield a suitable comparison of frequencies for the two dissimilar trailing edges discussed so far in this report. For the rounded trailing edge,  $N_{st}$  is of the order 0.45 to 0.5 compared to the more generally accepted values of 0.23 to 0.29 and observed for the blunt edge. Therefore, the use of the base thickness is only appropriate when the surface is blunted symmetrically with distinct corners. Gongwer (1952) has previously shown that some adjustment to the formula for blunt edges to the use of  $h$  is necessary when the boundary layers at the edge are thick. Aerodynamic fairing of the edges produces a thinner wake with higher predominant frequencies. A nondimensionalization based on the momentum thickness in the near wake was also found (Blake 1975) not to agree with the behavior shown by Hanson (1970). According to Hanson, a definition based on the momentum thickness seemed to account for the frequencies generated by trailing edges with aerodynamic shaping, notching, and splitter plates. The applicable functional form is (also see Roshko 1954, for application to circular cylinders)

$$S_{\theta} N_{Re} = 0.0725 \left[ N_{Re} - 1038 \right] \quad (11)$$

where

$$S_{\theta} = f_s \theta_f / U_s \quad (12)$$

and  $\theta_f$  is the momentum thickness of the wake at the end of the formation zone ( $X = x_f$ ) and  $U_s$  is given by Equation (7). While it satisfactorily predicts  $f_s$  for the 45° rounded edge, Equation (11) over predicts the vortex shedding frequency for the blunt trailing edge, by nearly a factor of 2.

An alternative definition of Strouhal number that does seem to agree with the presently measured tone frequencies for both edge geometries is Bearman's (1967). Bearman has suggested an alternative scaling using far-wake variables. This scaling is based on the Kronauer (1967) stability criterion which states that the stable cross-wake spacing  $b$  of the vortices in a wake with a periodic vortex street is of such a nature that a minimum drag is exerted on the body. Bearman's universal Strouhal number,  $S_B = f_s b_1 / U_s$ , was determined from the far-wake data of both the blunt and  $45^\circ$  rounded edges using his calculation procedure. The values are shown in Figure 15 as a function of shedding velocity  $U_s / U_\infty$ ; agreement with the trend of earlier data continues to support the applicability of the Bearman definition.

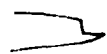
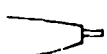
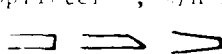
The nondimensionalization of  $y_f$  used in Figures 6, 9, and 10 is based on the hypothesis that the frequency of disturbances in the near wake passing a fixed point relative to the trailing edge will be determined by the local velocity there (taken as  $U_s$ ) and the cross-wake separation of the shear layers which constitute the near-wake. In the case of shear layers analytically modeled as a pair of parallel vortex sheets, Abernathy and Kronauer (1962) computed vorticity concentrations that resulted from instabilities of the layers. The streamwise spacing of these concentrations was suggestive nearly proportional to the separation of the shear layers. In fact, it seems that for the blunt edge, which sheds a pair of trailing edge vortices from the shear layers, the use of  $y_f$  in this context is appropriate.

In the case of the rounded trailing edge, the streamwise spacing of the vortices in the wake are not nearly as large as in the case of the blunt edge. A detailed stability analysis of the preferred hydrodynamic mode for the rounded trailing edge profiles of the type shown in Figure 8 would seem to be more appropriate than the type of analytical model used in the present manner. Since we are interested in only preferred wake tones, a detailed description of growth rates and disturbance amplitudes from a stability analysis can be useful. Gaster (1964) has shown that spatial and temporal stability analyses are not generally equivalent, that is, the growth rates as the growth rates of disturbances diminish. Specifically, if the complex wave number in the temporal stability analyses is  $C_r + iC_i$ , and the complex wave number in the spatial stability analysis is  $\alpha_r + i\alpha_i$ ; then, the two analyses will predict preferred frequencies when  $C_i/C_r$  and  $\alpha_i/\alpha_r$  are much less than unity. The present data indicate that parallel flows with mean velocity profiles of the type shown in

Figure 8 for the near wake of the trailing edge were all unstable. Furthermore, letting  $y_f$  be the cross-wake spacing between the inflection points of the profiles, it was then found that the preferred frequencies were bounded by  $0.85 < \omega y_f / U_0 < 1$ . Note that a precise computation of wake dynamics must account for change in the mean velocity profile over downstream distances which are small compared with a disturbance wavelength (see Crighton and Gaster, 1976).

The approximate generality of this definition of Strouhal number is also supported by Table 1 which draws on additional measurements of vortex shedding frequency from two other sources. Here,  $y_f$  and the characteristic velocity  $U_s$  as

TABLE 1 - STROUHAL NUMBERS BASED ON CROSS-WAKE LENGTH SCALE

Edge Shape	$\omega y_f / U_s$	Position of $y_f$
Blunt <sup>1</sup> 	0.97	$1.0 y_f$
Blunt with splitter plate*, $l/h=1$ 	0.92	$1.0 y_f$
Notched lifting** ( $N_{RE_0} = 6900$ ) 	0.78	$0.3 y_f$
Notched lifting** ( $N_{RE_0} = 4800$ ) 	0.87	$0.5 y_f$
Splitter**, $l/h=1$ ( $N_{RE_0} = 5930$ ) 	0.91	$0.4 y_f$
Splitter**, $l/h=1$ ( $N_{RE_0} = 9800$ ) 	0.94	$0.5 y_f$
Blunt: 45° round blunted, tapered edges with blunt base	0.85-1.0	$0.65 y_f$ , 45° round $0.8 y_f$ - $1.0 y_f$ , others

<sup>1</sup>From Bearman (1965)

\*\*From Hanson (1970)

<sup>†</sup>From W. Blake, et al. (1977)

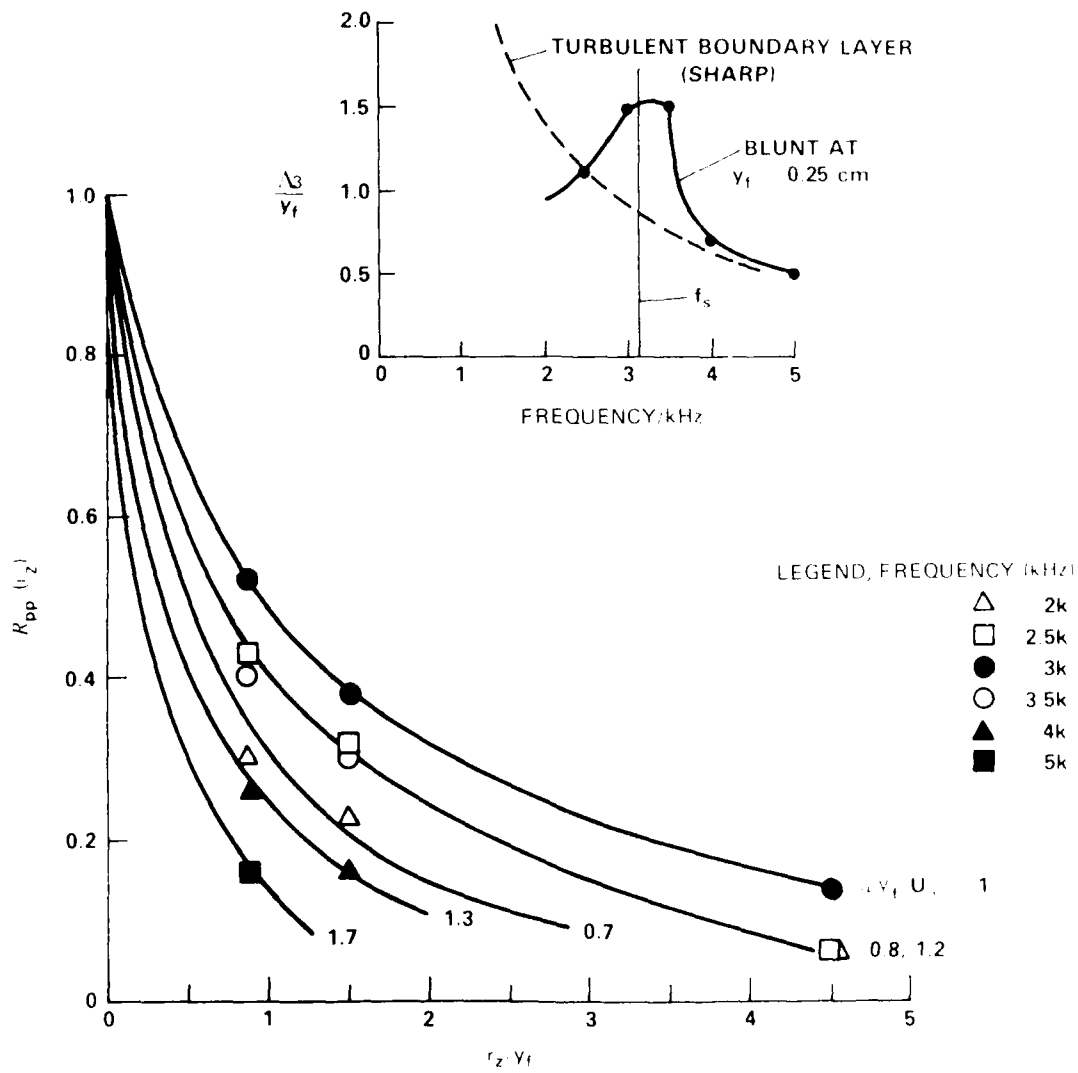


Figure 21 - Narrowband Cross-Spectral Densities and Spanwise Integral Scales of Surface Pressures on Blunt-Edged NACA 0012 Airfoil. Data Courtesy of Dr. T. Brooks, NASA, Langley.

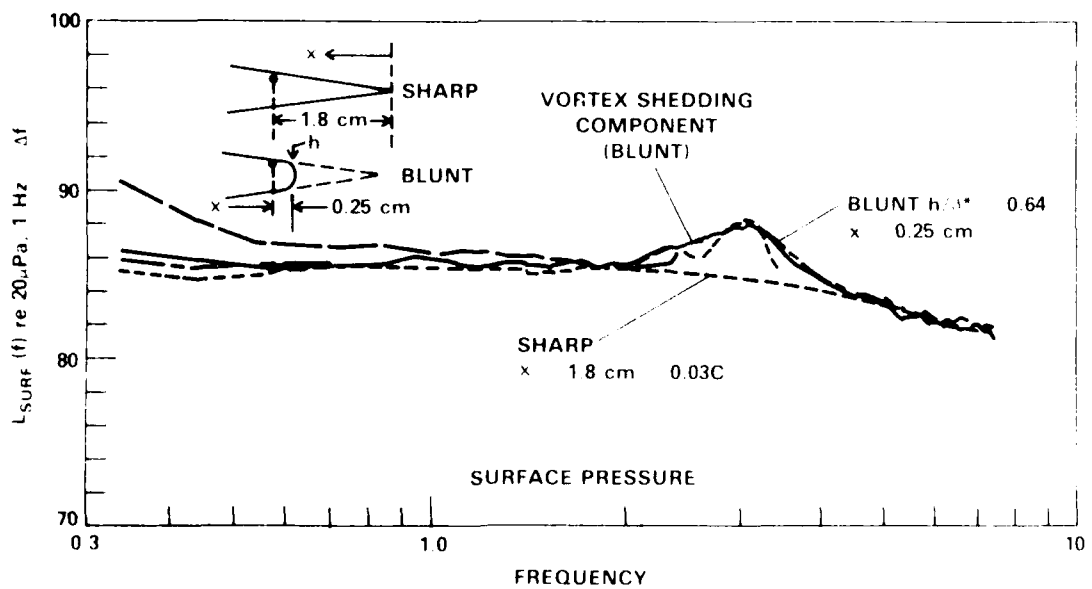
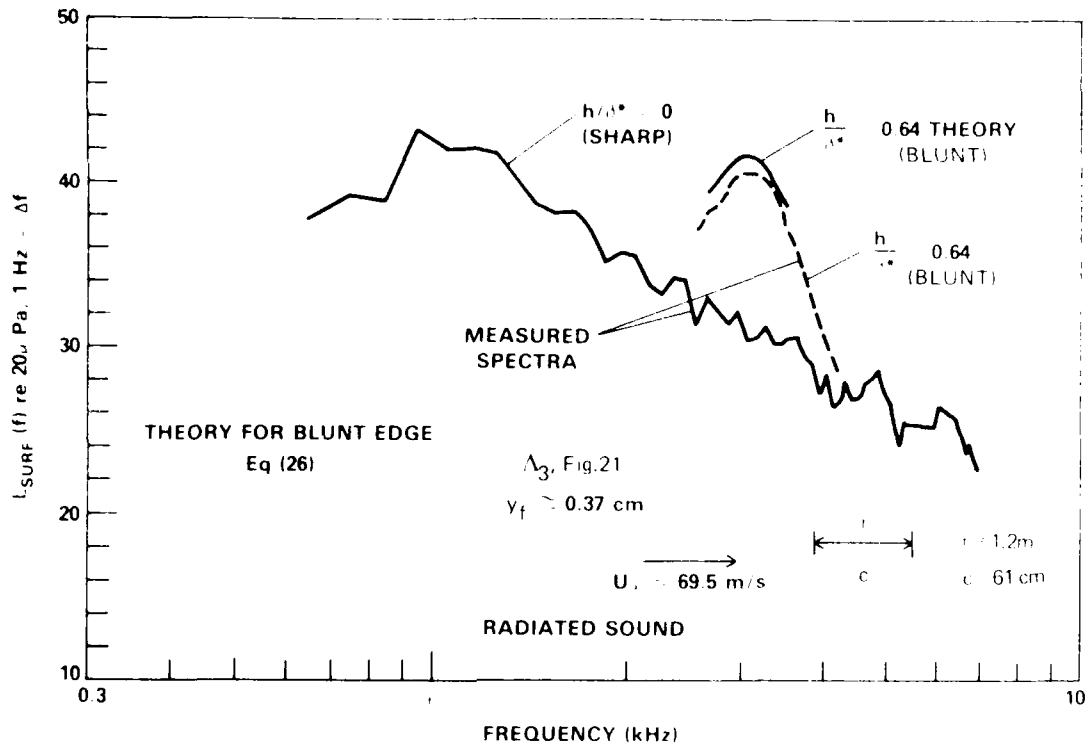


Figure 20 - Radiated Sound and Surface Pressure for Sharp and Blunt Edges of a NACA 0012 Airfoil with Leading Edge Tripping,  $U_\infty = 69.5$  m/s (Courtesy T. Brooks)

Thus the appropriate ratio of spectra is

$$\frac{\overline{p}_{\text{rad}}(\vec{x}, \omega)}{\overline{p}_s(x, \omega)} = \frac{1}{2\pi^2} \frac{U_s}{C_o} \frac{\ell_c}{y_f} \frac{|x - x_s|L}{r^2} |\sin \phi| \sin^2 \theta/2 \quad (26)$$

where  $C_o$  is the speed of sound, and where  $(x - x_s)$  must be selected close enough to the edge so that either Equation (20a) or Equation (20d) holds.

Experimental verification of Equation (26) can be determined from the results of Brooks and Hodgeson (1981). In their measurement program, far-field sound and trailing-edge surface pressures were measured for a NACA 0012 airfoil with a blunt trailing edge at  $0^\circ$  angle of attack. The Reynolds number based on edge thickness was quite low ( $hU_\infty/\nu = 1.1 \times 10^4$ ) and the ratio of twice the boundary-layer momentum-thickness-to-base-thickness was nearly 2. A tone was not generated, rather the pressure spectrum at the trailing edge was a broad bump, much like that shown in Figure 10 for  $U_s = 50\text{ft/s}$ . The surface pressure was measured at  $|x - x_s|/U_s = x/y_f = 0.69$ . Figure 20 shows a comparison between the measured sound spectrum and the theoretical estimate using Equation (26), with the surface pressure measured near the trailing edge. The surface pressures on the edge are also given. The spanwise correlation lengths for various frequencies were deduced from data supplied by Brooks (private communication) and evaluated by using a best fit of Equation (12). These are shown in Figure 21. A value of  $\lambda_3/y_f = 1.5$  is indicated at the vortex shedding frequency, which value is more in line with measurements to be discussed in Part 2 of this report, and this is considerably less than  $\lambda_3 = 3.5y_f$  discussed in Section 3. The reduced spanwise correlation length is undoubtedly the result of both lower Reynolds number and greater local turbulence since  $2\delta/h = 2$ .

#### 4.4 APPARENT DEPENDENCE ON REYNOLDS NUMBER

The preceding sections have shown the relationship between wake vorticity and surface pressure, and between surface and radiated sound pressures for specified operating conditions. It remains to offer some indications of the dependence of vortex strength on Reynolds number. To do this, we note that Equations (20a) and (20d) present unique relationships between mean-square surface pressure at a location  $x$  and the mean-square vortex strength at a point near the trailing edge. One can use this interchangeability between  $\overline{p_s^2}(x)$  and  $\overline{\Gamma_o^2}$  to deduce the behaviors of wake strengths

a random function of  $\xi_3$ . Evaluating the integral over  $\xi_1$  in Equation (23), we find

$$P_a(\vec{X}, \omega) = \frac{e^{ik_o r}}{4\pi R} \frac{1}{\sqrt{2}} \sqrt{\frac{k_o}{k_w}} \sin^{1/2} \phi \sin(\theta/2) \rho_o U_c \int_{-L/2}^{L/2} \gamma_o(k_w, \xi_3, \cdot) d\xi_3 \quad (24)$$

$P_a(\vec{X}, \omega)$ , is a random variable because of the stochastic nature of  $\gamma_o(k_w, \xi_3, \cdot)$  as a function of  $\xi_3$ . The spectral density of the radiated sound pressure  $\Phi_{\text{Prad}}(\vec{X}, \cdot)$  is then related to the ensemble average

$$\Phi_{\text{Prad}}(\vec{X}, \omega) \delta(\omega - \omega') = \langle P_a(\vec{X}, \omega') P_a(\vec{X}, \omega) \rangle$$

so that the mean square sound pressure in the far field is

$$\overline{P_{\text{rad}}^2}(\vec{X}) = \frac{1}{32\pi^2} \left( \frac{k_o}{k_w} \right) |\sin \phi| \sin^2(\theta/2) \rho_o^2 \overline{\gamma_o^2} \frac{c^L U_c^2}{r^2} \quad (25)$$

where  $\ell_c = 2\Lambda_3$  is the spanwise correlation length of the vorticity (Equation (9)) and by Equation (14)

$$\overline{\gamma_o^2} = \Gamma_o^2 k_w^2 / 4$$

is the mean-square vorticity at a point in the near-wake.

Now, Equations (20a) and (25) are fully consistent, the former giving the surface pressure in the immediate vicinity of the trailing edge, the latter giving the far field radiated sound pressure. Although the analysis of the radiated sound has assumed a negligible formation length, the ratio of Equations (25) to (20a) will give a relationship between the radiated sound and surface pressures near the edge that is applicable, even if  $k_w \delta_f$  is not negligible. This is because Equation (20d), which applies to the case of  $k_w \delta_f > 1$ , gives a pressure amplitude in the near field of the edge that is less than that of Equation (20a), but it has the identical dependence on  $x$ . Accordingly, the acoustic dipole strength of the trailing edge is simply reduced by  $\pi y_f / 2 \delta_f$  when the formation zone is extended sufficiently far downstream, while its spatial character remains fundamentally unchanged.

### 4.3 RADIATED SOUND FROM VORTEX SHEDDING

The sound pressure radiated to the farfield of a thin rigid edge that generates a vortex street wake, as described in the previous section, can now be determined. At low Mach number, the reduced wave equation in the Powell (1959) and Howe (1978) form for the edge-vortex geometry considered above is

$$\nabla^2 P_a(\vec{y}, \omega) + k_0^2 P_a(\vec{y}, \omega) = \frac{h}{\partial y_2} (\rho_0 \omega_3 U_c) \quad (21)$$

where  $P_a(\vec{y}, \omega)$  is a Fourier coefficient of the acoustic pressure and  $k_0$  is the acoustic wave number. Since the surface pressure is maximum at the trailing edge, we must use a theory which admits this maximum. Accordingly, the theory of Ffowce Williams and Hall (1970) will be used. Thus, the reduced sound pressure at  $\vec{X}$  is

$$P_a(\vec{X}, \omega) = -\iiint \rho_0 \omega_3 U_c \frac{\partial G(\vec{X}, \vec{\xi}, \omega)}{\partial \xi_2} dV(\vec{\xi}) \quad (22)$$

where the integral extends over the entire fluid region and  $G(\vec{X}, \vec{\xi}, \omega)$  is the half-plane Green function. When the region of vorticity is concentrated within an acoustic wavelength close to the edge and  $k_0 |\vec{X}|$  is much greater than unity, then the acoustic part of the Green function takes a particularly simple form. Then Equation (22) becomes

$$P_a(\vec{X}, \omega) = \frac{e^{ik_0 r}}{4\pi r} \frac{e^{-i\pi/4}}{2\sqrt{\pi}} \int_{-L/2}^{L/2} (2k_0)^{1/2} \sin^{1/2} \theta \sin^{-1/2} \theta \left( \gamma_0(k_w, \xi_3, \omega) U_c \right) \cdot \int_0^\pi \frac{1}{\sqrt{r_1}} e^{ik_w \xi_1} d\xi_1 d\xi_3 \quad (23)$$

where the acoustic field coordinates are  $X_1 = r \sin \theta \cos \phi$ ,  $X_2 = r \sin \theta \sin \phi$ ,  $X_3 = r \cos \theta$ ;  $\theta$  is measured from the wake in the 1,2 plane and the edge coincides with the  $\vec{X} = (0, 0, X_3)$  coordinate axis (see Figure 16). In deriving Equation (23) it has been assumed that  $k_w \xi_f \approx 0$ , and that, even though the plane of vorticity is parallel to the edge, it has a spanwise dependence that is weak enough to consider it constant over distances  $\Delta \xi_3 \approx 2\pi/k_w$ , but possibly variable over distances  $\Delta \xi_3 \sim L$ , where  $L$  is the total length of the span. Therefore,  $\gamma_0(k_w, \xi_3, \omega)$  is regarded as

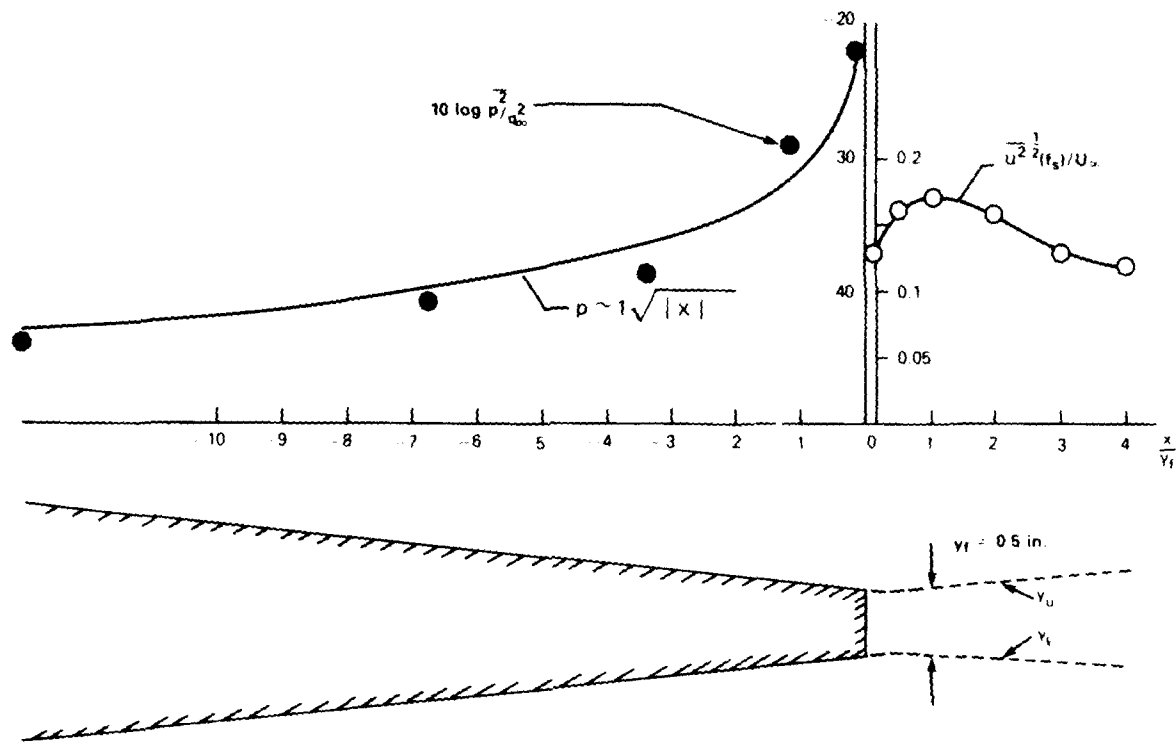


Figure 19 - Profiles of Surface Pressure and Velocity Fluctuations at the Blunt Trailing Edge of a Tapered Airfoil. Measurements Were Made at  $U_\infty = 100 \text{ ft/s}$

may be of order  $(\nu/\omega)^{1/2}$  and a conservative limiting condition could be

$$x/y_f > 0 \left( \frac{\nu}{y_f U_\infty} \frac{U_\infty}{y_f \omega} \right)^{-1/2}$$

$$> 0 (R/y_f)^{-1/2}$$

If an unsteady Kutta condition had been applied, then the measured pressures would not have been predicted. Instead, in the limit of  $|x| > 0$  the pressure would decrease to zero and the prediction of peak pressures at the edge would not have been possible.

for  $k_w \ell_f \gg 1$ , a smooth transition occurs for the asymptotic forms, Expressions (20b) and (20d). In all the expressions for the pressure, it can be seen that both the formation length and the wake thickness enter as pertinent length scales, depending on the domain of dependence. When  $k_w \ell_f$  is much less than unity, Expressions (20a) and (20c) show that when  $k_w \ell_f$  decreases toward zero, the pressure increases all values of  $k_w |x|$ . To compare the measured pressures with Expression (20), the vorticity amplitude  $\gamma_0$  was related to the measured velocity maxima in the wake,  $\overline{u^2}$ , and  $y_f$  using Equations (14) and (15). Figure 17 gives the surface pressures of all the trailing edges under consideration, and it shows the general significance of Expression (20). Very close to the edge, it is seen that the appropriate length parameter is  $|x - x_s|/y_f$  and the pressure depends also on the relative values of  $\ell_f$  and  $y_f$  as seen in Expressions (20a) and (20d).

The quantity  $x_s$  represents the approximate distance from the stagnation point on the trailing edge. This distance is illustrated in Figure 11 for a rounded edge together with the associated variation of the surface pressure tone. For the blunt, squared-off edges,  $x_s = 0$ .

Figure 19 illustrates the rise of the vortex-induced pressure measured on a tapered airfoil with a blunt trailing edge, together with the behavior  $p \sim 1/\sqrt{|x|}$ . The data shown in this figure have been included in Figure 18 and are denoted as Edge II. Also included is a profile of the unsteady fluctuations generated in the wake by the shed vorticity. The velocity profile allows a clear definition of both  $y_f$  and  $\overline{u^2}$  for use in Equation (15a) in determining the circulation factor  $\Gamma_0$ .

In a restricted parameter range, i.e., very near the edge and for  $k_w \ell_f > 1$ , Equation (20d) shows that  $\ell_f$  rather than  $y_f$  is the only dominant length scale, as held in a previous discussion by Blake (1976). It is seen that the available experimental data applies to  $k_w \ell_f > 1$ ; accordingly, Equations (20b) and (20d) are expected to agree with measurements best. For parameters of the available measurements, it is not possible to apply Equation (20b) because when the conditions of validity for  $x$  are reached,  $x$  also becomes comparable to the transverse correlation length  $2\Delta_3$ , so that the analysis in two dimensions no longer applies. At greater distances than  $2\Delta_3$ , the surface pressure will fall off more sharply than  $1/\sqrt{|x|}$ .

Very close to the edges, or to the rear stagnation point, i.e., as  $|x - x_s| \rightarrow 0$ , the  $1/\sqrt{|x|}$  behavior is expected at least until  $x$  is on the order of an approximately defined viscous length. In the case of a blunt edge with sharp corners, this length

in which the only important length scales are  $x$  and  $y_f$ ;

$$\frac{\overline{p^2}(x)}{\rho_o^2 U_s^2 (\Gamma_o/2\pi y_f)^2} \approx \frac{1}{4} \left( \frac{U_c}{U_s} \right)^2 \frac{y_f y_f}{|x| \ell_f} \text{ for } k_w |x| \gg k_w \ell_f > 1 \quad (20b)$$

and finally

$$\frac{\overline{p^2}}{\rho_o^2 U_s^2 (\Gamma_o/2\pi y_f)^2} \approx \frac{\pi}{4} \left( \frac{U_c}{U_s} \right) \frac{y_f}{|x|} \text{ for } k_w |x| \gg 1 \gg k_w \ell_f \quad (20c)$$

to complete the set of limits that apply whenever  $|x| \gg \ell_f$ . Expression 20a applies closer to the edge than a wake wavelength and it requires a very short formation zone. Expression (20c) applies at distances which are far from the edge, but still require a short formation zone. Expression (20b), on the other hand, applies at distances far from the edge when the formation zone is large.

In the alternative limit of  $\ell_f \gg |x|$  the  $\ln$  term in Equation (17) reduces to  $2j \sqrt{|x|/\xi_1}$  for the entire region of integration. The resulting integral is  $(1 - \text{Erf}(\sqrt{-ik_w \ell_f}))$ . Accordingly, when  $k_w \ell_f \gg 1$ , the expression for the pressure becomes

$$\frac{\overline{p^2}(x)}{\rho_o^2 U_s^2 (\Gamma_o/2\pi y_f)^2} \approx \frac{1}{4} \left( \frac{U_c}{U_s} \right)^2 \left( \frac{y_f}{\ell_f} \right) \left( \frac{y_f}{|x|} \right) \text{ for } k_w \ell_f \gg 1 > k_w |x| \quad (20d)$$

However, when  $k_w \ell_f \ll 1$ , the alternate limit for the error function leads to

$$\frac{\overline{p^2}}{\rho_o^2 U_s^2 (\Gamma_o/2\pi y_f)^2} \approx \frac{\pi}{4} \left( \frac{\ell_f}{y_f} \right) \frac{y_f}{|x|} \text{ for } 1 \gg k_w \ell_f \gg k_w |x| \quad (20e)$$

In all the above expressions, the  $k_w \ell_f$  has been rewritten as  $(U_s/U_c) (\ell_f/y_f)$ . Both Expressions (20a) and (20c) give similar values of  $\overline{p^2}$ , and, therefore, a smooth transition of parametric behavior in the overlap region of  $k_w \ell_f = k_w |x|$ . Similarly,

in which  $k_w$  regarded as having a small positive imaginary component in the limit  $\xi_1 \rightarrow \infty$ .

The integral simplifies into alternate forms depending on the relative magnitudes of  $x$  and  $\ell_f$ . In the case of  $|x| \gg \ell_f$ , the approximation

$$\ln \frac{\sqrt{|x|} - j\sqrt{\ell_f}}{\sqrt{|x|} + j\sqrt{\ell_f}} \approx -2j \left( \frac{\ell_f}{|x|} \right)^{1/2}, \quad |x|/\ell_f \gg 1$$

holds where  $x = -|x|$  on the surface. The integrals reduce to a pair (Gradshteyn and Ryzhik (1965)) (for  $|x| > \ell_f$ )

$$\begin{aligned} \frac{\sqrt{|x|}}{-ik_w} \int_{\ell_f}^{\infty} \frac{e^{ik_w \xi_1}}{\sqrt{\xi_1}} \frac{d\xi_1}{|x| + \xi_1} &= \frac{\sqrt{|x|}}{-ik_w} \left\{ \int_0^{\infty} \frac{e^{+ik_w \xi_1}}{\sqrt{\xi_1}(\xi_1 + |x|)} d\xi_1 - \right. \\ \left. \frac{1}{|x|} \int_0^{\ell_f} \frac{e^{+ik_w \xi_1}}{\sqrt{\xi_1}} d\xi_1 \right\} &= \frac{\pi}{-ik_w} \left\{ e^{-ik_w |x|} \left( 1 - \operatorname{Erf}(\sqrt{-ik_w |x|}) \right) (-i\pi k_w |x|)^{-1/2} \right. \\ &\left. \cdot \operatorname{Erf}(\sqrt{-ik_w \ell_f}) \right\} \end{aligned}$$

The limiting expressions for the error functions are given by Abramowitz and Stegun (1965) as

$$\begin{aligned} \operatorname{Erf}(\sqrt{-ik|x|}) &\approx 1 - (\pi k|x|)^{-1/2} \exp\left(+i(k|x| + \pi/4)\right) & k|x| > 1 \\ &\approx \sqrt{k|x|} \exp\left(+i(k|x| - \pi/4)\right) & k|x| < 1 \end{aligned} \quad (19)$$

A set of alternate first-order closed-form expressions for the mean-square amplitude of the surface pressure may now be given for various cases which depend on where  $k_w |x|$  and  $k_w \ell_f$  stand with respect to unity:

$$\frac{\rho_0^2 U_s^2 \left( \frac{\Gamma_0}{2\pi y_f} \right)^2}{P^2} \approx \frac{\pi^2}{16} \left( \frac{U_c}{U_s} \right) \frac{y_f}{|x|}, \quad \text{for } 1 > k_w |x| \gg k_w \ell_f, \quad (20a)$$

pressure. The vortex street generates a potential field  $\phi_h(x, y, t)$  which causes a pressure that is given by the unsteady Bernoulli equation,

$$\frac{-p(x, 0^+, t)}{\rho_0} = \frac{\partial \phi_h(x, 0^+, t)}{\partial t} + U_c \frac{\partial \phi_h(x, 0^+, t)}{\partial x} \quad (16)$$

where  $\phi_h(x, 0^+, t)$  is evaluated on the upper surface of the half plane,  $x < 0$ ,  $y = 0^+$ . Pressures on the opposite sides are out of phase, i.e.,  $p(x, 0^+, t) = -p(x, 0^-, t)$ . The potential needed is a real part of the complex value. The vortex-induced pressure magnitudes on all edges diminish approximately as  $1/(x-x_s)^{1/2}$ . Thus

$$\phi_h(x, y_0) = \text{Re}_j[\phi_h(Z_1, Z_0)]$$

where  $Z_1 = x + jy_0$ ,  $Z_0 = \xi_1 + \xi_2$ , and where  $\text{Re}_j$  is the real part of  $\phi_h(Z_1, Z_0)$  with respect to the complex notation  $j$ . This potential at  $x, y_0$  due to localized vorticity at  $x_0, y_0$  near a plane surface is given by Milne-Thompson (1960), mapped into the half-plane of this problem (see Blake (1976)) and integrated using Equation (13). The potential on the upper surface given by this process is

$$\phi_h(x, 0^+, t) = \frac{-j\gamma_0}{2\pi} \int_{\xi_f}^{\infty} \ln \left( \frac{\sqrt{|x|} - j\sqrt{\xi_1}}{\sqrt{|x|} + j\sqrt{\xi_1}} \right) e^{ik_w(\xi_1 - U_c t)} d\xi_1 \quad (17)$$

where Equation (13) has been used to model the continuous wavelike distribution of vorticity which begins at  $\xi_1 = \xi_f$  and continues downstream.

By integrating by parts we find the potential induced by the entire periodic wake as\*

$$\begin{aligned} \phi_h(x, 0^+, t) = & \frac{-\gamma_0}{2\pi} \int_{\xi_f}^{\infty} \frac{e^{+ik_w \xi_1}}{ik_w} \sqrt{\frac{|x|}{\xi_1}} \frac{d\xi_1}{|x| + \xi_1} \\ & + \frac{j\gamma_0}{2\pi} \left[ \frac{e^{+ik_w \xi_f}}{ik_w} \ln \left( \frac{\sqrt{|x|} - j\sqrt{\xi_f}}{\sqrt{|x|} + j\sqrt{\xi_f}} \right) \right] \end{aligned} \quad (18)$$

\*This analysis supersedes that in Blake (1976).

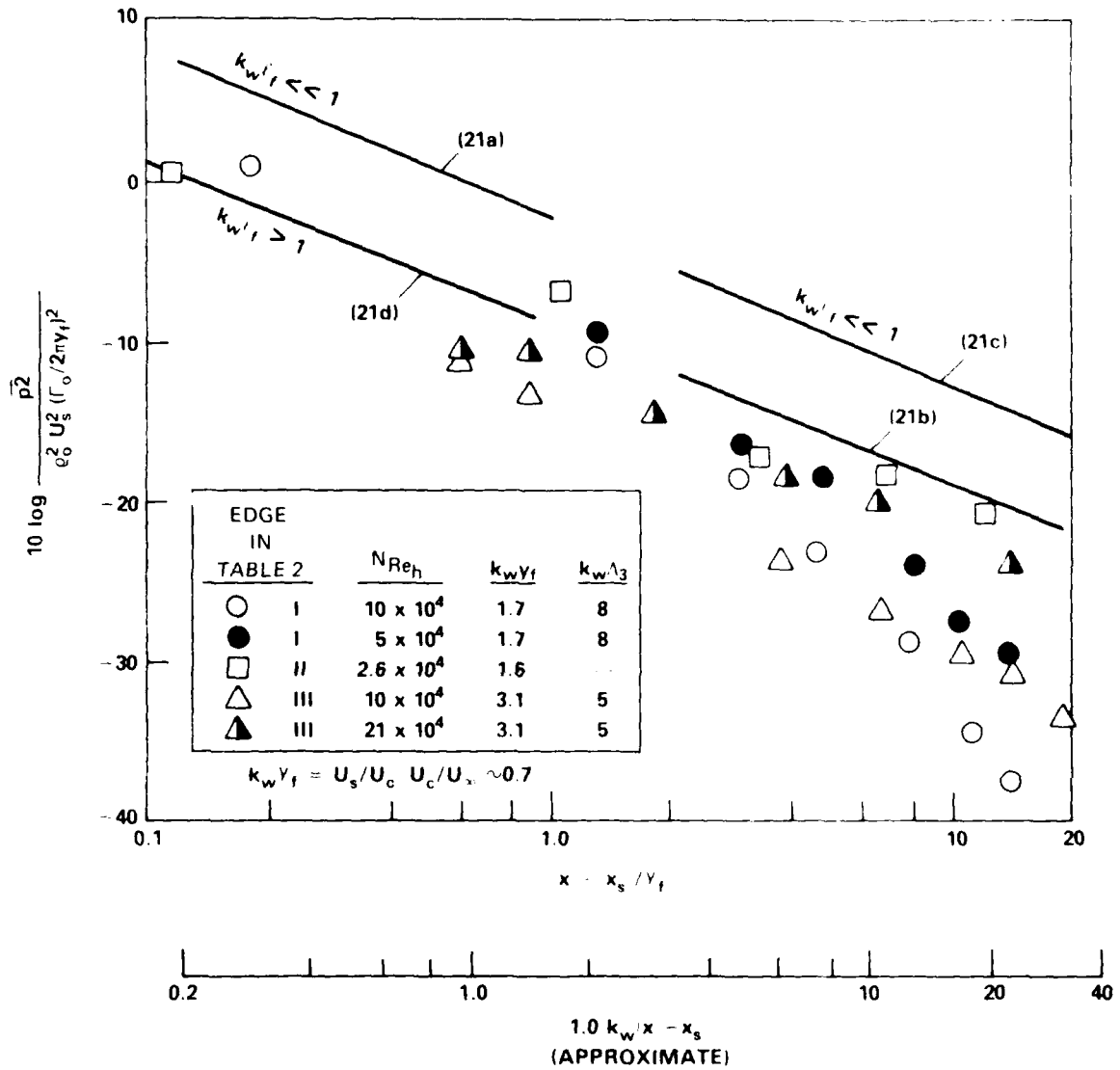


Figure 18 - Vortex-Induced Surface Pressures on Trailing Edges of Airfoils. Normalization is Based on Wake Variables: Circulations, Shear Layer Thickness, and  $U_s$

The surface pressure generated by the vortex street can be shown to be analytically singular at the trailing edge as  $x^{-1/2}$  as long as a complete Kutta condition is not applied. We now derive an explicit theoretical relationship for the surface

$$\Gamma_o^2 = \frac{\pi^2 u^2 y_f^2}{4} \quad (15a)$$

Equations (14) and (15) relate the analytical wake model to the experimental evaluations since we assume, following Schaefer and Eskinazi (1959), that a constitutive vortex has a core radius which is approximately  $y_f/4$ .

The pressures actually generated by the physical vortex street are maximum near the trailing edge or just upstream of the trailing edge stagnation point, as described above; the complete data set is collected in Figure 17. Additional data obtained on a third trailing edge (see Blake et al. 1977) is shown in Figure 18. The wake disturbance levels and the trajectories  $y_l$  and  $y_u$  for this edge were obtained as described in Section 3.3. The length  $x - x_s$  in Figure 17 is the distance upstream of the trailing-edge stagnation point. For the blunt edges  $x_s = 0$ .

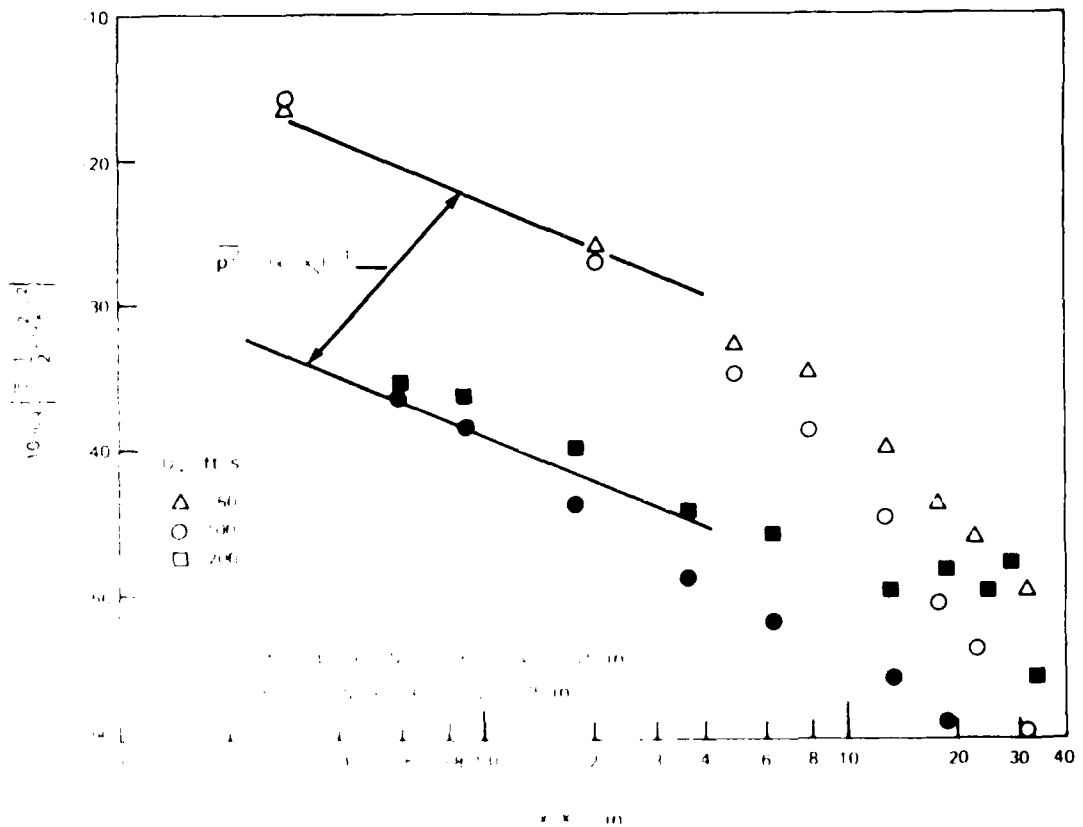
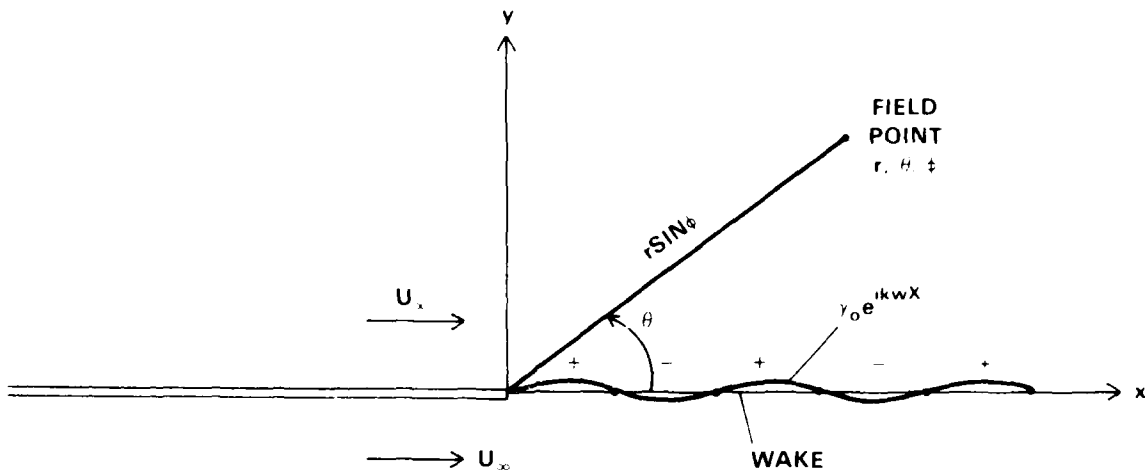
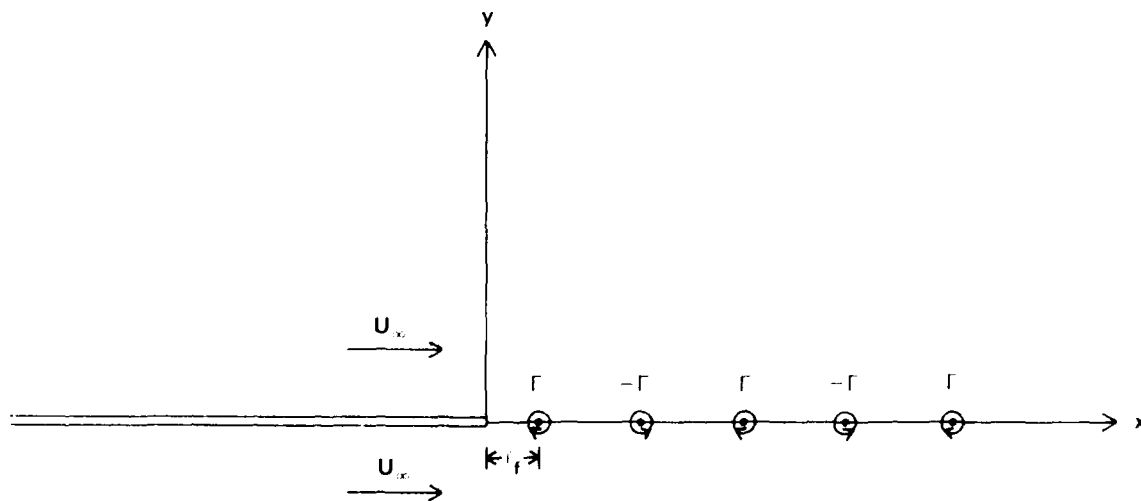


Figure 17. Maximum Pressure at Various Streamwise Distances from the Trailing-Edge Stagnation Point ( $x_s$ )



(a) Wavelike Vortex Sheet Model of the Wake



(b) Discrete Vortex Wake

Figure 16 - Idealizations of Vortex Wake Structures for Modeling of Surface Pressures and Radiated Sound

defined by either of Equations (5) or (7), yield dimensionless frequencies between 0.78 and 0.97. Thus, it appears that either a cross-wake dimension,  $y_f$  in the near wake or a dimension  $b$  in the far-wake, may both be used to define similar Strouhal number for vortex shedding for any shape trailing edge.

#### 4.2. MAGNITUDES OF THE SURFACE PRESSURE; ANALYTICAL MODEL

The measured correlation functions between the surface pressure and the wake velocities that are shown in Figures 7, 12, and 13 suggest the appropriateness of analytical modeling as a wavelike vorticity distribution in the wake. The surface pressure generated on a rigid half-plane by a two-dimensional wavelike vorticity distribution, downstream of and in the same plane as the surface, has been modeled by Blake (1976). The surface lies on the  $x < 0$  and  $y = 0$  plane, as shown in Figure 16, while the wake, which extends to  $x > 0$ , has a vorticity distribution approximated as

$$\omega_3(\xi_1, \xi_2, t) = \gamma_0 \delta(\xi_2) e^{ik_w(\xi_1 - U_c t)} d\xi_1, \xi_1 < \xi_f = 0 \quad (13)$$

where  $\xi_1$  is a dummy variable to express the wake coordinates separately from coordinates on the surface. The region  $0 < \xi_1 < \xi_f$  is the vortex formation zone. The circulation in one-half of a wavelength is

$$\begin{aligned} \Gamma_0 &= \int_{x - \pi/2k_w}^{x + \pi/2k_w} r_0 e^{ik_w(\xi_1)} d\xi_1 \\ \Gamma_0 &= 2r_0/k_w = 2r_0 U_c / v_s \end{aligned} \quad (14)$$

For a vortex of core radius  $r_0$  and tangential velocity  $u$  at the edge of the core (see the discussion in Section 3.2) another measure of the circulation of the vortex that causes the half wave is

$$\Gamma_0 = 2\pi r_0 u \quad (15)$$

which is related to the wake thickness and mean square intensity

for various trailing edge shapes as a function of Reynolds number. It is necessary only to note the behavior of  $\overline{p^2(x_0)}$  at a specific value of  $x/y_1$ , and convert it to the equivalent value of  $\Gamma_0^2$  using either Equation (20a) and (20d).

Figure 22 shows values of  $\Gamma_0^2$  over a range of 0.26 Reynolds number for the two principal trailing edges of this study, Edges I and III, the trailing edge shown in Figure 17 (Edge II), the blunt edge airfoil of Brooks and Hodgeson and the 25° rounded edge that is discussed in Part 2. Table 2 summarizes the important parameters of each edge. For  $U_\infty y_1/\nu$  less than  $2 \times 10^4$  for blunt edges, the vortex strength increases systematically with increasing Reynolds number. For the 25° and

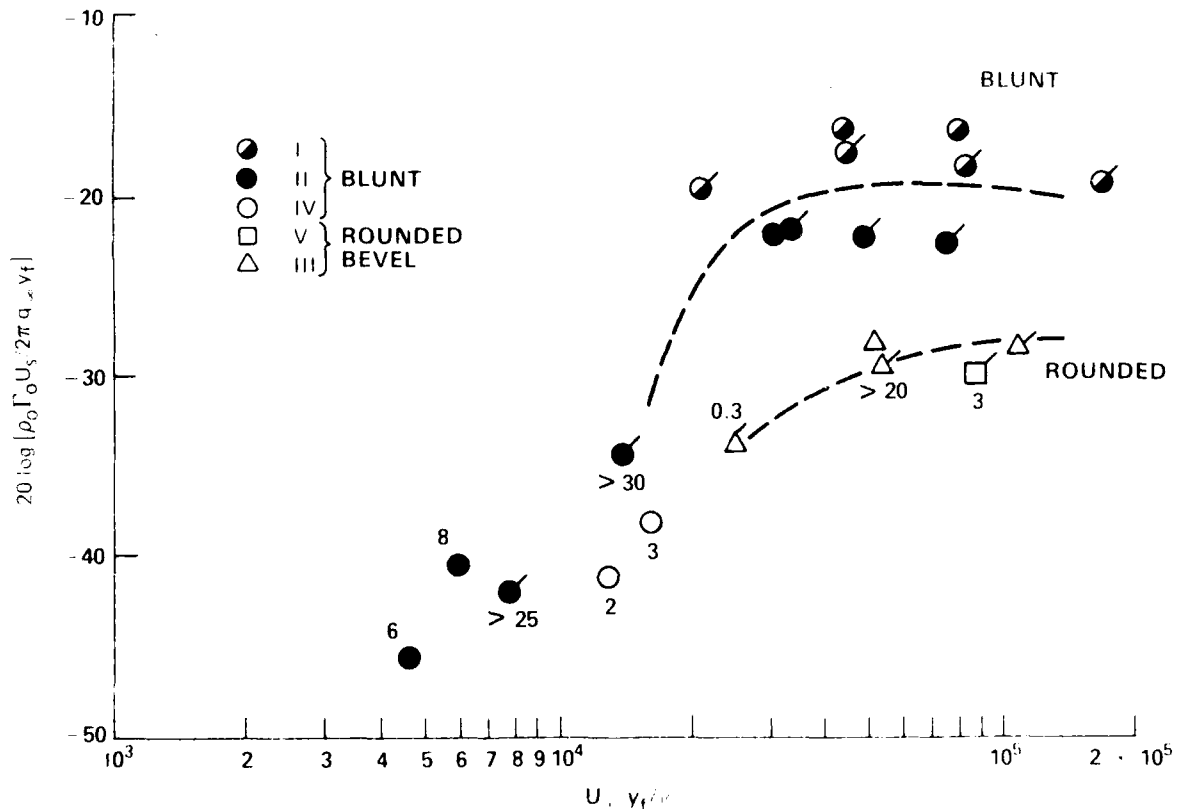
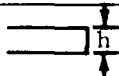
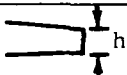
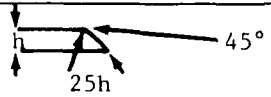
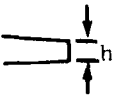


Figure 22 - Mean-Square Vortex Strengths for Various Trailing Edges with Vortex Shedding. Unflagged Points Obtained with Wake Intensity Measurements and Eq. (17a), Flagged Points Obtained with Surface Pressure Measurements and Eq. (21d). Numbers Denote Quality Factors  $1/\Gamma_0 = 0$  For  $Q < 30$ . Dashed Lines Represent Trends for Blunt and Rounded Bevel Edges. See Table 2 for Edge Notation.

TABLE 2 - PARAMETERS FOR TRAILING EDGES WHICH PRODUCE TONES

Edge Type	$2\theta/h$	$\omega y_f / U_s$	$y_f/h$	$f_s/y_f$	$\Delta_3/y_f$
I. 	0.06	1.0	0.8	0.94	3.5
II. 	0.26	0.85	1.0	0.9	--
III. 	0.05	1.0	0.5	2.0	3.5
IV. NACA 0012 	2	1.0 (assumed)	1.5 (estimate)	--	1.5
V. 	-0.05	1.0	0.37	-2	--

45° rounded trailing edges, the deduced vortex strengths are much less intense and also increase with Reynolds number. It is anticipated that other trailing edge shapes will have similar dependence.

As the Reynolds number increases in each case the tonal quality of the vortex-induced pressures improves; the flagged points denote conditions for which the surface or sound pressure has a continuous spectrum. The number by each point denotes the approximate quality factor,  $f_s/\Delta f$ , at each Reynolds number. The  $\Delta f$  are measured at the "half-power" points of the pressure or velocity spectra.

Pressures on blunt edges for Reynolds numbers greater than  $10^4$  are tones; in the case of the 45° rounded-edge tones occur for  $R_h > 10^5$ . These limiting values are dependent on the nature of the boundary layer upstream of the edge. The measurement of Brooks and Hodgeson shows this with a  $f_s/\Delta f = 3$  and a thick boundary layer at the trailing edge (see Table 2). The vortex strength behind the 25° rounded trailing edge was observed only at the highest Reynolds number of the test, it had a broad bandwidth, and represented a threshold of onset of vortex shedding.

## 5. CONCLUSIONS

For two trailing edge geometries, differences in the structures of the near wakes that relate to the production of tonal disturbances have been elucidated. As would be expected, a disruption of the formation of regular disturbances reduces the intensity of the tonal pressure produced. In the present instance, this disruption is brought about by the asymmetry in the upper and lower shear layers in the wake, and made possible by asymmetrically beveling the trailing edge. The growth phase of ordered wake structure occurs only after both the upper and lower shear layers pass the apex of the edge and it occurs within a half wavelength of oscillation. The completed formation of a vortex in the wake thus occurs before the shedding of the next vortex of opposite circulation. This process is dependent on Reynolds number, the geometry of trailing edge, the relative thicknesses of the upstream boundary layer, and the cross-wake separation of the shear layers that constitute the near wake.

The important parameters affecting the level of vortex-induced surface and aerodynamic sound pressure are: the wake width,  $y_f$ , measured between shear layers at the end of the formation zone, the length of the zone, the strength of the shed vorticity, and its spanwise correlation length. For the limited range of parameters examined, the spanwise correlation length  $l_c = 2 \cdot \lambda_3$  appears to be of the order of  $0.5y_f$  to  $0.7y_f$ . It is to be emphasized that these values apply for rigid edges only.

Vortex-induced surface pressure were found to increase as the trailing edge is beveled. This clearly disposes of any question of application of a complete "Kutta" condition that would null the fluctuating pressure at the trailing edge. It is shown, however, in Part 2 that analyses which do apply a "Kutta" condition to predicting the generation of continuous-spectrum pressure by turbulence convected past the edge appear to be valid.

The observation is made here that at low Reynolds number the 45° rounded trailing edge generates a continuous spectrum pressure centered on the same frequency that discrete vortex shedding would have occurred, i.e.,  $\omega y_f / U_s \approx 1$ . In this case, however, the correlation between the surface pressure and the velocities fluctuations is generally high only in the immediate vicinity of the edge. These continuous spectrum pressures are basically generated in the immediate velocity of the separation zone at the edge rather than the induction field of the wake, as it would be for tonal pressures; yet the primary frequency is still governed by the same  $y_f$  and

$U_s$  as in the tonal case. We explore the generality of this observation to other trailing edge geometries in Part 2.

#### ACKNOWLEDGMENTS

The assistance of L. Maga, R. Armstrong, and R. Dwyer in gathering experimental results is much appreciated. This work was sponsored by the Naval Sea Systems Command, SEA 55X4.

#### REFERENCES

- Abernathy, F.H. and R.E. Kronauer, (1962), "The Formation of Vortex Streets," *Journal of Fluid Mechanics*, 13, p. 120
- Abramowitz, M. and I.A. Stegun (1965), "Handbook of Mathematical Functions," Dept. of Commerce, N.B.S. Publication No. 55.
- Bearman, P.W. (1965), "Investigation of the Flow Behind a Two-Dimensional Model with a Blunt Trailing Edge and Fitted with Splitter Plates," *Journal of Fluid Mechanics*, 21, pp. 241-255.
- Bearman, P.W. (1967), "On Vortex Street Wakes," *Journal of Fluid Mechanics*, 28, pp. 625-641.
- Blake, W.K. (1970), "Turbulent Boundary-Layer Wall Pressure Fluctuations on Smooth and Rough Walls," *Journal of Fluid Mechanics*, 44, p. 1.
- Blake, W.K. (1975a), "A Statistical Description of Pressure and Velocity Fields at the Trailing Edges of Flat Struts," DTNSRDC Report 4241.
- Blake, W.K. (1975b), "Periodic and Random Excitations of Streamlined Structures by Trailing Edge Flows," Proc. 4th Biennial Symposium on Turbulence in Liquids, Rolla, Mo.
- Blake, W.K. and L.J. Maga (1975), "On the Flow-Excited Vibrations of Cantilever Struts on Water II - Surface Pressure Fluctuations and Analytical Predictions," *J. Acoust. Soc. Am.* 57, pp. 1448-1464.
- Blake, W.K. (1976), "A Near-Wake Model for the Aerodynamic Pressures Exerted on Singing Trailing Edges," *J. Acoust. Soc. Am.* 60, pp. 594-598.
- Blake, W.K., L.J. Maga and G. Finkelstein (1977), "Hydroelastic Variables Influencing Propeller and Hydrofoil Singing," *Noise and Fluids Engineering*, Am. Soc. Mech. Eng., N.Y.
- Brooks, T.F. and T.H. Hodgeson (1981), "Trailing Edge Noise Prediction Using Measured Surface Pressures," *J. Sound Vib.* 78, pp. 69-117.
- Chandirmani, K.L. (1974), "Diffraction of Evanescent Waves with Applications to Aerodynamically Scattered Sound and Radiation from Unbaffled Plates," *J. Acoust. Soc. Am.* 55, pp. 19-29.
- Clase, D.M. (1975), "Noise Radiated from an Edge in Turbulent Flow," *AIAA Journal*, 13, pp. 1041-1047.
- Chevray, R. and L. Kovaszny (1969), "Turbulence Measurements in the Wake of a Thin Flat Plate," *AIAA Journal* 7, pp. 1041-1043.

- Crighton, D.G. and M. Gaster (1976), "Stability of Slowly Diverging Jet Flow," J. Fluid Mech. 77, pp. 397-413.
- DeMetz, F.C. and M.J. Casarella (1973), "An Experimental Study of the Intermittent Properties of the Boundary Layer Pressure Field During Transition on a Flat Plate," NSRDC Report 4140.
- Eagleson, P.S. et al. (1961), "Turbulence in the Early Wake of a Fixed Flat Plate," Massachusetts Institute of Technology Hydrodynamics Laboratory Report 46.
- Ffowcs Williams, J.E. and L.H. Hall (1970), "Aerodynamic Sound Generation by Turbulent Flow in the Vicinity of a Scattering Half-Plane," J. Fluid Mech. 40, pp. 657-670.
- Gaster, M. (1964), "A Note on the Relation Between Temporally-Increasing and Spatially Increasing Disturbances in Hydrodynamic Stability," J. Fluid Mech. 14, pp. 222-224.
- Gongwer, G.A. (1952), "A Study of Vanes Singing in Water," Journal of Applied Mechanics, 19.
- Gradeshteyn, I.S. and I.M. Ryzhik (1965), "Table of Integrals Series and Products," Academic Press.
- Greenway, M.E. and C.J. Wood (1973), "The Effect of a Beveled Trailing Edge on Vortex Shedding and Vibration," Journal of Fluid Mechanics, 61, pp. 323-335.
- Hanson, C.E. (1970), "An Investigation for the Near-Wake Properties Associated with Periodic Vortex Shedding from Airfoils," Massachusetts Institute of Technology Acoustics and Vibration Laboratory Report 76234-5.
- Hekestad, G. and D.R. Olberts, "Influence of Trailing Edge Geometry on Hydraulic-Turbine-Blade Vibration Resulting from Vortex Excitation," Transactions of the American Society of Mechanical Engineers, Journal of Engineering for Power, 82, pp. 103-110.
- Howe, M. (1978) "A Review of the Theory of Trailing Edge Noise," J. Sound Vib. 61, pp. 437-465.
- Klebanoff, P.S. (1955), "Characteristics of Turbulence in a Boundary Layer with Zero Pressure Gradient," National Advisory Committee for Aeronautics Report 1247.
- Kronauer, R.E. (1964), "Predicting Eddy Frequency in Separated Wakes," Paper presented at the International Union of Theoretical and Applied Mathematics Symposium on Concentrated Vortex Motions in Fluids, University of Michigan Ann Arbor, Mich (6-11 Jul 1964); also, referred to by Bearman (1967).

- Leverton, J.W. (1973), "The Noise Characteristics of a Large 'Clean' Rotor,"  
Journal of Sound and Vibration 27, pp. 357-376.
- Milne-Thompson, L.M. (1960), "Theoretical Hydrodynamics," Macmillan Co.
- Perry, A.E. and P.M. Joubert (1963), Journal of Fluid Mechanics, 17, 193.
- Powell, A. (1959), "On the Aerodynamic Noise of a Rigid Flat Plate Moving at Zero  
Incidence," J. Acoust. Soc. Am. 31, pp. 1649-1653.
- Roshko, A. (1954), "On the Drag and Shedding Frequency of Two-Dimensional Bluff  
Bodies," National Advisory Committee for Aeronautics Technical Note 3969.
- Schaefer, J.W. and S. Eskinazi (1959), "An Analysis of the Vortex Street Generated  
in a Viscous Fluid," Journal of Fluid Mechanics, 6, p. 241.
- Schlichting, H. (1960), "Boundary Layer Theory," McGraw-Hill Fourth Edition, New  
York.
- Toebes, G.H. and P.S. Eagleson (1961), "Hydroelastic Vibration of Flat Plates Related  
to Trailing Edge Geometry," Transactions of the American Society of Mechanical  
Engineers," Journal of Basic Engineering, 18.

## PART 2. RANDOM PRESSURE AND VELOCITY FLUCTUATIONS

### ABSTRACT

An experimental determination of the turbulent field quantities which exist at trailing edges has been made. The investigation was carried out on a rigid strut with parallel sides and circular leading edge; the strut was not yawed to the flow. Discussions in Part 1 cover cases of trailing edges that produce predominantly periodic wakes; discussions in this part cover trailing edges that produce predominantly random wake structures. In each case, the time-averaged, boundary-layer characteristics, streamwise turbulence intensities, and fluctuating surface pressures have been spatially mapped in the region of each edge. Correspondence between surface pressures and turbulent fields in both the immediate vicinity of and in the far wake of each edge were determined by correlation analyses. Results show some general features of both random and tonal pressure generation that are common to both ordered and disordered flows. The random surface pressures on the edges discussed in this part are generated by a large-scale eddy structure caused by turbulent flow separation on one side of the airfoil rather than by the wake extending downstream. The large eddies are formed in the separation process at the edge, and the frequency spectra of the random pressures are expressed in a dimensionless form that has also been found suitable for describing tonal surface pressures of periodic wakes.

## 1. INTRODUCTION

In Part I the connection between the periodic pressures generated on a trailing edge and the large, paired-vortex structure in the wake was quantified. In this part, we shall see that when vortex growth does not occur, the surface pressure fluctuations are not periodic, but rather distributed over a broad frequency range centered on a characteristic frequency that appears to scale on the same variables as the tonal pressure of the frequency. There is a class of trailing edges, which shall be called "nonsinging," which does not generally produce tonal pressures, and behind which the flow pattern at the trailing edge is a hybrid of an attached boundary layer with an adverse pressure gradient and a separated flow without reattachment. Figure 1 shows the schematic of the interchangeable geometries used on a basic strut as well as rough classifications denoted as "singing" or "nonsinging" edges. Part I dealt with discussions of the organized, vortex street wake flow behind the blunt edge and the edge with a  $45^\circ$  rounded bevel. In this part we discuss the fluid dynamics of the remaining two edges, each with a  $25^\circ$  bevel. These two edges are recommended by Heskestad and Olberts (1960) as geometries useful for the prevention of "singing of lifting surfaces"; the  $25^\circ$  knuckle edge, which was not

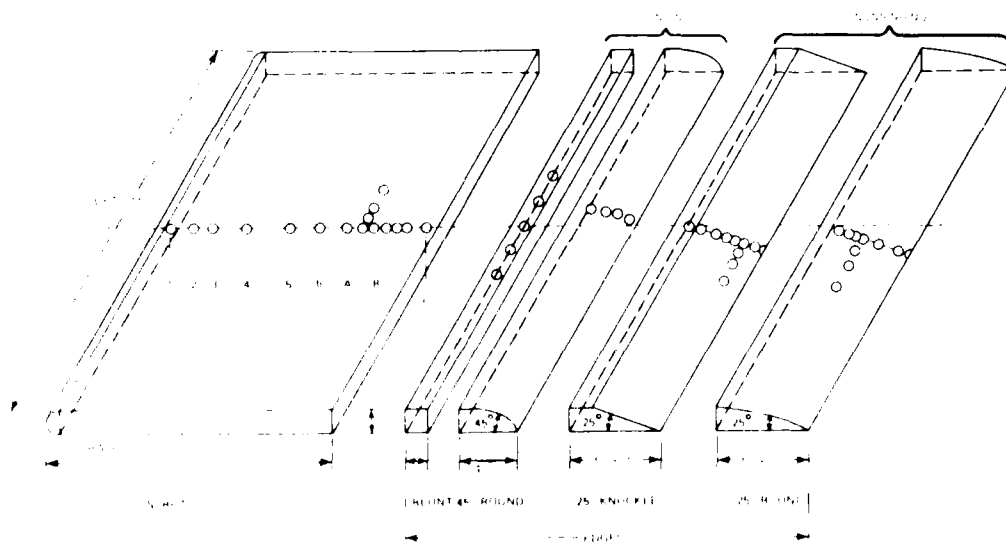


Figure 1 - A View of the Strut Showing the Orientation of Trailing Edges and Schematic Locations of Microphones

rounded, has boundary layer separation over the wedge region with an extensive zone of large-scale motion. The other edge has a more gradually induced separation afforded by the 10-in. radius of curvature that removes the knuckle and that permits an extensive region of boundary layer flow, with and adverse pressure gradient that gives rise to a less intense separation zone. In the discussions to follow, we describe the turbulence field near each trailing edge in considerable detail, the surface pressures it induces, the statistical relationship extant between the pressures and the eddy structure in the near wake, and the theoretically-based aerodynamic sound-producing qualities of the flow. Further, we attempt to delineate between the meanings of generating "tonal" and "nontonal" disturbances, particularly with regard to predictions.

The microphone measurement Locations A through G are illustrated in Figures 1, 2, and 3. All details of the experimental method and of the boundary-layer characteristics on the strut have been described in Part 1, and in Part 2, Tables 1 and 2, and by Blake (1975).

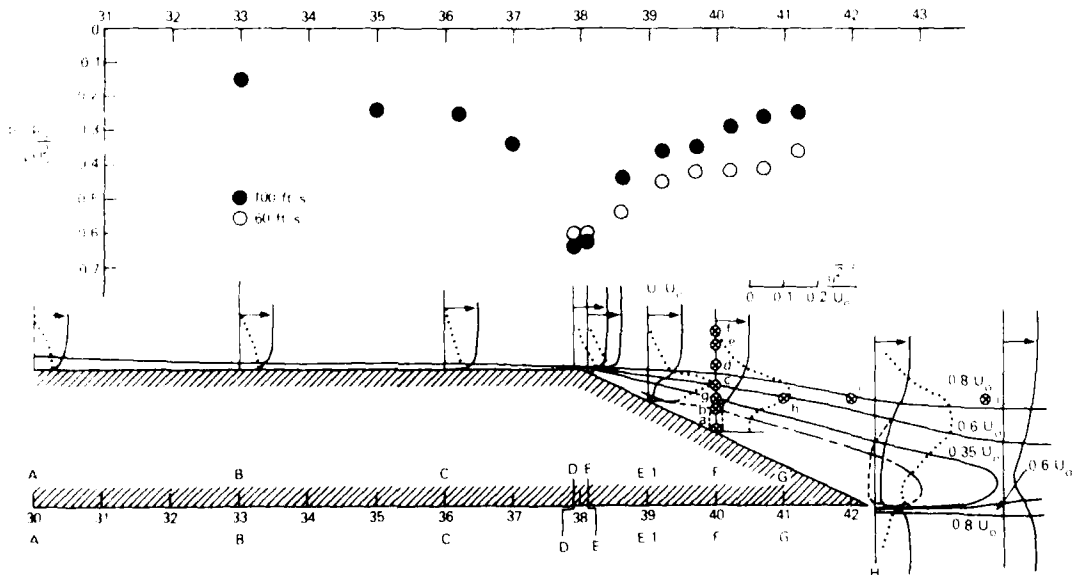


Figure 2 - Flow Patterns and Static Pressure Distributions on the 25° Knuckle Beveled Edge. The Flow Patterns are Shown for  $U_{\infty} = 100$  ft/s; Static Pressures for the Speeds Shown

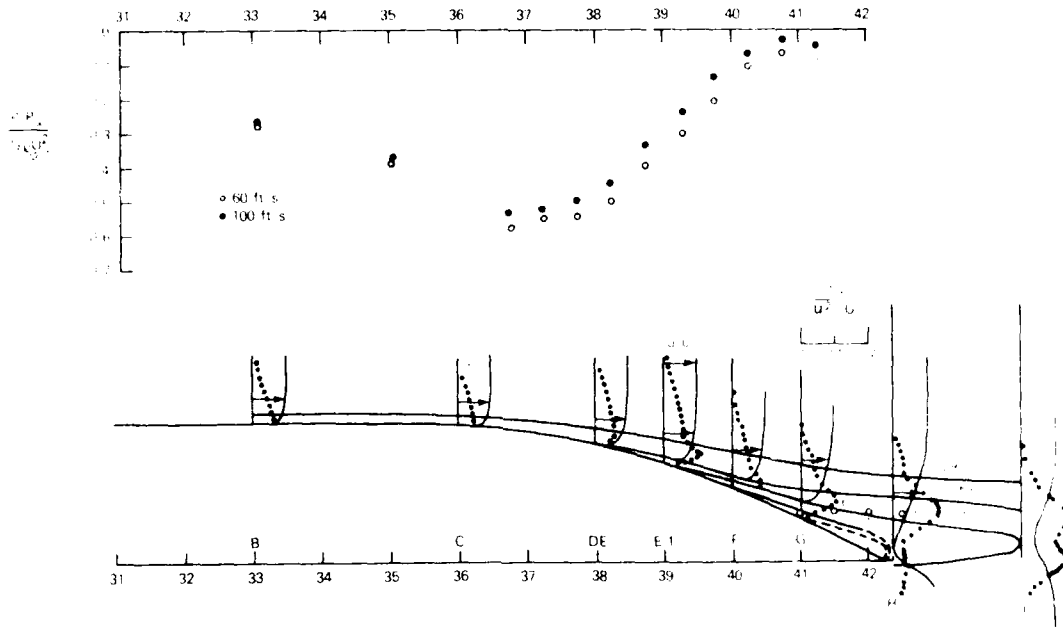


Figure 3 - Flow Patterns at  $U_\infty = 100$  ft/s Pressure Distribution Near the  $25^\circ$  Rounded Level

TABLE I - MEAN BOUNDARY-LAYER PROPERTIES FOR THE  $25^\circ$  KNUCKLE TRAILING EDGE

Position	50 fps				100 fps			
	$\delta$	$\delta^*$	$\theta$	H	$\delta$	$\delta^*$	$\rho$	H
A	--	--	--	--	0.65	0.09	0.073	1.23
B	--	--	--	--	0.67	0.103	0.074	1.4
C	--	--	--	--	0.62	0.0705	0.0564	1.245
D	0.09	0.084	0.0795	1.055	0.56	0.05	0.0475	1.06
E	--	--	--	--	0.5	0.07	0.0525	1.34
E-1	1.33	0.45	0.135	--	0.88	0.316	0.114	2.765
F	1.6	0.81	0.181	4.47	1.29	0.596	0.217	2.75

All dimensions are in inches,  $H = \delta^*/\theta$ .

TABLE 2 - MEAN BOUNDARY-LAYER PROPERTIES FOR THE 25° ROUND TRAILING EDGE

Position	60 fps				100 fps			
	$\delta$	$\delta^*$	$\theta$	H	$\delta$	$\delta^*$	$\theta$	H
4	0.575	0.0735	0.061	1.21	0.435	0.0603	0.048	1.26
A	--	--	--	--	--	--	--	--
B	0.8	0.093	0.08	1.17	0.63	0.073	0.059	1.23
B-1	--	--	--	--	0.615	0.0668	0.0565	1.16
C	--	--	--	--	0.5	0.045	0.04	1.14
DE	0.8	0.0915	0.059	1.56	0.62	0.093	0.0495	1.88
E-1	0.95	0.157	0.082	1.93	0.65	0.118	0.0676	1.74
F	1.35	0.285	0.133	2.12	0.95	0.231	0.095	2.43
G	1.96	0.52	0.215	2.42	1.36	0.451	0.129	3.47

All dimensions are in inches,  $H = \delta^*/\theta$ .

## 2. SEPARATED FLOW AT BEVELED TRAILING EDGES

In these cases, the boundary layers incident on the edges experience adverse pressure gradients before being shed by the strut. For these nonsymmetrical edges, the flow on one side of the strut separates upstream from the apex, or tip, of the trailing edge and periodic vortex streets do not appear to be formed. This section describes the mean and unsteady velocities that occur on the two beveled trailing edges with a 25°-included angle. Much effort was spent on a clear identification of the separation points and large-scale vortex structures in the absence of sophisticated flow-visualization techniques.

### 2.1 TURBULENT FLOW NEAR 25° KNUCKLE-BEVELED EDGE

As the boundary layer approaches the edge, it first experiences a favorable pressure gradient, followed by an adverse gradient just downstream from the knuckle. This is shown in Figure 2 for the two tunnel speeds  $U_\infty = 50$  and 100 ft/s. The pressure recovery appears to be more apparent at the higher speed since the pressure coefficients are less negative at 100 than at 50 ft/s. Boundary-layer characteristics were obtained at the Positions A through F (see Figure 2) on the surface of the edge as well as in the near wake downstream from the edge. Before discussing

the quantitative measurements, it is appropriate to mention that an oil streak experiment, identical to that described in Part 1, showed separation at Position F. Oil accumulated in a streak approximately 0.1 in. in width at the downstream from Position F. This confirms that an expected steady separation occurs at the knuckle followed by a large-scale and intermittent separation zone further downstream.

Results of a survey of the boundary layer on the edge, performed at upstream flow velocity  $U_\infty = 100$  ft./s, are shown in Figure 2. Flow profiles for 50 ft/s are similar. Table 1 gives thickness parameters for the boundary layer. At Position E, which is 0.1 in. downstream from the knuckle, the flow reversal that accompanies separation could not be observed with the hot-wire anemometer. The total velocity sensed by the anemometer cannot discriminate between components parallel to and vertical to the surface when the mean velocity is small. The "mean" and root-mean-square velocities on the knuckle are of the same order as the mean velocity; and as shown by Simpson et al. (1977), the standard interpretation of the anemometer output gives anomalously high mean velocities when the mean and fluctuating quantities are of comparable value. Furthermore, the anemometer is indiscriminately sensitive to all flow directions in these cases. What the velocity profiles do show is the general structure of the separated flow field. The total root-mean-square turbulence intensities of the boundary layers are shown as dotted lines for each location and they show important features. The first is a local maximum in turbulence intensity that coincides with a maximum in the vertical gradients of mean velocity  $dU/dy$ . These local maxima show an absolute maximum\* in excess of  $\overline{u^2}/U_\infty^2 = 0.23$ , where  $U_\infty$  is the local mean free stream velocity which occurs near Position H with an intensity at Position I comparable to that at Position H. The second feature is that near the wall, where  $dU/dy = 0$ , the gradient  $d(\overline{u^2}/U_\infty^2)/dy$  also vanishes. Furthermore, at Position F the root-mean-square turbulence intensity indicated in this region near the wall is approximately one-half the measured local mean velocity, and, therefore, the peak fluctuations of velocity probably exceed the mean velocity near the wall. Lines of constant speed, which describe streamlines, have also been drawn in Figure 2. The dashed line which encloses the region near the wall for which  $dU/dy < 0$  is considered as also roughly enclosing the region of separated flow.

---

\*Two normalization velocities are used;  $U_\infty$ , the average upstream velocity and  $U_\infty^*$ , the local free-stream velocity at the position in question.

The region of separation between Position E-1 and the tip (shown in Figure 2), as bounded by the line (---), is not a zone of constant flow reversal. Rather, it is a zone of oscillatory motion with equal tendency of flow upstream and downstream. This tendency was indicated by space-time correlations of streamwise velocity fluctuations (see Blake (1975)). For a probe pair separated in the streamwise direction and placed outside the separation zone, a convection velocity of the same order as the local velocity was measured. When the probe pair was situated in the zone marked by the boundary line (---), there was no time delay between the probes and, therefore, no mean streamwise convection. Furthermore when a pair of probes was oriented across the stream normal to the surface, one inside and one outside the boundary with no streamwise displacement of probes, the velocity fluctuations were positively correlated. Thus, motions on either side of the boundary (---) are oppositely phased. To the extent that the unsteady motions in the separation zone may be characterized by a vortex-like structure, these correlations then give the indications of a vortex whose center nearly coincides with the boundary (---), and bounded roughly by the surface of the strut and the streamline  $U = 0.6 U_0$ , which is given by the locus of turbulence maxima in the shear flow. Thin cotton tufts fixed to the surface substantiated this interpretation. The tufts were long enough to be trapped in the recirculation zone and they alternately twirled in the flow or were carried upstream and downstream along the surface. The alternations of motion were most irregular in occurrence. Thus, it appears the separation zone can be described as a vortex formed at Position E, growing and translating along the edge at a velocity of order  $0.35 U_0$ , and behind which is a temporarily reattached flow. When the vortex translates far enough downstream, separation reoccurs at Position E. The net upstream and downstream motions very near the surface is such as to give zero mean convection. Unfortunately, both the high velocities used in this study and the geometry required in the facility (surface pressure measurements received no attention and this dictated facility selection) made it impossible to use some of the more recent flow visualization techniques.

The frequency spectral content of turbulence above Positions F and H was broadband. When scaled on the local velocity and  $v^*$ , the nondimensionalized spectra were quite similar to those normally measured in attached turbulent boundary layers, say, in the stream of the trailing edge. This means that the wave-number spectrum of detached turbulence at a given location along the bevel was set by the general

The theoretical noise-producing qualities of this geometry depend on the convection velocity of the separated vorticity past the trailing edge. Cross-spectral densities between pressure at Position F, i.e.,  $p(x_F, t)$  and other positions, i.e.,  $p(x_F + r_x, t)$ , are shown in the center of Figure 13. The cross spectrum is defined as

$$\begin{aligned} \phi(r_x, 0, \omega) &= \frac{1}{2\pi} \int_{-\infty}^{\infty} \langle p_F(x_F, t) p(x_F + r_x, t + \tau) \rangle e^{i\omega\tau} d\tau \quad (3) \\ &= |\phi(r_x, 0, \omega)| e^{i\alpha(r_x, \omega)} \end{aligned}$$

where  $x_F$  represents the location of Position F. In Figure 13, the cross-spectral density is normalized on the product of the individual autospectra denoted by

$$\langle \phi_p(\omega) \rangle = [\phi_p(x_F, \omega) \phi_p(x_F + r_x, \omega)]^{1/2} \quad (4)$$

The phase of the cross spectrum,  $\alpha$ , has a smooth variation both with separation  $r_x$  and frequency, as also shown in Figure 13. The near-linear dependence of this phase is representable as

$$\alpha(r_x, \omega) = \frac{\omega r_x}{U_c} \quad (5)$$

where  $U_c$  is an eddy convection velocity,  $U_c = 0.55 U_\infty$ , which appears to be constant from Position E-1 to the apex and over the frequency range  $0.7 < \omega y_F / U_\infty < 1.0$ . The phase has been extrapolated and referred to zero at the apex of the edge as if the reference microphone had been located there.\* Interpreting this phase as due to a mean convection, then, the phase in the form shown in Figure 13, i.e.,

$$\alpha_0 = \frac{\omega x}{U_c} = k_c x \quad (6)$$

where  $k_c$  is interpreted as a convection wave number and  $x$  points upstream from the apex.

\*In Figures 12 and 13, it is to be noted that measurement locations were extended to within  $\frac{1}{4}$  in. from the apex of the edge using thin strain gage microphones.

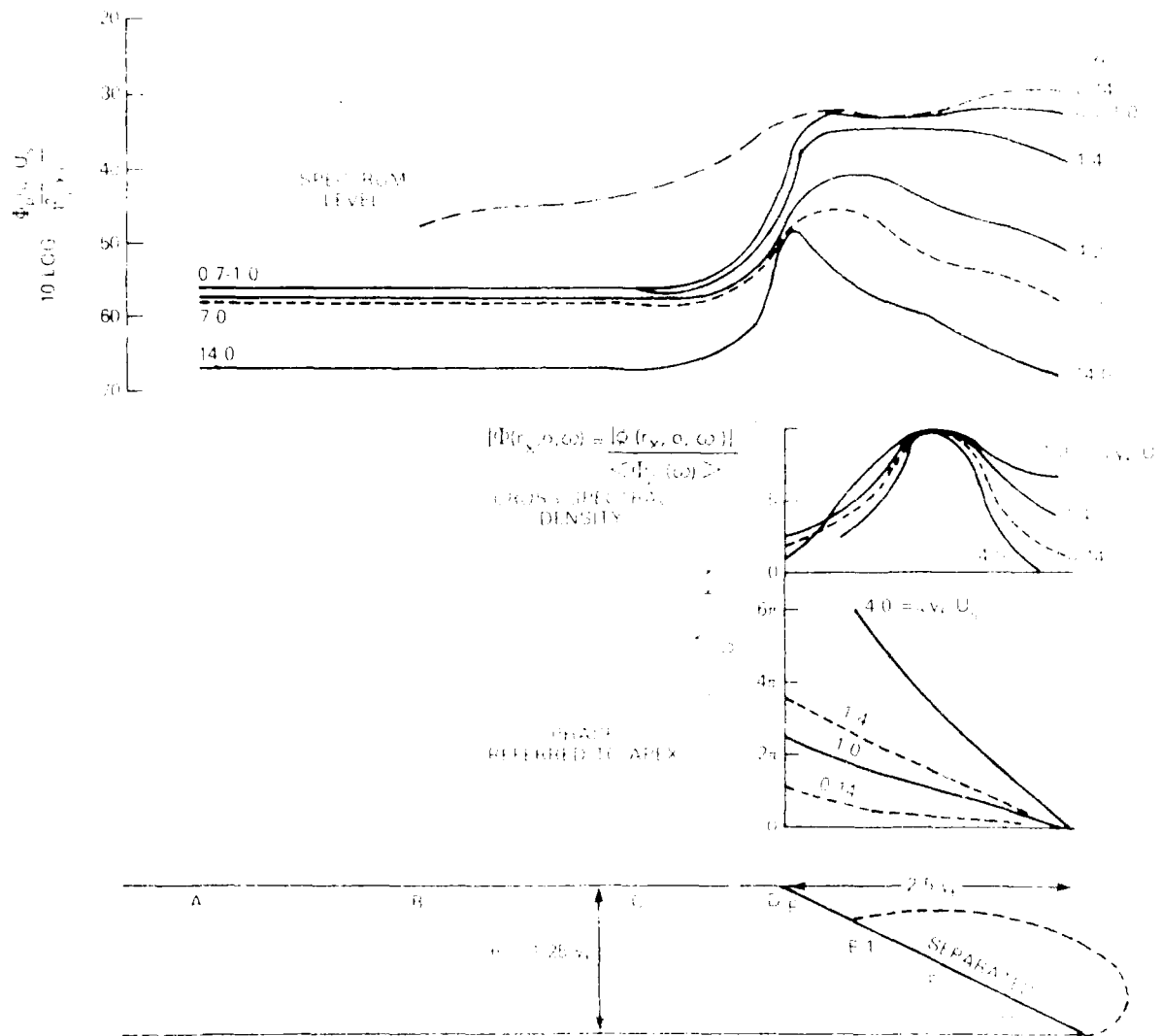


Figure 13 - Distribution and intensity of pressures on the bench (cut in pipe at  $x_1/z_0 = 1$ ,  $U_0 = 100 \text{ ft/sec}$ ).

showing an abrupt increase in pressure level at the knuckle at selected values of  $x_1/z_0$  and at a free-stream velocity of  $U_0 = 100 \text{ ft/sec}$ . For  $x_1/z_0 = 1$ , the values for the spectrum at the knuckle, but at  $x_1/z_0 = 1$ , they remain reasonably constant over the entire level. This particular case was selected for more intensive evaluation because of the large and relatively stable region of flow that it provided.

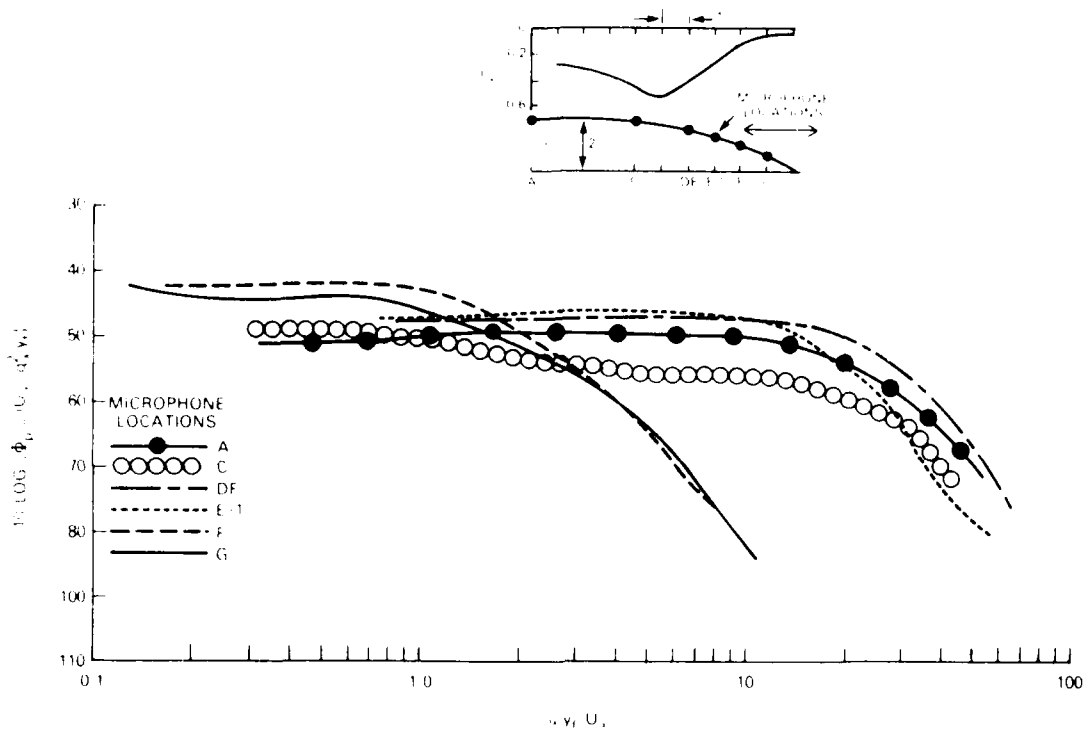


Figure 12 - Spectral Densities of Surface Pressures at a Rounded-Bevel Trailing Edge. The Double Arrow in the Inset Indicates the Zone of Separation. Parameters: Edges 5 Tables  $N_{Reh} = 10^5$ .

The surface pressure spectra on the  $25^\circ$  rounded edge, previously nondimensionalized on local  $y^*$  in Figure 6, are normalized on  $y_f$  and  $U_s$  in Figure 12. Now it can be seen that, in the separation zone, the pressures stabilize to a common spectral form which, as seen above, appears to be somewhat typical of separation-induced pressure fluctuations. A comparison of Figures 10 through 12 permits the general statement that the spectral form of pressures beneath a separation zone differs considerably from that of pressures in an attached boundary layer and show greatly enhanced values at frequencies less than  $f y_f / U_s \approx 1$ .

## 5.2 LARGE-EDDY STRUCTURE IN THE SEPARATION ZONE OF THE BEVELED EDGE

It was shown in Sections 3 and 5.1 that the pressure fluctuations on the beveled edges fall into distinctly different groupings, according to whether they occur on the bevel or upstream on the base strut. Figure 13 further expresses this point,

Autospectra of pressures on the blunt trailing edges, discussed in Part I, are shown in Figure 11. It is now seen that  $\omega y_f / U_s = 1$  defines both the frequency of the vortex shedding tone and the cutoff frequency above which the continuous-spectrum pressures decrease with increasing frequency. The arrows shown in Figure 11 indicate the spectral levels of the tones. Any of the spectra shown in Figures 10 and 11 is expressible in the general analytical form

$$\frac{p_{cs}(\omega) U_s}{q_c^2 y_f} = \frac{[1 - p_s(\omega y_f / U_s)]_{cs}}{q_c^2} + 1/2 \frac{p_s^2}{q_c^2} \left[ \delta(\omega y_f / U_s - 1) + \delta(\omega y_f / U_s + 1) \right] \quad (2)$$

where  $p_{cs}$  refers to the continuous spectrum part,  $p_s^2$  to the tonal component if it exists and which is represented by the heads of the arrows in Figure 11, and  $\delta(\pm 1)$  is the Dirac delta function which is unity only when  $\omega = +1$  or  $-1$ . The particular spectral densities shown in Figures 10 and 11 have been selected in order to give representative continuous-spectrum values in either the separation zone or the near-maximum tonal levels selected for small values of  $x = x_c / y_f$  where  $x = 1$  is the streamwise location of the trailing edge stagnation point as discussed in Part I.

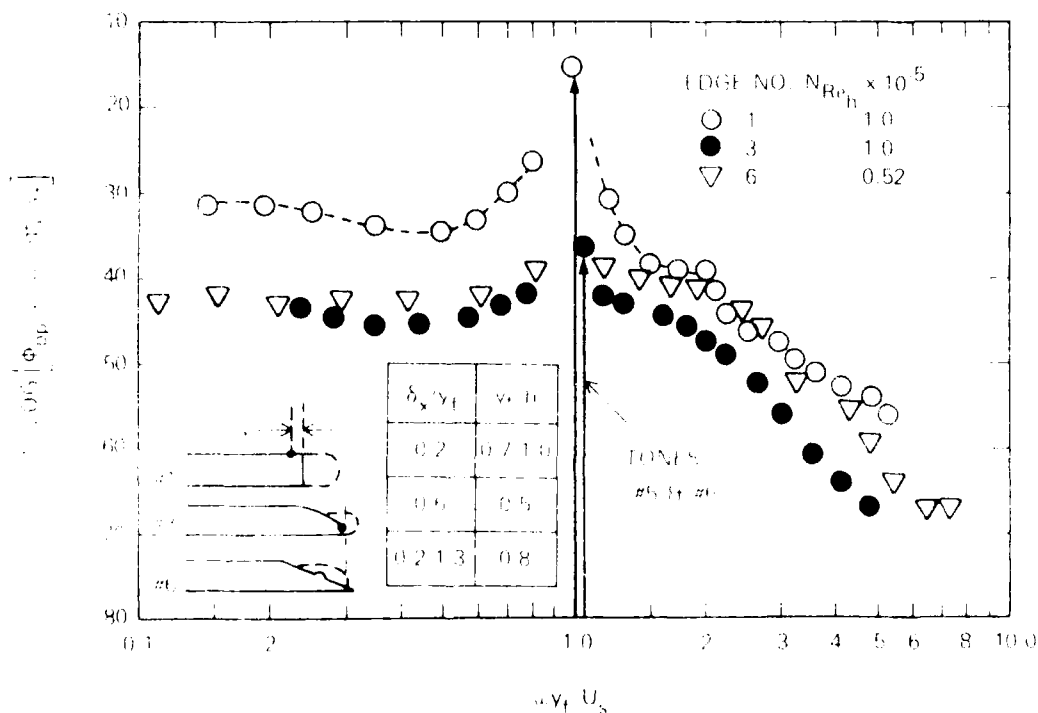


Figure 11 - Surface Pressure Spectra at Trailing Edges for Conditions with Varying Degrees of Vortex Shedding Periodicity. Numbers Refer to the Listing in Table 3.

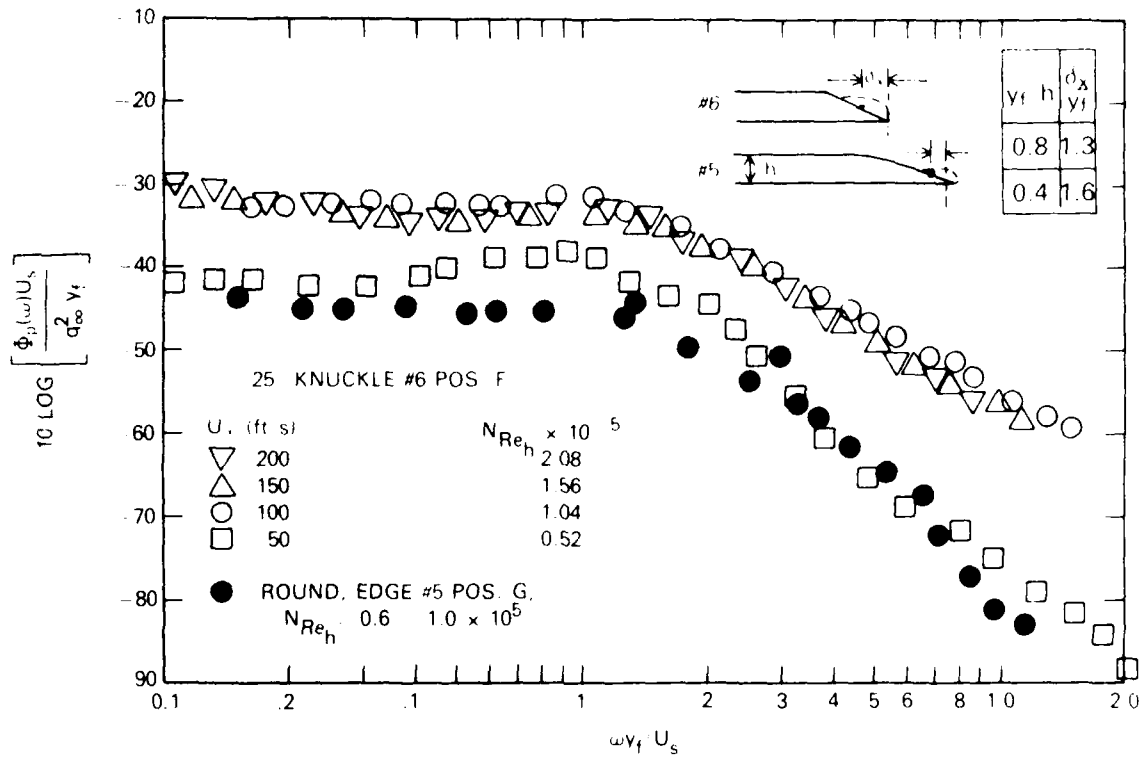


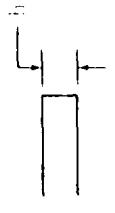
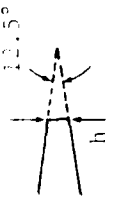
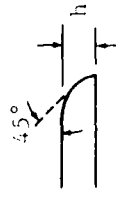
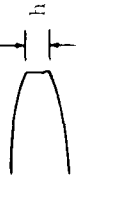
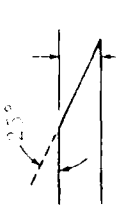
Figure 10 - Surface Pressure Spectra Beneath Flow Separation at Trailing Edges Which Do Not Ordinarily Generate Periodic Vortex Street Wakes. Open Points: Pos. F on Knuckle-Beveled Edge,  $y_f = 0.7 h$ ,  $C_{p_s} = -0.3$ ; Closed Points: Pos. G on Round-Edge,  $y_f = 0.037 h$ ,  $C_{p_s} = -0.1$ .

these pressures, now normalized on  $y_f$  and on

$$U_s = U \sqrt{1 - C_{p_s}} \quad (1)$$

where  $C_{p_s}$  is the static pressure coefficient beneath the separated flow. The pressures on the knuckle edge appear to stabilize to a common dimensionless form at velocities greater than 50 ft/s. No such obvious speed dependence was observed for the nondimensionalized pressures on the 25° rounded edge. The shapes of all spectra are all similar and  $\omega y_f / U_s = 1$  marks a limiting dimensionless frequency below which the spectrum is reasonably flat.

TABLE 1 - SUMMARY OF PARAMETERS FOR TRAILING EDGE FLOW

Geometry	Dimensionless Reynolds Number Virtual Leading	$h/\lambda$	$\lambda/\delta$	$\lambda/\delta$	Remarks
	$8 \times 10^3$	0.06	0.8	3.5	Truly random pressures not observed for $N_{Re} \frac{y_f}{\lambda} > 3000$ .
	$4 \times 10^3$	0.26	1.0	--	Tonal, or near tonal, pressure superimposed on a random field.
	$2.6 \times 10^4$	0.05	0.5	3.5	Value of $\Lambda_3$ for periodic pressures only.
NACA 0012 	$8 \times 10^3$	2.2	$\sim 1.5$	1.5	Value of $\Lambda_3$ for periodic pressures only, $y_f$ deduced on the basis $v_s' y_f / U_s = 1$ . This is a blunted NACA 0012 section for which $h/h_m = 0.26$ and 0.034.
	$8 \times 10^4$	--	$\sim 0.4$	--	Near-periodicity only observed in wake velocities at highest velocity attainable.
	$1.6 \times 10^5$	0.05	0.8	$\leq 1.0$	No periodicity could be observed in the wake at any $N_{Re} \frac{y_f}{\lambda}$ , for $y_f$ see Section 6.1.

correlation function is more representative of the boundary layer pressure than the wake-induced pressure. It appears that, in both cases, one can generalize the pressures and correlation functions as being "boundary-layer-like" and "wake-like" in nature. The pressures generated beneath fully attached flows are generated by a rather disordered field producing  $R_{pu}$  of the "boundary-layer type." Conversely, the pressures locally generated beneath a separated turbulent flow with large-scale structure, or by an ordered wake are of the "wake-like" type.

In Figures 8 and 9, the length scale  $y_f$  has been introduced, a consequence of the apparent wake-like mechanics of pressure generation. This cross-wake dimension is defined, as it was in Part 1, as the distance between intensity maxima, as these indicate the shear-layer location. For these beveled edges, the absolute maxima in  $u_{rms}$  occurs at or slightly downstream of Position H. Accordingly, for the knuckle edge  $0.7 < y_f/h < 0.8$ , and for the  $25^\circ$  rounded edge  $0.2 < y_f/h < 0.3$ ; the values chosen were  $y_f = 0.8 h$  and  $0.37 h$ , respectively. A curious similarity between the edges is that the streamwise extent of the separation appears to be of order  $2 y_f$  in both cases.

A comparison of the general characteristics of all the trailing edges that are discussed in this and the first part is given in Table 3. Although a full discussion of all the columns in the table will unfold in the succeeding sections of this paper, it will put the various flow types into perspective. Edges 1 through 5 generate tonal or nearly tonal pressures, depending on the Reynolds number involved, while Edges 3 through 6 generate fully random, or nearly periodic pressures, again, depending on the Reynolds number. As we shall see in Section 5, both the vortex-shedding pressures and the fully-random pressures fall into individual categories for which general dimensionless formats may be used to describe them. Spanwise integral length scales of the surface pressures,  $\Lambda_3$ , (see Section 6.2) were only measured on four of the six edges.

## 5. DETAILS OF THE PRESSURE SPECTRA IN REGIONS OF SEPARATED TRAILING EDGE FLOW

### 5.1 GENERALIZATIONS REGARDING THE STATISTICAL PROPERTIES OF THE SURFACE PRESSURE

Pressures at Position G on the  $25^\circ$  rounded edge and at Position F on the knuckle edge are typical of pressures in the separation zone. As indicated on the knuckle edge, the pressures through the separated zone are fairly constant. Figure 10 shows

the fully-developed flow, the correlations are typical of those measured elsewhere. In the near wake over and downstream of the knuckle, along a trajectory which approximately follows the locus of maximum velocity fluctuations, the correlations have a very different behavior. They have only one negative peak which occurs at increasingly later time delays as the anemometer probe location is moved downstream. As noted in Blake (1975), the maximum values of  $\overline{p u}$  occur at the location of maximum turbulence intensity. These correlations are normalized on  $U_\infty$  as they were in Figures 7, 12, and 15 of Part 1. Comparison of  $\langle p_F u \rangle$  in Figure 8 with the correlations in Figures 12 of Part 1 shows some qualitative similarities, but the magnitudes of the correlations over the knuckle edge are about one-half those over the  $45^\circ$  rounded edge. Furthermore, the pressure is correlated with  $-u$  in the near wake, but with  $\partial u / \partial t$  in the boundary layer flow. This latter conclusion is supported by the correlation function of Position B shown in Figure 8, which has a single maximum of  $\partial R_{pu} / \partial \tau$  occurring at  $\tau = 0$ . In the case of discrete vortex shedding downstream of blunt edges, the pressure is also correlated with  $-u$ , but that correlation remains significant for values of  $\vec{r}$  well downstream of the trailing edge.

Similar general behavior can be seen for the flow field of the  $25^\circ$  rounded edge in Figure 9. In the flow Position F, which is near the point of separation, the

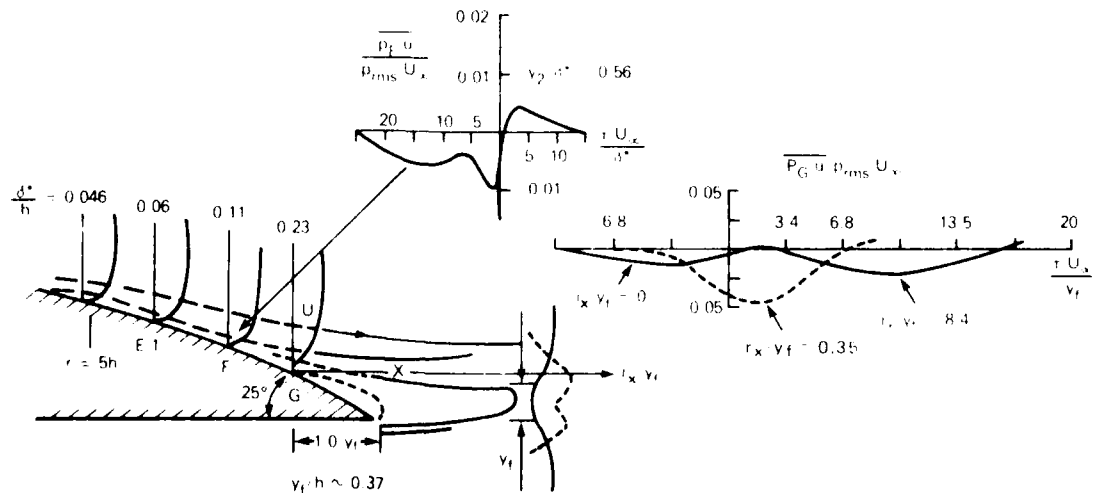


Figure 9 - Pressure-Velocity Correlations in the Near Wake and Separation Zone of the  $25^\circ$  Rounded Trailing Edge.  $r_x$  is Measured from Position G

#### 4. CONNECTION BETWEEN SURFACE PRESSURE AND LOCAL FLOW STRUCTURE

The regions of the shear flow which control the surface pressure are elucidated by pressure-velocity correlations, much as done previously in Part 1 for the tone generation at blunt trailing edges. Similar correlations have also been obtained for boundary layer flows by Willmarth and Woolridge (1963) and by Burton (1971). In the case of fully-developed turbulent boundary layers, correlation of the type

$$\langle p(\vec{y}, t) u(\vec{y}+\vec{r}, t+\tau) \rangle = \overline{pu}$$

where the brackets  $\langle \rangle$  denote a time-averaged product, and where  $p(\vec{y}, t)$  represents the instantaneous pressure at the wall location  $\vec{y}$ , suggest features of flow structure which control the pressure. Figure 8 shows the correlations obtained upstream of the edge in the region of the knuckle-trailing edge. Upstream of the edge, in

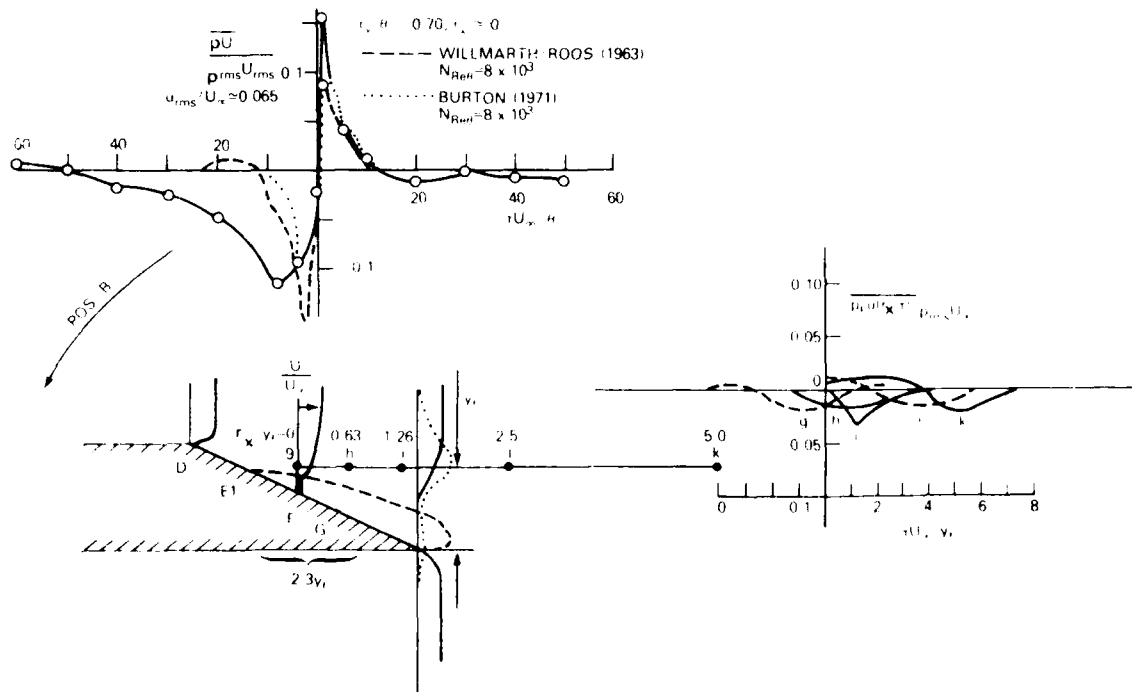


Figure 8 - Pressure-Velocity Correlation in the Near Wake and Separation Zone of the 25° Knuckle Trailing Edge

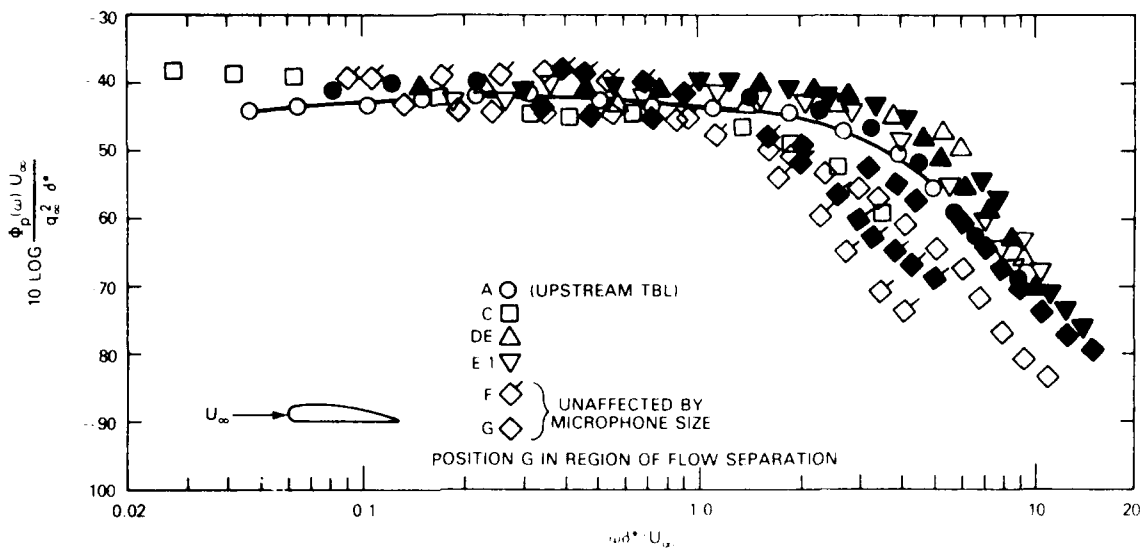


Figure 6 - Dimensionless Pressure Spectra on the 25° Rounded Bevel Trailing Edge. Open Points,  $U_\infty = 100$  ft/s; Closed Points  $U_\infty = 60$  ft/s

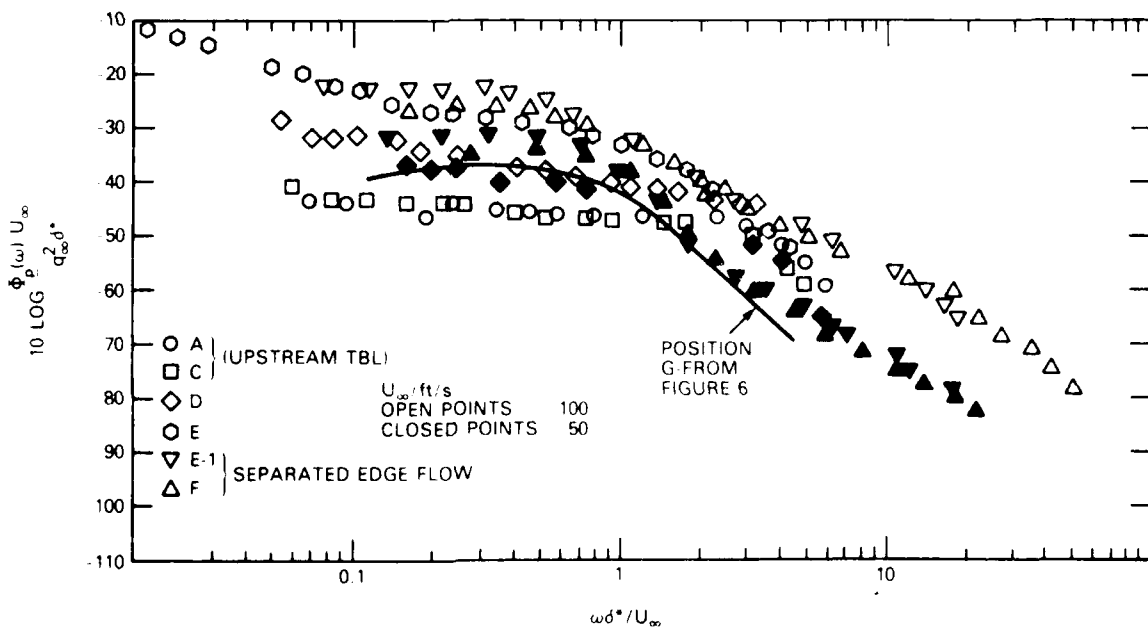


Figure 7 - Dimensionless Pressure Spectra of 25° Knuckle Trailing Edge

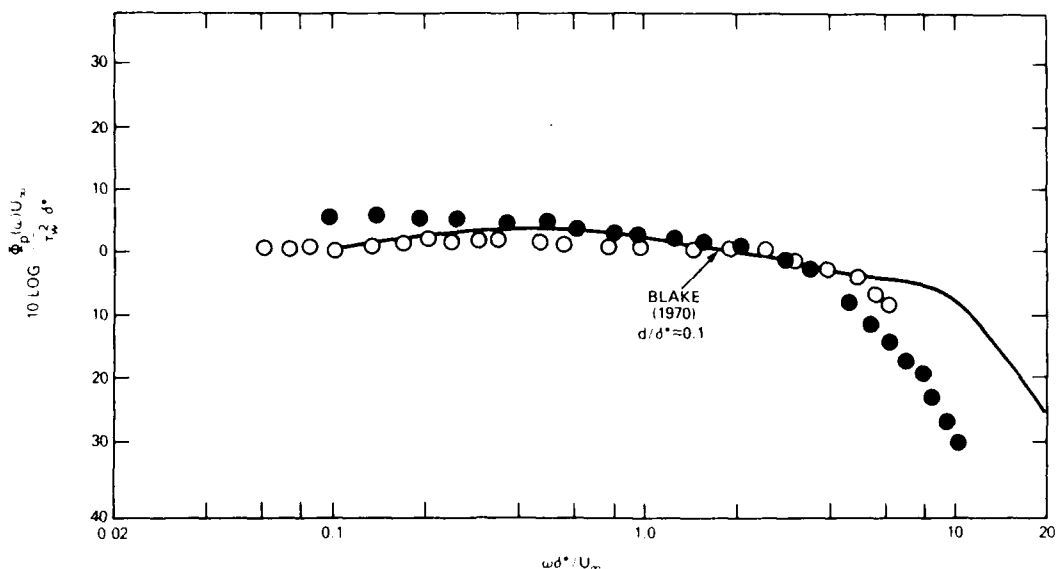


Figure 5 - Wall Pressure Spectral Densities at Position B Normalized on Local Wall Shear, Displacement Thickness, and  $U_\infty$ . Open Points  $U_\infty = 100$  ft/s, Closed Points  $U_\infty = 60$  ft/s

rounded edge, the pressures (Figure 6) have increasingly more low-frequency content as Position F is approached. From Positions E-1 to G, there is a systematic reduction in high frequency pressures; this reduction is highly significant especially when it is recalled that the values of  $\delta^*$  used also increase as the edge is approached. From Positions DE to G, there is a 5-fold increase in  $\delta^*$  given in Table 2. The autospectra of pressures on the knuckle edge, and given in Figure 7, show a marked lack of  $\delta^*$ -similarity with pressures upstream in the fully developed layer. The results do show clearly two distinctly different spectra, depending on location upstream in the standard boundary layer or in the zone of separated flow. Pressures at Position D are intermediate. It is notable, that throughout the separation zone, (i.e. at Positions E, E-1, and F) the dimensionless pressures are roughly the same, especially at low frequencies. The pressures are also much less intense than those on the edge with the rounded-off knuckle; however, pressure spectra at Positions E-1 and F on the knuckle edge are within the 6 dB and similarly shaped. This is a feature which will be reexamined in Section 5.1. On the nonbeveled, flat, side of the edge the spectrum levels were the same as those measured upstream, say at Position A.

typical of attached boundary-layer flow. This similarity implies that the length scales, or wave number spectrum, of the turbulence is determined by the local shear layer. The turbulence dynamics for the separation zones of both these trailing edges seem qualitatively quite similar; the rounded trailing edge, however, generates a much smaller scale separation zone. As seen by comparing turbulence intensities of Position H of both edges (Figures 2 and 3) the turbulence intensities of the shed shear layers differ by roughly a factor of 2.

### 3. AUTOSPECTRA OF PRESSURE FLUCTUATIONS: GENERAL FEATURES

For both 25° trailing edges, the frequency distribution and the spatial correlation characteristics of the surface pressures have been measured. In this section we compare these results to previously published wall pressure statistics in equilibrium boundary layers and to earlier measurements in adverse pressure gradients.

In Part 1, it was shown that the mean velocity profile and the streamwise turbulence intensities at a point were similar to those that are well known for equilibrium boundary layers. The autospectra of the wall pressures at Position B are shown in dimensionless form in Figure 5; normalization has been made so that

$$\frac{\overline{p^2}}{t_w^2} = \int_{-\infty}^{\infty} \frac{\phi_p(\omega) U_{\infty}}{t_w^2 \delta^*} d\left(\frac{\omega \delta^*}{U_{\infty}}\right) \quad (5)$$

The results compare favorably with those of Blake (1970) for a boundary layer on a smooth, flat wall. For  $\omega \delta^* / U_{\infty} > 4$  the results diverge because of the spatial averaging of small-scale disturbances over the microphone as discussed by Corcos (1963), an effect which becomes severe when  $\omega d / U_c > 2$ , where  $d$  is the diameter of the microphone and  $U_c \approx 0.6 U_{\infty}$ . In this case,  $d = 0.3 \delta^*$ . The spectra also diverge slightly at lower frequencies. This divergence was not observed in the earlier work (Blake 1970); in this case it may be due to the influence of leading-edge separation. Nonetheless, these spectra are considered representative of the equilibrium turbulent boundary layer and, therefore, they are a standard of comparison for spectra measured at points on the trailing edges.

Autospectra of pressures at these two trailing edges show progressive effects of flow separation. We first examine the gross trends of the pressures in the non-dimensional form typically used for turbulent boundary-layer pressure. On the

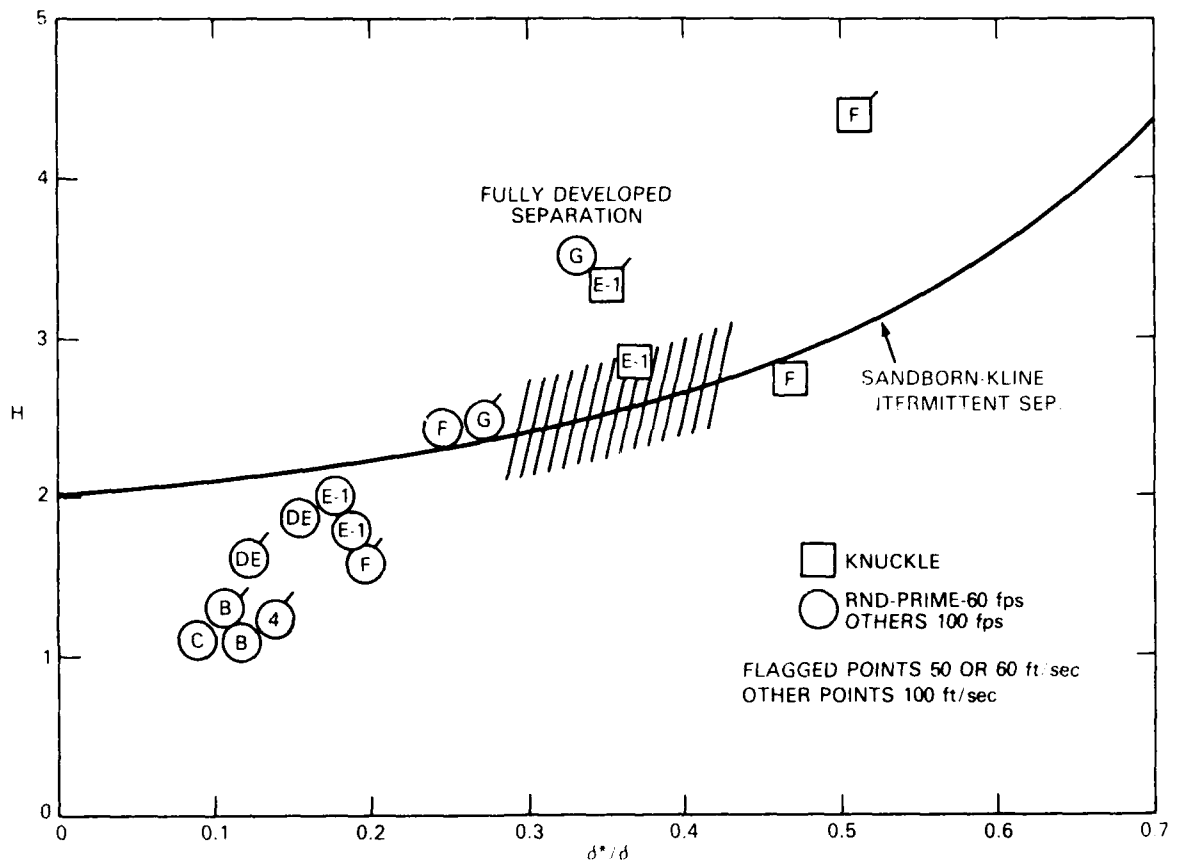


Figure 4 - Relationship Between Shape Factor and  $\delta^*/\delta$  for Various Positions on the Trailing Edges and for Sanborn and Kline's Experiment with Intermittent Separation

velocity. This suggests that the flow separation on the knuckle edge should be more intermittent as the wind speed is increased. As previously discussed, the mean turbulent velocity measurements on this edge indicate more turbulent activity at 100 ft/s than at 50 ft/s. For the knuckle edge however, Position E in Figure 2 is clearly the separation point.

The frequency spectra of the longitudinal velocity fluctuations near this trailing edge show the same property of local convection that has been shown for the boundary layers with vanishing pressure gradients. Spectra, normalized on the local velocity and boundary-layer displacement thickness are all similar to those that are

dimension of the local shear layer. Therefore, the frequency spectra of velocity fluctuations progressed to lower and lower frequencies as the flow passed along the bevel.

## 2.2 TURBULENT FLOW NEAR 25° ROUNDED-BEVELED EDGE

The surveys of the boundary layer and the static pressure distribution on the 25° rounded, beveled edge are shown in Figure 3. Downstream of Position F, the static pressure was nearly constant for speeds  $U_\infty = 60$  and 100 ft/s; however, the gradient of pressure was adverse for points downstream of 37 in. from the leading edge. The mean velocity slows markedly with distance downstream from this point, while the fluctuating velocities increase, reaching an apparent maximum in the vicinity of Positions H and I. The balance of mean momentum measured for the boundary layer on the edge (Blake (1975)) shows that separation occurs somewhere between Positions F and G. Table 2 gives the mean properties of the boundary layer on this rounded trailing edge. The favorable pressure gradient upstream from Position C causes the boundary layer to contract so that its momentum and displacement thicknesses decrease and the shape factor decreases to 1.14. Although a rough measurement of the mean momentum balance suggests that this is accompanied by an increase in  $C_f$  (compared to the values of local skin friction at Positions A and B, see also Figure 2), the survey of the boundary layer was not made with close enough streamwise separations for the calculated momentum integrals to give local values of  $C_f$  precisely. Flow visualization by oil streaks demonstrated that flow separation occurred just upstream from Position F. Distinct flow reversal was not clearly disclosed because the very low velocities near the wall were insufficient to cause significant movement of the oil. In drawing streamlines in Figure 3, Position F has been selected as the separation point.

The criterion for intermittent separation of Sandborn and Kline (1961) relates the local value of shape factor  $H^*/\delta$  to  $\delta^*/\delta$ . Their criterion for turbulent flow separation is compared to measured values on the trailing edges in Figure 4. At Position G, flow separation appears to be assured for both speeds of 60 ft/s and 100 ft/s, while, at Position F, separation is assured by this criterion only at 100 ft/s. Thus, as speed increases beyond 100 ft/s, the tendency for the existence of steady-state separation appears to be more persistent. Similarly-obtained parameters for the knuckle trailing edge are also shown as squared letters. In this case, by the Sandborn and Kline criterion, the values of Position H decrease with increasing

The normalized cross-spectrum magnitude  $\langle \rho(r_x, 0, \omega) \rangle$  represents a spatial correlation coefficient of pressures of the wave number  $k_c$  over a coordinate distance  $r_s$  along the chord. The cross spectrum shown indicates that the pressures are reasonably well correlated, over more than half of the bevel, especially at frequencies near  $\omega y_f / U_s = 1$ . The correlation scale of the pressure is  $k_c = \omega / U_c$  as shown by the further computation in Figure 14. Here,  $\langle \rho(r_x, \omega) \rangle$  is shown for a variety of speeds and microphone combinations. Especially, at speeds in excess of 50 ft/s, this function can be represented as a function of  $k_c r_x$ , primarily so the

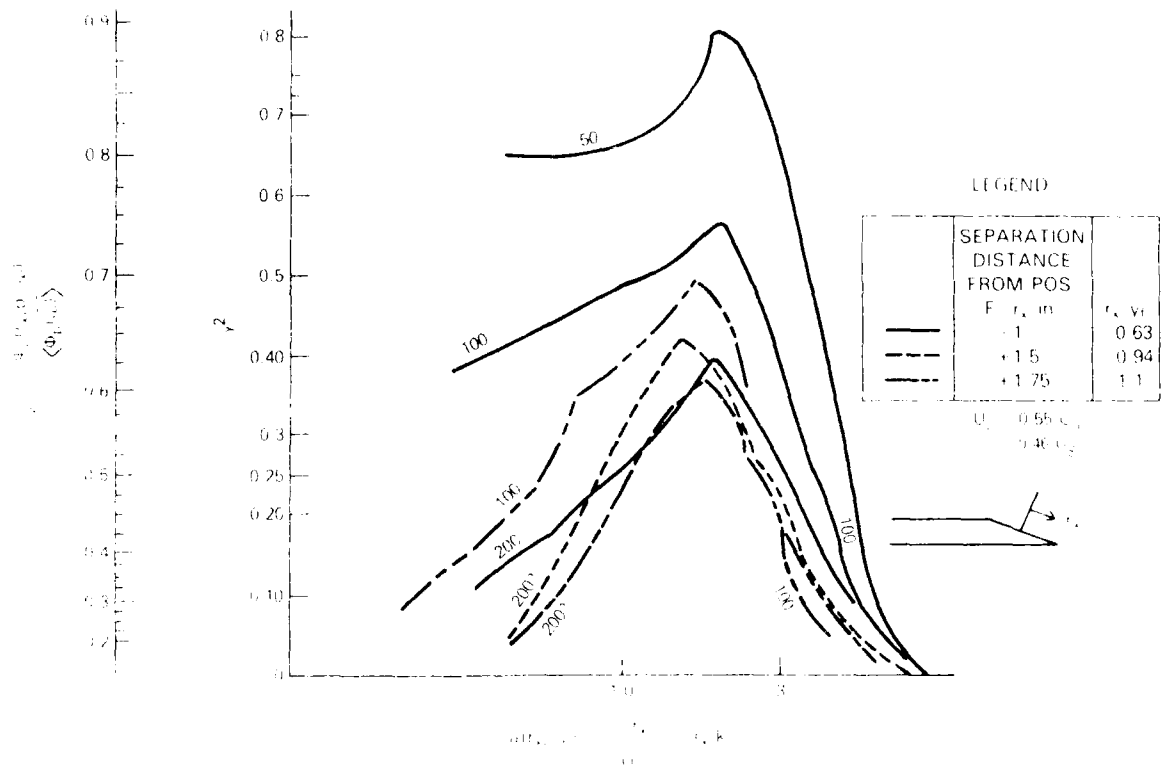


Figure 13 - Cross-Spectral Densities of Surface Pressure with Chordwise Distances in the Separation Zone of the 25° Knuckle Edge. The Reference Pressure is at Position F in the Center of the Bevel and 2 in. Upstream of the Apex of the Edge. Numbers Shown in the Figure Pertain to Flow Velocities of 50, 100, and 200 ft/s.

complete cross spectrum can be approximated in the form

$$\phi(r_x, \omega) \approx \phi(\omega y_f / U_s) \phi(\omega r_x / U_c) e^{i\omega r_x / U_c} \quad (7)$$

where  $\phi(\omega y_f / U_s)$  is shown in Figure 10. As indicated in Figure 13, the eddy lifetime of the most correlated turbulence in the bevel area appears to be of such duration that eddies retain their identities over streamwise separation distances  $\Delta r_x$  upstream and downstream of the center of the bevel (Position F) of order  $\Delta r_x \approx 2/k_c$ . This is confirmed by the peak of large correlation at  $\omega r_x / U_c \approx 2$  shown in Figure 14 for all free-stream speeds. For the characteristic frequency,  $\omega y_f / U_s = 1$  and  $U_c = 0.46 U_s$ , this means that  $\Delta r_x \approx 2 (0.46) y_f$  and a measure of the total extent in a Lagrangian reference frame of correlated existence of eddies responsible for this frequency is roughly  $2y_f$ , or the entire length of both the bevel and zone of separation. Thus, the characteristic eddy field is formed just downstream of the knuckle and convects at a speed  $U_c \approx 0.55 U_\infty$  (or  $0.46 U_s$  in this case) past the apex of the edge with little change in its statistical identity. As we saw earlier, the trajectory of the eddy center roughly corresponds to the  $0.35 U_0$  streamline in Figure 2, i.e., near the zone marked (---) as discussed in Section 2.1. Noting that the local free-stream velocity  $U_0$  is approximately the same as  $U_s$  over the separated flow =  $0.46 U_0$ , the convection velocity of  $0.55 U_\infty$  suggests that the vortex moves slightly faster than the streamline, with average velocity  $0.35 U_0$ . As suggested by the pressure velocity correlations in Figure 8, the field continues its convection downstream of the apex of the edge with a diminishing influence in creating the surface pressures.

### 5.3 WALL PRESSURE STATISTICS ON ROUNDED-BEVEL TRAILING EDGES

Just upstream of separation region of the rounded edge (i.e., upstream of Positions F and G in Figure 3), the boundary layer is controlled by a strong adverse pressure gradient. The longitudinal cross-spectral densities of surface pressures in this region, defined by Equations (3) and (4) and shown in Figure 15, have a rather erratic behavior. Convection velocities could be computed from the measurements because the phase  $\alpha(r_x, \omega)$  increased systematically with frequency and streamwise separation of the microphones. For locations nearest the separation point, Figure 16 shows that the pressure convection velocity slows down to roughly  $0.55 U_\infty$ .

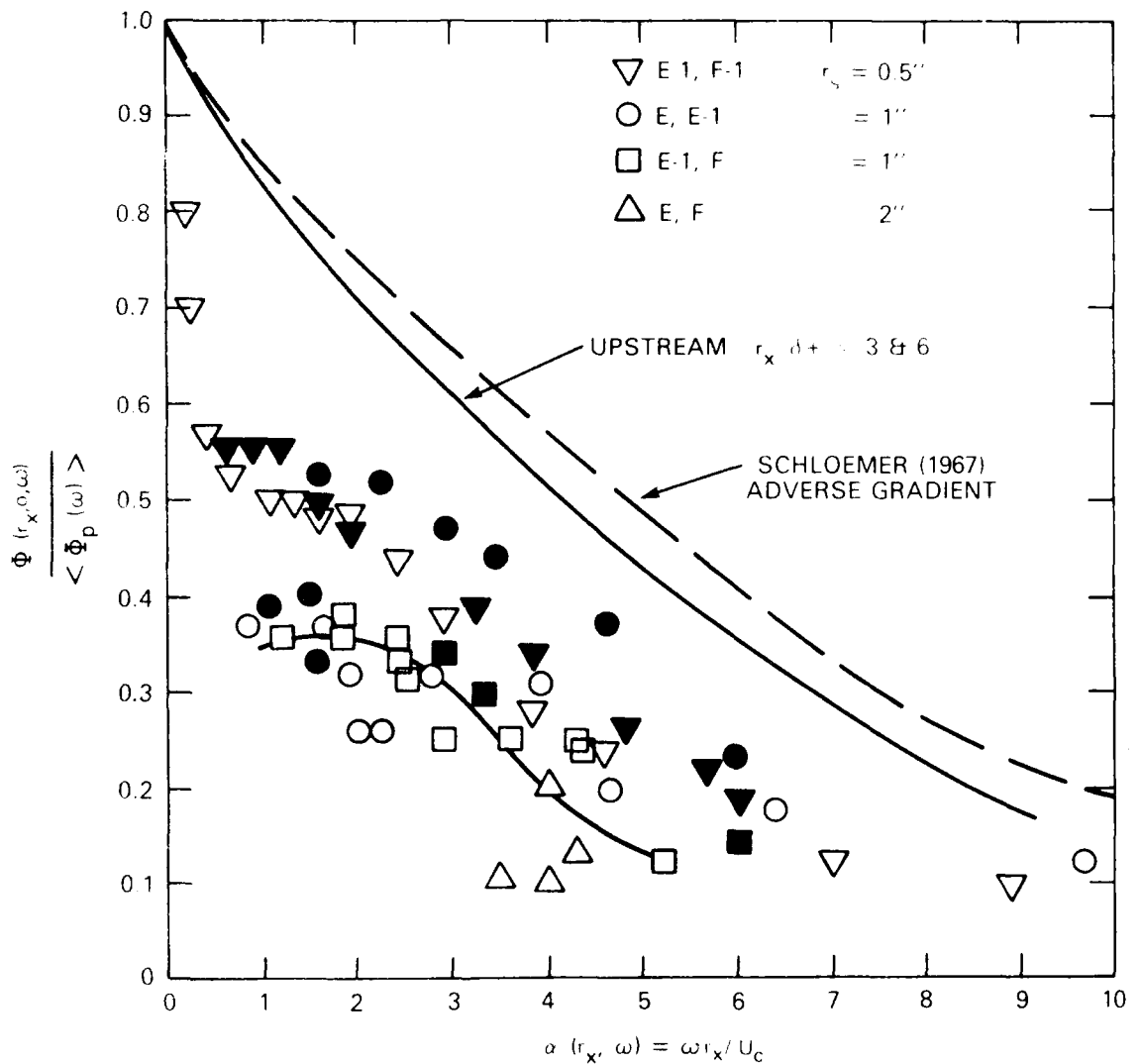


Figure 15 - Normalized Longitudinal Cross-Spectral Density Magnitudes of Fluctuating Surface Pressures on 25° Rounded Bevel Edge

The considerable lack of spatial homogeneity of the flow in this region of this trailing edge makes in-depth interpretation of these data impossible. There is a suggestion by the Positions E-1 to F cross-spectra that, as the separation zone is approached,  $\Phi(r_x, 0, \omega)$  approaches the form shown in Figure 14. The most significant correlation between these positions exists over the range of  $\alpha = \omega r_x / U_c$  between 1 and 2. Since  $\delta^* = 0.7$  to  $0.9 y_f$  for these locations, and since  $U_c / U_s = U_c / U_\infty = 0.55$

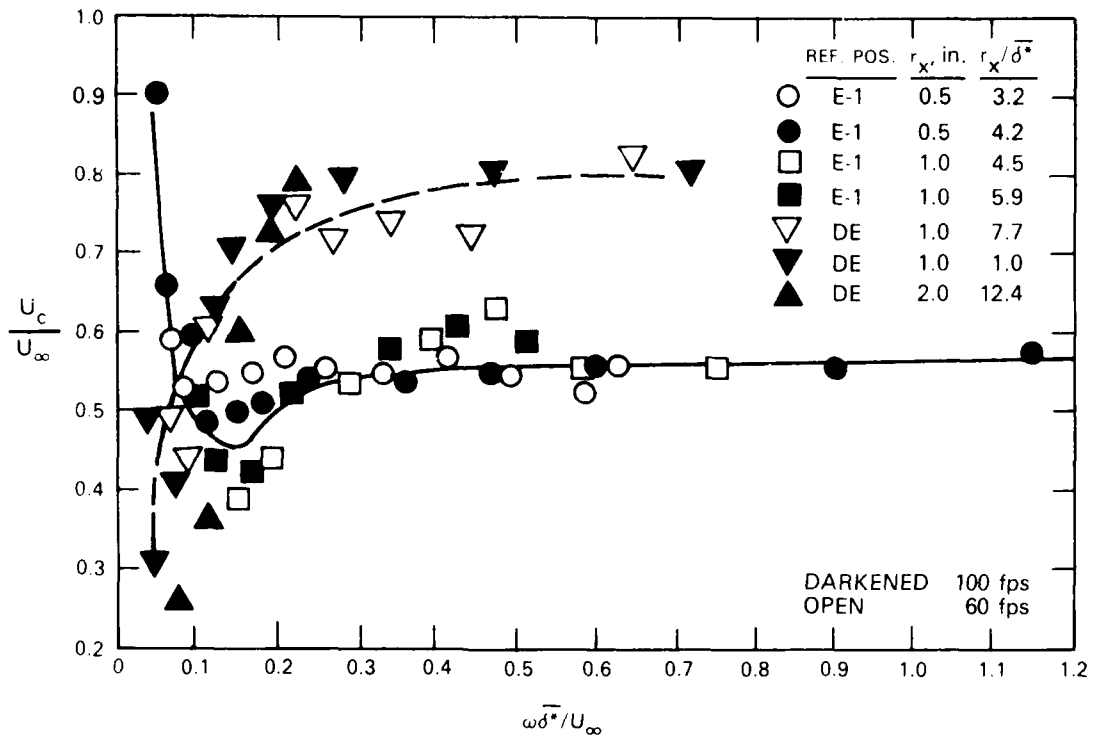


Figure 16 - Wall Pressure Convection Velocities at Two Positions on the Strut with 25° Rounded Bevel Trailing Edge. All Values of  $r_s$  are Toward the Edge, and  $\delta^*$  is the Average Value of  $\delta^*$  for the Two Measurement Locations

the Lagrangian correlation distance  $r_x$  for disturbances of the characteristic frequency  $\omega y_f / U_s \approx 1$  is between  $0.55 y_f$  and  $1.1 y_f$ , just as in the case of the knuckle bevel. Thus, in comparison to the knuckle bevel, the rounded bevel appears to generate a qualitatively similar flow but with a less intense pressure field in its less extensive separation zone. The leading edge of this separation zone is not as well defined for this edge as it is for the knuckle.

## 6. IMPLICATIONS FOR AERODYNAMIC SOUND GENERATION AND SPANWISE PRESSURE CORRELATIONS

### 6.1 ELEMENTS OF THE THEORY OF AERODYNAMIC SURFACE PRESSURES AT TRAILING EDGES

The separated flow over the trailing edges discussed in this paper has been shown to be essentially dominated by locally generated, convected eddy fields with

no new disturbances being generated as a result of near-wake shear-layer instabilities. The surface pressures on the knuckle bevel have been shown to be nearly constant throughout the separation zone, or perhaps slightly decreasing, as the apex of the trailing edge is approached from the upstream flow direction. Correlations between the surface pressures on opposite sides of knuckle-bevel trailing edges were unmeasurable within the available averaging time of the instrumentation which, in work subsequent to Blake (1975), permitted measurement of correlation coefficients of 0.03 between transducers on opposite sides of the foil and situated 1/4-in. upstream of the apex of the edge. Further, the pressure spectrum levels beneath the attached boundary layer on the opposite side are essentially the classically reported values. Therefore, the separated flow may be regarded as a one-sided turbulent field convected past the apex. Interaction between the shear layers was, therefore, sufficient to maintain a tangential mean flow at the apex and the interaction did not generate any growing disturbances in the downstream wake. This is in marked contrast to the shear-layer interactions responsible for the generation of tones at the blunt trailing edges.

The noise theory of Howe (1978), which applies to the generation of continuous-spectrum aerodynamic sound and surface pressures in cases such as those described here, is summarized below. It is used to account for the observed differences in surface pressure in terms of deduced vortex structure. Postulating that the source region above and downstream of the edge constitutes a region of nonvanishing  $\nabla \cdot (\vec{\omega} \times \vec{U})$ , where  $\vec{\omega}$  and  $\vec{U}$  are the aerodynamic vorticity and velocity fields, respectively; and where  $\nabla$  is the divergence operator, Howe obtains an expression for the surface pressures (on  $y = 0$ ) and at a location  $(x, z)$  on the surface (illustrated in Figure 17) and time  $t$  which is

$$p_s(x, z, t) = \frac{-\rho_0}{2} \int_0^x \int_{-\infty}^{\infty} \int_{-\infty}^{\infty} dy' dk_1 dk_3 d\omega \int_0^{\infty} dy \left\{ 1 + \text{sgn}(y) \text{Erf}(\sqrt{ix}(k_1 + i\epsilon)) \right\} \left\{ \left( 1 - \frac{U_w}{U_c} \right) \vec{u} \cdot (\vec{\omega} \times \vec{U}_c) \right\} \frac{e^{i\sqrt{k_0^2 - k^2} y'}}{\sqrt{k_0^2 - k^2}} e^{i(\vec{k} \cdot \vec{x} - \omega t)} \quad (8)$$

$U_c$  is the average local convection velocity of the eddies at a distance  $y'$  from the surface,  $\text{sgn}(y) = +1$  for pressures on the same side of the surface as the flow  $y = 0^+$  and  $\text{sgn}(y) = -1$  for pressures on the opposite side ( $y = 0^-$ ). The error function,

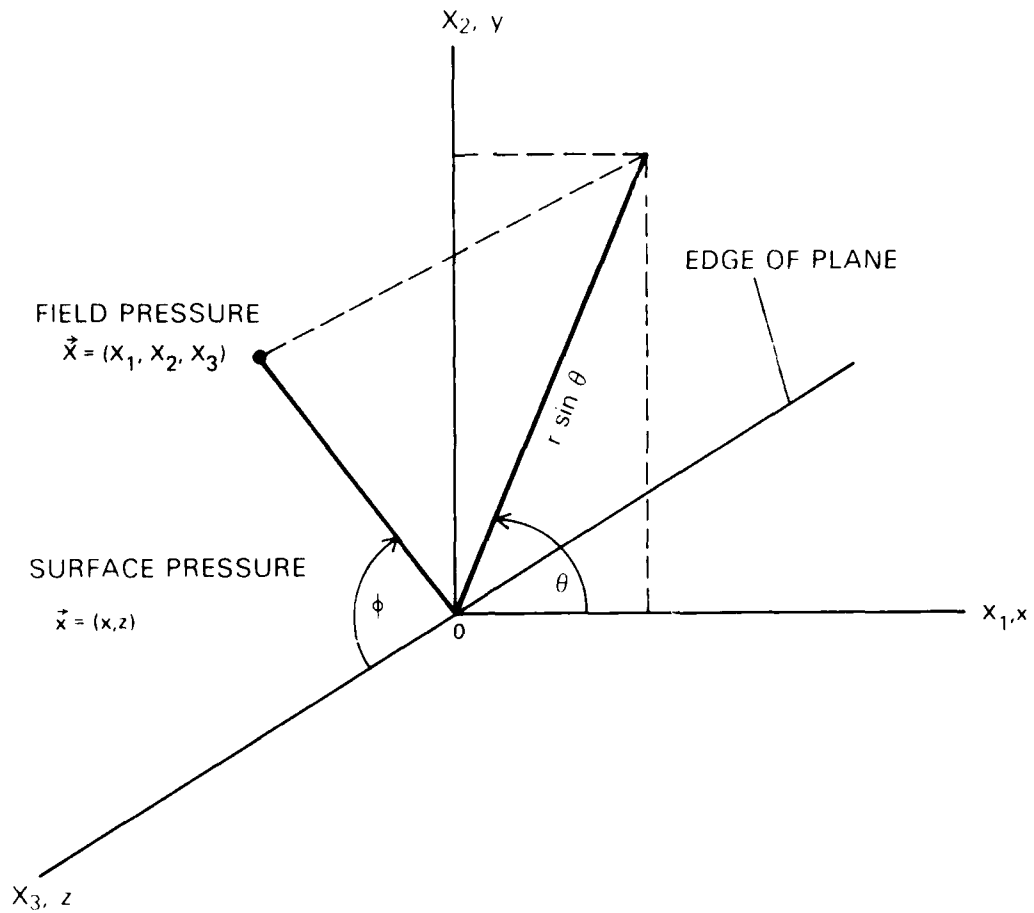


Figure 17 - Geometry and Coordinate System for Trailing Edge Problems

$\text{erf}(\xi)$  has the asymptotic values given by Equation (19) in Part 1. The complex wave numbers are

$$\vec{\mu} = (k_x, -\sqrt{k_o^2 - k_z^2}, k_z),$$

$$\vec{k} = (k_x, k_z)$$

$$\kappa = (\text{sgn } k_o) \sqrt{k_o^2 - k_z^2}, \quad k_o > k_z$$

$$= i \sqrt{k_z^2 - k_o^2}, \quad k_z > k_o$$

is the acoustic wave number,  $\omega/c_0$  and  $\vec{\omega}$  is the generalized Fourier transform of the source vorticity defined as

$$\vec{\omega}(\vec{k}, y', \omega) = \frac{1}{(2\pi)^3} \iiint_{-\infty}^{\infty} e^{-i(\vec{k} \cdot \vec{x} - \omega t)} \vec{\omega}(\vec{x}, t) dx dz dt \quad (9)$$

In the theory, the complete Kutta condition was evoked at the edge to remove any possibility of a discontinuous pressure between the upper and lower surfaces. This insures tangential flow at the apex, accounts for the error function, and for the presence of  $U_w$ , which is a convection velocity of eddies in the wake. These eddies are generated in the wake in just sufficient quantity to insure parallel flow at the edge. In writing down Equation (8), the general result has been specialized to a flow vector perpendicular to the edge, and an eddy convection Mach number less than unity.

Pertinent assumptions made in the derivation of Equation (8) for our purposes are:

1. The eddy field is frozen during the time that it translates past the edge.
2. The eddy convection velocity  $U_c(y')$  is equal to the local mean velocity in the boundary or shear layer.
3. The wake vorticity created in response to the eddy-edge interaction via the imposition of the Kutta condition is concentrated in a thin sheet,  $\delta(y)$ , and is convected in frozen fashion at velocity  $U_w$ . The velocities  $U_c(y)$  and  $U_w$  are parallel to the wall.
4. The source term  $\vec{\omega} \times \vec{U}$  is such that  $\vec{\omega} \times \vec{U} \approx \vec{\omega} \times \vec{U}$ . This requires that

$$\nabla(\vec{\omega} \times \vec{U}) \gg \nabla \frac{d\bar{U}_1}{dy} \vec{k}_z \times \vec{u}$$

where  $\vec{k}_z$  is the unit vector parallel to the edge and  $\vec{u}$  is the fluctuating velocity vector. If the above inequality does not hold, it will affect the results through the form of the shed vorticity arising from imposition of the Kutta condition. As shown by Crighton and Leppington (1971) a half-plane is a suitable approximation to a wedge as long as the included angle is small enough; by their theory a  $25^\circ$  included angle wedge yields less than 10% change in the theoretical dependence of radiated sound on Mach number with the half-plane.

Equation (8) is too complicated for our purposes so it will be recast to give a spectrum function for the surface pressures. The definition of the vorticity

spectrum of the type given by Equation (9) is approximately valid as far as the trailing-edge noise is concerned because of the limited range of  $k_c r_x$  over which the pressures are shown to be correlated in Figure 13, compared to the extent ( $k_c \Delta x$ ) over which the vorticity field exists. The vorticity field, as indicated by the behavior of the surface pressure, is, thus, approximately locally homogeneous. Thus, in relation to the acoustical effect of edge scattering, any noise due to the upstream vortex generation process is assumed negligible.

The cross spectrum of surface pressures, referred to a coordinate  $\vec{x}$  with separation  $r$  is  $\phi_p(\vec{x}, \vec{r}, \omega)$  and it may be regarded as having a spanwise wave number spectrum

$$\phi_p(\vec{x}, r_x, k_z, \omega) = \frac{1}{2\pi} \int_{-L_3/2}^{L_3/2} e^{-ik_z r_z} \phi_p(\vec{r}, \omega) dr_z \quad (9)$$

as long as the field is statistically homogeneous along the span,  $L_3$ . The span also must exceed the spanwise correlation length  $2\Lambda_3$ , defined by Equation (9) of Part 1. This assumption, therefore, also applies to the vorticity field. Accordingly, Equation (8) yields a spectral density at Position  $x$  with zero streamwise separation (i.e.,  $r_x = 0$ )

$$\begin{aligned} \phi_p(x, k_z, \omega) = & \frac{1}{4} \int_0^\infty dy \int_0^\infty dy' \rho_0^2 [U_c - U_w]^2 \int_{-\infty}^\infty e^{-k_x(y+y')} \\ & |1 + \operatorname{sgn}(y) \operatorname{Erf}(\sqrt{ix}(k_x + k_z))|^2 \phi_{\omega_3\omega_3}(k_x, k_y, \omega, y, y') dk_x \end{aligned} \quad (10)$$

where  $\phi_{\omega_3\omega_3}$  is the spectrum of the vorticity field. The auto spectral density of the pressure at Position  $x$  is given by an integral of  $\phi_p(x, k_z, \omega)$  over all spanwise wave numbers,  $-\infty < k_z < \infty$ . The spanwise correlation length of the pressure is related to its wave number spectrum by

$$\Lambda_3 = \pi \lim_{k_z \rightarrow 0} [\phi_p(x, k_z, \omega) / \phi_p(x, \omega)] \quad (11)$$

Further simplifications of Equation (10) are possible. We have argued above that the streamwise correlation of wall pressure follows approximately the behavior

shown in Figure 14, and is thus confined to a limited range of  $k_c r_x$ . This indicates that the corresponding wave number spectrum of the vorticity will be confined to a region  $\Delta k$  centered on the convection wave number  $k_c$ . If we model the vorticity spectrum using a vortex sheet of the type introduced by Equations (13) and (15a) in Part I, then the parameters of this spectrum may be collected in the groupings given by

$$\phi_{\omega_3 \omega_3}(k_x, k_z, \omega, y, y') \sim \overline{u_m^2} \phi(\omega, k_x, k_z) (\omega y_f / U_c)^2 \delta(y - y_0) \delta(y - y') \quad (12)$$

where  $\overline{u_m^2}$  is the local maximum value of streamwise velocity fluctuation and  $y_0$  is the trajectory of the vorticity. The term  $\phi(\omega, k_x, k_z)$  is a spectrum function normalized on  $\overline{u_m^2}$  and peaked about  $k_x = k_c$  as described above.

This function is roughly independent of  $k_z$  as long as  $k_z < \pi/l_3$  and systematically decreases as  $k_z > \pi/l_3$ . To the extent that  $\omega/U_c \gg \pi/l_3 \gg k_0$ , the argument of the error function in Equation (10) thus simplifies to  $k_c$ . The error function also may now be dropped in accordance with its being small-valued for  $k_c x > 1$ . The surface pressure spectrum then behaves parametrically as (assuming  $U_c \propto U_w \propto U_s$ )

$$\phi_{pp}(x, \omega y_f / U_s) \sim \rho_0^2 \overline{u_m^2} U_s^2 e^{-2k_c y_0} \phi(\omega y_f / U_s, x) \quad (13)$$

for positions far enough upstream from the apex that  $k_c x \gg 1$ . The term  $\phi_{pp}(x, \omega y_f / U_s)$  is a dimensionless spectrum function. Equation (13) accounts for part of the observed level difference between the surface pressure at Position F on the knuckle edge and at Position G on the round edge that is shown in Figure 10. Since  $k_c y_0 = (\omega y_f / U_s) \cdot (U_s / U_c) \cdot (y_0 / y_f)$ , and since at the respective positions  $y_0 / y_f = 0.4$  and  $0.6$  for the knuckle (K) and round (R) edge, respectively, the ratio of surface pressures on the two edges is given in order of magnitude.

$$10 \log \left\{ \frac{[\phi_{pp}(x, \omega y_f / U_s)]_K}{[\phi_{pp}(x, \omega y_f / U_s)]_R} \right\} \\ \approx 10 \log \frac{(\overline{u_m^2})_K}{(\overline{u_m^2})_R} \cdot \frac{(U_s)_K^2}{(U_s)_R^2} \cdot \exp \left\{ -2 \left( \frac{\omega y_f}{U_s} \right) \left[ \left( \frac{U_s y_0}{U_c y_f} \right)_K - \left( \frac{U_s y_0}{U_c y_f} \right)_R \right] \right\}$$

$$\begin{aligned}
&= 10 \log \left\{ (1.7)^2 \left[ \frac{1.28}{1.2} \right]^2 \left[ \frac{1.28}{1.2} \right]^2 \exp \left\{ -2 \frac{\omega y_f}{U_s} \left[ \frac{0.6}{0.54} - \frac{0.4}{0.46} \right] \right\} \right\} \\
&\approx 6 - \log \left[ e^{-0.44 (\omega y_f / U_s)} \right] \\
&= 8 \text{ at } \omega y_f / U_s = 1
\end{aligned}$$

The factors in the exponential for the knuckle and round edge are determined by  $U_c/U_s = 0.46$  and  $0.54$  at  $y_o/y_f = 0.41$  and  $0.6$ , respectively. The distance  $y_o$  from the surface is the location of the turbulence maximum. Of the 12 dB difference in spectra shown in Figure 10, therefore, 8 dB can be accounted for by a reduced intensity shear layer and a greater displacement of  $y_o$  relative to  $y_f$ .

The presence of the error function in Equations (8) and (10) account for pressure contributions due to local scattering at the trailing edge. Subject to the conditions  $k_c \gg \pi/\Lambda_3 \gg k_o$ , these effects are confined to the region well within an aerodynamic wavelength such that  $k_c y_o < 1$ ; a perception of how close this region is to the apex can be deduced from the phase information in Figure 13 which shows  $\alpha = k_c x$ . For  $\omega y_f / U_s \geq 1$ , nearly all measurement locations were outside the region affected by the error function. A similar restriction holds for the measurements taken on the rounded bevel edge. Thus, dropping that function in discussing present data is justified. The work of Brooks and Hodgeson (1981) does examine this behavior at very thin edges without separation.

## 6.2 DEDUCTIONS REGARDING AERODYNAMIC SOUND

In Part 1, an expression was derived that related the radiated sound pressure to the autospectrum and the spanwise correlation length of surface pressures in the case of tonal sound generation. For continuous-spectrum sound, similar relationships have been derived by Howe (1978), Chandiramani (1974), and Chase (1975). Howe's (1978) result for the spectral density of the far-field radiated sound due to aeroacoustic scattering from the rigid half plane is written

$$\phi_{\text{rad}}(\hat{X}, \omega) = \frac{1}{8\pi^2} \sin^2 \theta \left| \sin \theta \right| m_c \frac{2L\Lambda_3}{r^2} v(\omega) \quad (14)$$

where  $\rho(\omega)$  represents the integrated influence of the entire vortical source region, and  $m_c$  represents the average convection Mach number of turbulence past the edge,  $U_c/C_0$ . The function  $\rho(\omega)$  is related to the spectral density of the surface pressure by

$$\rho(\omega) = \frac{\pi}{\Lambda_3} \phi_p(x, k_z = k_0 \cos \phi, \dots) \quad (15)$$

when  $k_c x = \omega/U_c \gg 1$ . Since, as proposed above,  $\pi/\Lambda_3 \gg k_0$ , Equation (15) reduces to

$$\rho(\omega) = \phi_p(x, \dots) \quad \omega/U_c \gg 1 \text{ and } m_c = k_0/k_c \ll 1 \quad (16)$$

using Equation (11). For Equation (14), the half plane lies in the  $X_2 = 0$  plane, the edge lies along  $X_1 = 0$ ;  $X_2 = 0$ ; as shown in Figure 17, coordinates of the acoustic field points are  $X_1 = r \sin \phi \cos \theta$ ;  $X_2 = r \sin \phi \sin \theta$ ;  $X_3 = r \cos \phi$ . Equation (14) with Equation (16) is analogous to Equation (27) of Part 1, and it has been verified experimentally by Brooks and Hodgeson (1981).

The important parameters used to describe the sound pressure in each case are the surface pressure spectra shown in Figure 10, the convection velocity of the vorticity, and the spanwise correlation length to be described below for the beveled-edge flows.

Spanwise cross-spectral densities at Position F-1 on the rounded edge are shown in Figure 18, and are typical of those to be expected beneath attached flow in adverse pressure gradients. The correlation length indicated by these measurements is a function of frequency, since the length scale determining the cross spectrum is  $U_c/\omega$ . For this edge, according to the definition used in Equations (9) and (10) of Part 1

$$\Lambda_3 \approx 1.2 U_c/\omega = 1.2/k_c \quad (17)$$

Fully developed boundary layers have a slightly longer correlation length at a given value of  $k_c$ , as indicated in Figure 18.

More interesting behavior is shown by the spanwise functions beneath separated flow for Position F of the knuckle edge as shown in Figure 19. Here the functions have an envelope that is bounded closely by a shape such as that drawn in Figure 18;

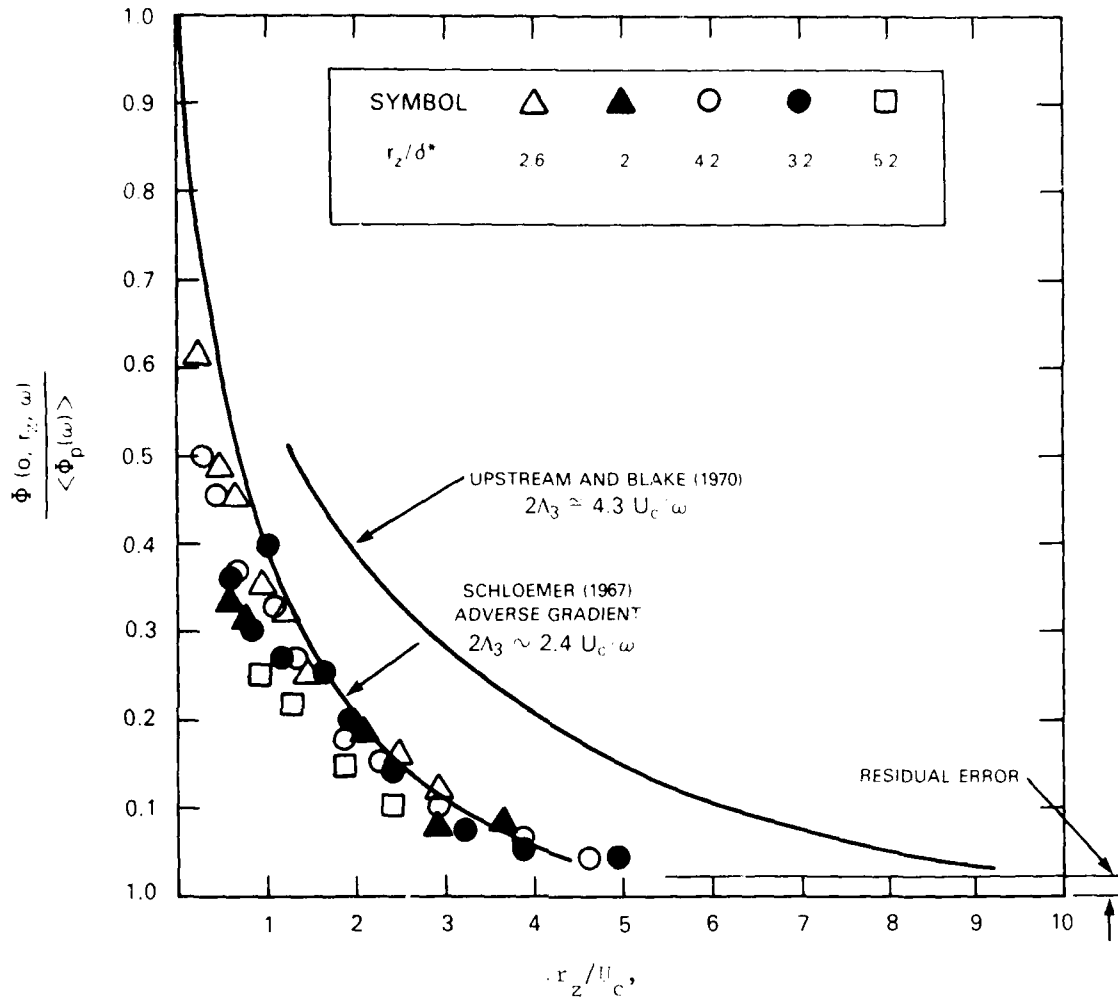


Figure 18 - Normalized Lateral Cross-Spectral Density Magnitudes of Fluctuating Surface Pressure at Position E1 on 25° Rounded Bevel Edge. Open Points,  $U_m = 100$  ft/s; Closed Points  $U_c = 60$  ft/s,  $U_c \approx 0.55 U_m$ .

for this envelope

$$\Lambda_3 \approx 2.2 U_c/\omega \quad (18a)$$

which is actually similar to that existing in attached boundary-layer in zero pressure gradient. At small values of  $r_z/U_c$ , the cross spectrum flattens; for each value of  $r_z$ , the value of  $\omega/U_c$ , at which  $\phi(r_z, \omega)$  departs from the relatively smooth

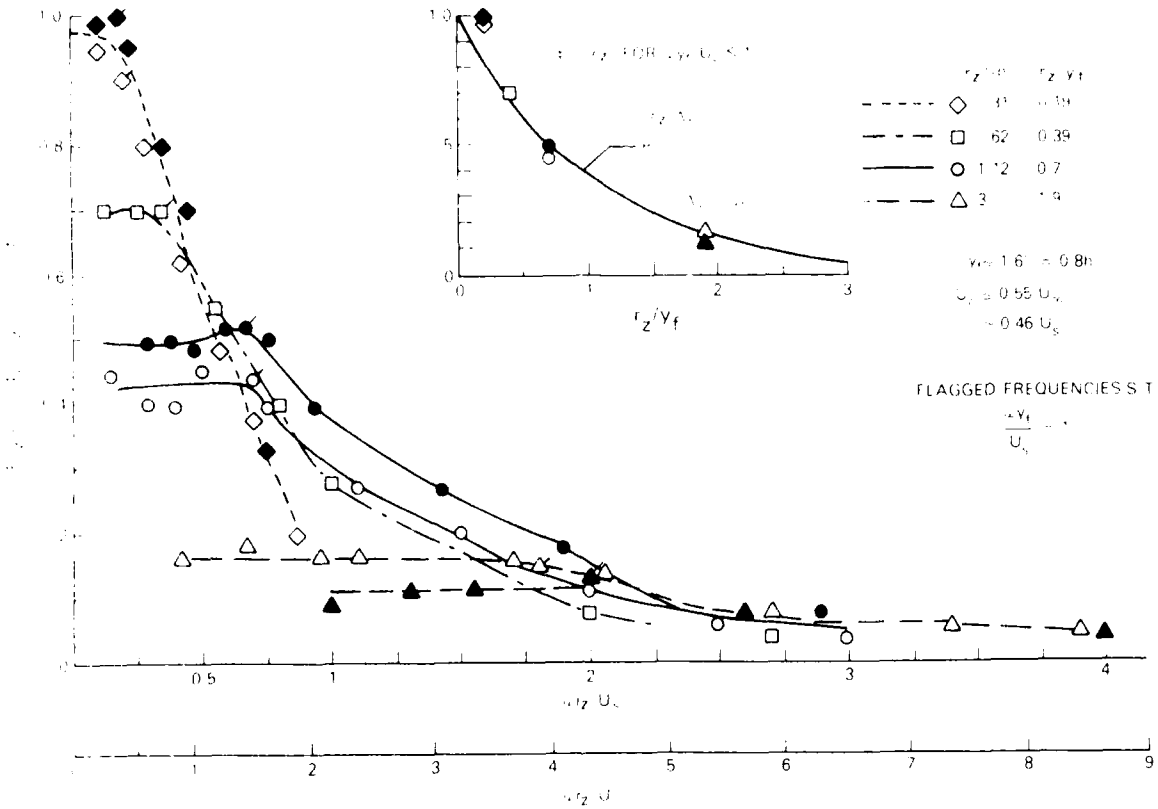


Figure 19 - Cross-Spectral Densities of Pressures in the Zone of Separated Flow on the 25° Knuckle Trailing Edge. Flagged Points Denote Frequencies for Which  $\omega y_f / U_s = 1$ . The Inset Gives the Correlation of Low Frequency  $\omega y_f / U_s < 1$  Pressure Which are Shown as Plateaus at Small Values of  $\omega r_3 / U_c$  in the Main Figure.

exponential-like behavior, corresponds to  $\omega y_f / U_s = 1$ . These points are marked by a flag (see Figure 19). The inset shows  $r_{p_3}(z)$  for a sample of frequencies, such that  $\omega y_f / U_s < 1$ , as a function of  $r_3 / y_f$ . The knuckle bevel appears to generate two spanwise scales which depend on frequency, thus:

$$\lambda_3 = y_f \quad \omega y_f / U_s \geq 1 \quad (18b)$$

and from Equation (18a) with  $U_c / U_s = 0.46$ , and

$$\lambda_3 = y_f \left( \frac{\omega y_f}{U_s} \right)^{-1} \quad \omega y_f / U_s < 1 \quad (18c)$$

The value of  $\Lambda_3$  for low frequency contrasts to the values of  $3.5 y_f$  for the blunt trailing edges with tones. These integral scales and the spectra of Figures 10 and 12 may be used to predict aerodynamic sound from airfoils fitted with these edges. For nonseparated flow, values lying between that given in Equation (18) and about double that value (with  $U_c \approx 0.6 U_\infty$ ) may be used. For separated flow values,  $\Lambda_3$  given by Equations (18b) and (18c) may be used.

## 7. CONCLUSIONS

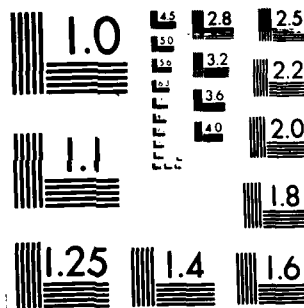
### 7.1 GENERAL COMMENTS

A few general statements may now be made concerning the trailing edge flows of lifting surfaces. The turbulent flows off thin airfoils with sharp trailing edges are not expected to produce tones, as measurements of Chevray and Kovaszny (1969) have shown. Practicalities often dictate the necessity that some finite trailing edge thickness may produce tones or enhanced continuous spectrum pressures. Such behavior has been observed in the sounds radiated by helicopters such as presented by Leverton (1973). Even when the edge is beveled at such a small angle as to prevent the generation of an aerodynamically unstable vortex sheet, large-scale motions that have many aerodynamic features qualitatively in common with discrete vortex shedding will be generated. Trailing edge pressures, however, which develop from the vortex street formation on the one hand, or from the less-ordered large-scale separation on the other, will generate pressure fields of very different magnitudes, though the frequency spectrum of each type of pressure will be describable in terms of  $y_f$  and  $U_s = U_\infty \sqrt{1 - C_{p_s}}$ ;  $y_f$  is the cross-wake dimension at the end of the vortex formation zone, or near the apex of the edge in the case of continuous-spectrum pressures, and  $C_{p_s}$  is the static-pressure coefficient in the separation zone.

### 7.2 MINIMUM REYNOLDS NUMBER FOR PERIODIC WAKE GENERATION

Periodic, or nearly periodic, disturbances were generated on the blunt edge and on the  $45^\circ$  rounded edge above a certain onset speed, as described in Part 1. A low amplitude, nearly periodic, disturbance was also observed in the near wake of the  $45^\circ$  rounded edge at the highest test velocity available. Although classified as nonsinging in this and previous work of Beekstedt and Olberts (1969), even this relatively thin edge may generate a periodic disturbance above some suitable





MICROCOPY RESOLUTION TEST CHART  
NATIONAL BUREAU OF STANDARDS 1963-A

Reynolds number, as shown in Part 1, Figure 22. Using a definition of Reynolds number based on the wake parameter  $y_f$ , these limiting speeds corresponded to  $U_\infty y_f / \nu = 5.2 \times 10^4$  for the 25° edge,  $3.3 \times 10^4$  for the 45° edge, and roughly  $10^3$  for the blunt edge. Length scales have been taken as  $y_f = 0.37 h$  and  $0.5 h$  for the 25° and 45° round edge, respectively, and  $0.8 h$  for the blunt edge. Note the consistent increase in onset Reynolds number as the apex angle of the edge is decreased. Since the nearly periodic disturbance for the 25° rounded edge was observed in the wake and in the surface pressures only at the maximum speed capability of the facility, it, therefore, could not be studied in any detail.

Although a universal Strouhal number based on a geometric length of the trailing edge has not been isolated in this study, an approximate dimensionless frequency is  $\omega_s y_f / U_s \approx 1$ . The length  $y_f$  for the blunt and rounded-beveled edges has been given above. Other dimensionless forms have been proposed by other authors for specific trailing-edge forms, and they may give frequencies more precisely in those cases; however, none appear to have both a practical and a universal application. When shedding does not occur, the random pressures are bounded by the upper limit in frequency  $\omega y_f / U_s \approx 1$ . Here, values of  $y_f$  are the same as those given previously for tones; for the 25° knuckle-beveled edge,  $y_f$  is approximately 0.7 to 0.8 h and  $U_s / U_\infty \approx 1.15$

### 7.3 MAGNITUDES OF SURFACE PRESSURE

The levels of all continuous-spectrum pressures generated on the trailing edges of this study appear to be reasonably well bounded by a 10 dB spread as noted by examining Figures 10 and 11. In a rough sense, and for a given edge geometry, the spectrum shapes are all similar functions of  $\omega y_f / U_s$ . For the 25° rounded bevel, the pressures generated closest to the apex and in the upstream extremity of the separation at low frequencies were only slightly greater than or comparable to pressures generated upstream in the attached boundary layer. At frequencies greater than  $\omega y_f / U_s > 1$ , the pressures of fully attached turbulent boundary layers may actually be much greater than the pressures generated in a trailing-edge separation zone if it occurs. However, the pressures generated in this zone may have enhanced cross-stream correlation. The flow separation thus generates a flow field of predominantly large-scale convected vortical disturbances. On the basis of aerodynamic noise theory, one would therefore expect a blunt edge with a limited separation zone such as the 25° rounded edge to generate less high frequency sound (i.e.,  $\omega y_f / U_s > 1$ ) than a thin airfoil with no separation whatsoever.

Prediction of the magnitudes of unsteady pressures beyond the general guidelines given here appears quite impossible with current knowledge. Not enough is known of the effects of upstream history on separation and on the unsteady motions produced in the near wake to make realistic magnitude estimates. For blunt edges which produce tones, however, even though there is some dependence of the strength of the vortex street wake on the thickness of the upstream boundary layer relative to the geometric thickness of the trailing edge, the pressures and vortex strengths of the near-wake vorticity seem reasonably well bounded. The current results may therefore be used in a predictive sense for cases involving airfoils of fairly uniform thickness, small camber, small ratios of upstream boundary layer thickness to base thickness, and moderately large curvature of the trailing edge to promote flows sufficiently dominated by trailing edge geometry. In the case of tone generation, the results shown in Part 1, Figure 22, and Equation (26), may be used for lifting surfaces. This was demonstrated when the theory was compared with Brooks and Hodgson's (1981) measurement of aerodynamic sound from a blunt trailing edge.

#### ACKNOWLEDGMENTS

The assistance of L. Maga, R. Armstrong, and R. Dwyer in gathering experimental results is much appreciated. This work was sponsored by the Naval Sea Systems Command, SEA 55X4.

## REFERENCES

- Blake, W. K., (1970), "Turbulent Boundary-Layer Wall Pressure Fluctuation on Smooth and Rough Walls," *Journal of Fluid Mechanics*, 44, p. 1.
- Blake, W. K., (1975), "A Statistical Description of Pressure and Velocity Fields at the Trailing Edges of Flat Struts," DTNSRDC Report 4241.
- Blake, W. K., (1982), "Structure of Trailing Edge Flow Related to Sound Generation," Part 1-Tonal Pressure and Velocity Fluctuations submitted to *J. Fluid Mech.*
- Brooks, T. F. and T. H. Hodgeson, (1981), "Trailing Edge Noise Prediction Using Measured Surface Pressures," *J. Sound Vib.*, 78, pp. 69-117.
- Burton, T. W., (1971), On the Generation of Wall Pressure Fluctuations for Turbulent Boundary Layers Over Rough Walls, Massachusetts Institute of Technology, Acoustics and Vibrations Laboratory Report 70208-4.
- Chandiramani, K. L., (1974), "Diffraction of Evanescent Waves with Applications to Aerodynamically Scattered Sound and Radiation from Unbaffled Plates," *J. Acoust. Soc. Am.* 55, pp. 19-29.
- Chase, D. M., (1975), "Noise Radiated from an Edge in Turbulent Flow," *AIAA Journal*, 13, pp. 1041-1047.
- Chevray, R. and L. Kovasznay, (1969), "Turbulence Measurements in the Wake of a Thin Flat Plate," *AIAA Journal*, 7, pp. 1041-1043.
- Corcos, G. M., (1963), *J. of the Acoust. Soc. Am.*, 35, pp. 192-199.
- Crighton, D. G. and F. G. Leppington, (1971), *J. Fluid Mech.*, 46, pp. 577-591.
- Heskestad, G. and Olberts, (1960), "Influence of Trailing Edge Geometry on Hydraulic-Turbine-Blade Vibration Resulting from Vortex Excitation," *Transactions of the American Society of Mechanical Engineers, Journal of Engineers, Journal of Engineering for Power*, 82, pp. 103-110.
- Howe, M., (1978), "A Review of the Theory of Trailing Edge Noise," *J. Sound Vib.*, 61, pp. 437-465.
- Sandborn, V. A. and S. J. Kline, (1961), *ASME Journal of Basic Engineering*, 83, pp. 317-327.
- Scholemer, H. H., (1967), *Journal of the Acoustical Society of America*, 42, pp. 93-113.
- Simpson, R. L., J. H. Strickland and P. W. Barr, (1977), *Journal of Fluid Mechanics*, 79, pp. 553-594.

Willmarth, W. W. and E. F. Wooldridge, (1963), "Measurement of the Correlation Between the Fluctuating Velocities and the Fluctuating Pressures in a Thick Turbulent Boundary Layer," Advisory Group for Aerospace Research and Development Report 456.

Leverton, J. W. (1973), "The Noise Characteristics of a Large 'Clean' Rotor" *Journal of Sound and Vibration*, 27, pp. 357-376.

INITIAL DISTRIBUTION

Copies		CENTER DISTRIBUTION		
		Copies	Code	Name
1	NRL (Hanson)			
5	NAVSEA	1	01	
	1 SEA 063R-31 (Pierce)			
	1 SEA 55N2 (Paladino)	1	15	
	1 SEA 55N5 (Weiczorek)	1	1504	
	1 SEA 55W33 (Sanberg)	1	152	
	1 PDS 350 (Firebaugh)	1	154	
2	CONR			
	1 (Whitehead)	1	154.1	Yin
	1 (Reischman)	1	154.2	Cumming
1	NUSC NPT (Kittredge, Code 3634)	1	1521	Day
		1	1521	Remmers
2	NUSC NLON			
	1 (Ko)	1	1542	Huang
	1 (Schloemer)	1	1542	Groves
		1	1542	Burke
12	DTIC	1	1544	Peterson
		1	1544	Fuks
3	NASA	1	1544	Caster
	1 (D.P. Beneze (AMES))	1	1544	Boswell
	1 (J. Harden) (Langley)			
	1 (T. Brooks) (Langley)	1	1802.1	Lugt
		1	1844	Dhir
2	MIT			
	1 (Prof. Patrick Leehey)	1	19	
	1 (Prof. C. Choysostomedes)	1	1905.1	
1	Univ of Minn	1	1905.4	
	Prof. R.E.A. Arndt	1	194	
1	Lehigh Univ	1	1942	Fisher
	Prof. Donald Rockwell	1	1942	Huang
		1	1942	Geib
1	Univ of Notre Dame	1	1944	Maga
	Prof. Thomas Meuler	1	1944	Paladino
3	ARL/PSU	1	1944	Nole
	1 (R. Henderson)	1	1944	Gershfeld
	1 (G. Lauckle)	1	1944	Kippel
	1 (D. Thompson)	1	1962	Kilcullen
1	Univ of Houston	10	5211.1	Reports Distribution
	Prof. A.K.M.F. Hussain	1	522.1	TIC (C)
		1	522.2	TIC (A)

END

DATE

FILMED

7-85

DT